February 2023
Ph.D. Dissertation

Synthesis and Characterization of Silole Derivatives and Application as Chemosensors for the Detection of Chemical Explosives

Graduate School of Chosun University

Department of Chemistry

Md Hasanul Haque

Synthesis and Characterization of Silole Derivatives and Application as Chemosensors for the Detection of Chemical Explosives

실올 유도체의 합성과 특성 분석 및 폭발물 탐지를 위한 화학센서로의 응용

February 24, 2023

Graduate School of Chosun University

Department of Chemistry

Md Hasanul Haque

Synthesis and Characterization of Silole Derivatives and Application as Chemosensors for the Detection of Chemical Explosives

Advisor: Prof. Honglae Sohn

This dissertation is submitted to the Graduate School of Chosun University in partial fulfillment of the requirements for the degree of Doctor of Philosophy in Science

October 2022

Graduate School of Chosun University

Department of Chemistry

Md Hasanul Haque

This is to certify that the Ph.D. dissertation of Md Hasanul Haque has successfully met the dissertation requirements of Chosun University.

위원장 조선대학교 교수 김 호 중 (인)

위 원 KIST 책임연구원 유 남 호 (인)

위 원 조선대학교 교수 이 종 대 (인)

위 원 조선대학교 교수 임 종 국 (인)

위 원 조선대학교 교수 손 홍 래 (인)

January 2023

Graduate School of Chosun University

TABLE OF CONTENTS

III. CHAPTER 3

IV. CHAPTER 4

V. CHAPTER 5

VII. CHAPTER 6

ABBREVIATIONS

AIE	Aggregation-induced emission
ICT	Intermolecular charge transfer
NACs	Nitroaromatic compounds
TNT	2,4,6-Trinitrotoluene
DNT	2,4-Trinitrotoluene
PA	2,4,6-Trinitrophenol
DCB	1,4- Dichlorobenzene
λ_{ex}	Excitation Wavelength
λ_{em}	Emission Wavelength
QY	Absolute Quantum Yield
σ	Sigma
π	Pi
mg	Milligram
A.U	Arbitrary Units
ppm	Parts per Million
UV-Vis	Ultraviolet-visible spectrophotometry
PL	Photoluminescence
nm	Nanometer
M	Molarity
CB	Conduction band
VB	Valence band
HR-MS	High resolution mass spectra
PXRD	Powder X-ray diffraction
NMR	Nuclear magnetic resonance
GPC	Gel permeation chromatography
M_w	Weight average molecular weight
M_n:	Number average molecular weight

PDI	Polydispersity index
SEM	Scanning electron microscopy
TGA	Thermogravimetric analysis
DSC	Different scanning calorimetry
DLS	Dynamic light scattering
PET	Photo-induced electron transfer
Eg	Bandgap
δ	Chemical shift
τ	Fluorescence lifetime
f_w	Water fraction
h	Hours
min	Minutes
TMS	Trimethylsilyl

LIST OF FIGURES

Chapter 1

Chapter 2

Chapter 3

Figure 12. (a) Fabrication of polymer film and sensing performance of TNT. (b) Real-time fluorescence intensity profiles (quenching followed by recovery) of P1 in response to TNT vapors. The arrows indicate the points when quencher vapor was introduced and removed.

Figure 13. Quenching PL spectra of increasing fraction by each concentration of TNT (a) and PA (b) in THF solution for **P1**; TNT (c) and PA (d) for **P2**.

Figure 14. Quenching PL spectra of increasing fraction by each concentration in polymer nanoaggregates solution of TNT (a) and PA (b) for **P1**; TNT (c) and PA (d) for **P2**.

Figure 15. Stern–Volmer plot showing sensing efficiencies for TNT and PA in THF solution (a) P1, (c) P2, and in polymer nanoaggregate solutions (b) P1 and (d) P2.

Figure 16. The interaction between the polymers in the presence of analytes. (a) Schematic diagram of electron-transfer mechanism for photoluminescence quenching and (b) HOMO–LUMO energy profiles of polymers, PA and TNT from the *ab initio* calculations at the B3LYP/6-31G(d) level.

Figure 17. Fluorescence lifetime decay profile of P1 a) in THF solution and b) in H_2O/THF (H_2O fraction: 99%) with an increasing amount of PA (λ_{ex} = 379 nm). Inset: Fluorescence lifetime (τ_o/τ) are independent of added PA.

Figure 18. X-ray diffraction (XRD) patterns of polymer powders **P1**–**P2** in solid states.

Chapter 4

Chapter 5

Figure 5. a) PL spectra of P1 in the THF/H_2O mixture with different H_2O fractions. b) Plots of maximum emission intensity and wavelength of P1 versus the water fraction in the THF/H_2O mixture c) DLS data shows the particle size of P1 at f_w-50% (d)SEM images of P1 prepared from spin-coating from 50% water fraction. Inset: images of P1 with different H_2O fractions under UV light at 365 nm

Figure 6. Fluorescence photograph of the P1 in different volumetric fraction of water.

Figure 7. DLS data showing when the water fraction increases then the particle size of P1 nanoaggregate were decreased.

Figure 8. (a) Quenching PL spectra and (b) Stern–Volmer plot showing sensing efficiency by increasing in THF solution for P1 (c) Quenching PL spectra and (d) Stern–Volmer plot showing sensing efficiency by increasing TNT in THF/water solution (50% water) for P1

Figure 9. The TGA curve of P1

Figure 10. X-ray diffraction (XRD) patterns of polymer powders P1 in solid states.

LIST OF SCHEMES

Chapter 2

Chapter 3

Chapter 4

Chapter 5

LIST OF TABLES

Chapter 2

Chapter 3

Chapter 4

Chapter 5

LIST OF PUBLICATIONS

MH Haque, H Sohn*, Comparison of aggregation-induced emission enhancement effect between π-σ* and σ-σ* conjugation on silole and application in explosives detection. **Dyes and Pigments**, 2022, 201, 110175.

MH Haque, H Sohn*, Aggregation-Induced Emission Enhancement of Fluorene-Substituted 2,5-Silole Polymer and Application as Chemosensor. **Journal of the Korean Physical Society**, 2022, **80**, 1060–1064.

MH Haque, H Sohn*, Synthesis of Allyl Functionalized Silacrown Ethers and Their Application-A Review, **Journal of the Chosun Natural Science**, 2020,13,41.

MH Haque, H Sohn*, Synthetic Methods and Applications of Silicon Nanowire: A Review, **Journal of the Chosun Natural Science**, 2017, 10, 65.

Abstract

Synthesis and Characterization of Silole Derivatives and Application as Chemosensors for the Detection of Chemical Explosives

Md Hasanul Haque

Advisor: Prof. Honglae Sohn

Department of Chemistry

Graduate School of Chosun University

Detection of nitroaromatic compounds (NACs) are highly desirable for our environment, national security, and human health. Conjugated fluorescent polymers play very important role for detecting NACs by various way such as fluorescence quenching, colorimetric sensing, real-time sensing and so on. Silole has unique and unusual optical properties among all others five-membered ring of heterocyclopentadienes, due to the σ*-π* conjugation between Si atom of silole core and butadiene moieties. This conjugation gives rises to the low-lying LUMO of silole and increases its electron affinity. Herein, a series of conjugated silole derivatives were successfully synthesized. The synthetic process,

details of spectroscopic characterizations and some of unique photophysical property such as mehcanocromic, solvetocromic, pieozocromic will be address, and various type of sensing methods were also reported. Synthesized siloles showed high thermal stability at high temperature confirmed by thermogravimetric analysis (TGA). The obtained compounds such as dimer and polymers are conjugated through σ-σ*, and σ-π* in 1,1-position and π-π* in 2,5-position of silole core. We have investigated their photophysical properties and they exhibit unique aggregation-induced emission (AIE) properties by increasing the emission intensity in THF/water mixtures. Furthermore, we observed excellent sensitivity for sensing explosives by silole derivatives. High Stern-Volmer constant was observed during quenching of photoluminescence (PL) intensity upon adding explosives. In addition, for the practical application, we investigated the real-time sensing by fluorescence recovery process and 2,5-phenyl substituted silole polymer showed great respond through NACS. Moreover, we also examined the colorometric and paper strips investigation and the polymers reveal that it may be a promising candidate in solid state for NACs detection.

초록

실올 유도체의 합성과 특성 분석 및 폭발물 탐지를 위한 화학센서로의 응용

박사과정: 앰 디 하 산 을 하 퀴

지도교수: 손 홍 래

조 선 대 학 교 화 학 과

니트로방향족 화합물(NAC)의 검출은 우리의 환경, 국가 안보 및 인간 건강에 매우 바람직합니다. 공액 형광 고분자는 형광 소광, 비색 감지, 실시간 감지 등 다양한 방법으로 NAC 를 감지하는 데 매우 중요한 역할을 합니다. Silole 은 silole 코어의 Si 원자와 부타디엔 부분 사이의 σ*-π* 접합으로 인해 헤테로시클로펜타디엔의 다른 모든 5 원 고리 중에서 독특하고 특이한 광학 특성을 가지고 있습니다. 이 접합은 silole 의 낮은 위치에 있는 LUMO 를 발생시키고 전자 친화력을 증가시킵니다. 합성 과정, 분광 특성화에 대한 세부 사항 및 메카노크로믹, 솔브토크로믹, 압전크로믹과 같은 고유한 광물리 특성에 대해 설명하고 다양한 유형의 감지 방법도 보고되었습니다. 합성된 사일로는 열중량 분석(TGA)에 의해 확인된 고온에서 높은 열적 안정성을 보였다. silole core 의 1,1-position 에서 σ-π*, 2,5-

position 에서 π-π*, σ-σ*, σ-π*를 통해 이량체 및 고분자와 같은 결합 화합물. 우리는 그들의 광물리학적 특성을 조사했으며 THF/물 혼합물에서 방출 강도를 증가시켜 독특한 응집 유도 방출(AIE) 특성을 나타냅니다. 또한, 우리는 silole 유도체에 의한 폭발물 감지에 대한 우수한 감도를 관찰했습니다. 폭발물을 첨가할 때 광발광(PL) 강도의 소광 동안 높은 Stern-Volmer 상수가 관찰되었습니다. 또한 실제 적용을 위해 형광 회복 과정에 의한 실시간 센싱을 조사한 결과 NACS 를 통해 2,5-페닐 치환 실롤 폴리머가 큰 반응을 보였다. 또한, 우리는 또한 비색 및 종이 스트립 조사를 조사했으며 폴리머는 NAC 검출을 위한 고체 상태의 유망한 후보가 될 수 있음을 보여줍니다.

Chapter 1 – Introduction

Background

1.1 Silole

Silole is a five-membered (silacyclopentadienes) silacycle, conjugated through the orbital interaction of the σ* orbital of its silylene moiety with the π* orbital of its butadiene fragment. This conjugation increases the electron affinity by lowering its LUMO energy level compared to other conjugated five membered heterocycles such as pyrrole, thiophene, and furan.[1–3]. Silole possess unique and unusual optical properties. The property of a silole fluorophore is sensitive due to substituents. The substituent effect helps in further molecular design and exploration in high-tech applications. There are only few reports have discussed about such investigation. 1,1-Substituent on the photoluminescence (PL) of siloles' rings through the inductive effect was reported by Yamaguchi et al [4]. Silole molecule with different substituents at the 2,5-positions were successfully synthesized and tuned by Pagenkopf et al [5,6]. On the other hand, 3,4-diarylsiloles are virtually non-emissive in solution and their poor luminescence condemns them to a dark future in applications which is coming from 3,4-substitution [7–10].

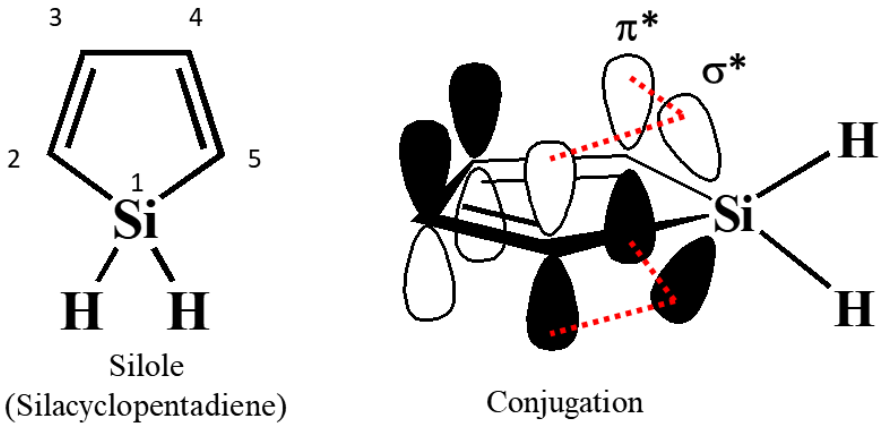

Figure 1: Skeleton of silole with positions numbered and conjugation system.

1.2 Conjugated Silole

A schematic energy-level diagram for conjugation system on silole is shown figure 2. Silole can be conjugation through 1,1-position in silole core. This conjugation occurred between two Si atom of silole core brings σ-σ* conjugation (figure 3). Different groups can be introduced in the 1,1-position. When the alkyl groups take place in between two silole core then we can observe the σ-π conjugation.

Accordingly, 1,1-substituents usually show to slightly longer absorption maxima due to the more electronegative [11].

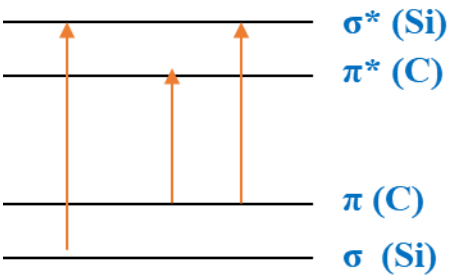

Figure 2: Schematic energy-level diagram silole conjugation

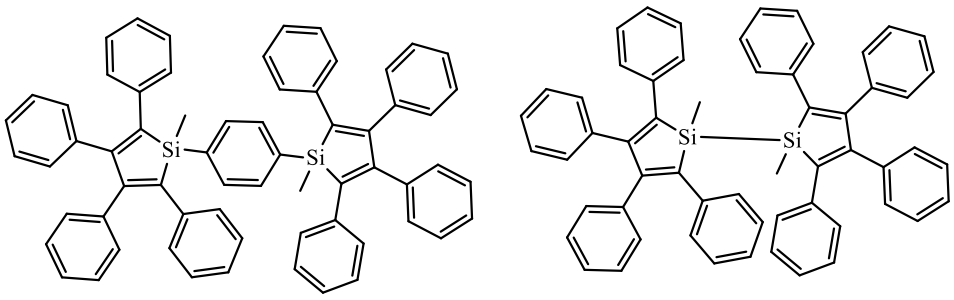

Figure 3: Silole in 1,1-position conjugated through σ-π* and σ-σ* conjugation

On the other hand, 2,5-position plays vital role for the photophysical properies of silole. π-π* conjugation usually seen in this position on silole core. Several studies

have been reported about the effects on this position. in the 2,5-positions of silole with the aryl groups and absorption, fluorescence and cyclic voltammetry are varied investigated Yamaguchi et al [7]. Figure 4 showed some the monomers attached in 2,5-position such as fluorene, ethylbenzene, octaloxy benzene and iptycene. Due to the π-π* conjugation their optical property could be differed and principally inductive effects on the electronic and optical properties of siloles. On the electronic and optical properties of silole depends on σ and π effects of 2,5-substituents. Many of electron-rich or electron-poor heteroaromatic rings can be combined with silole ring in the 2,5-positions can be examined the redox potentials of siloles.

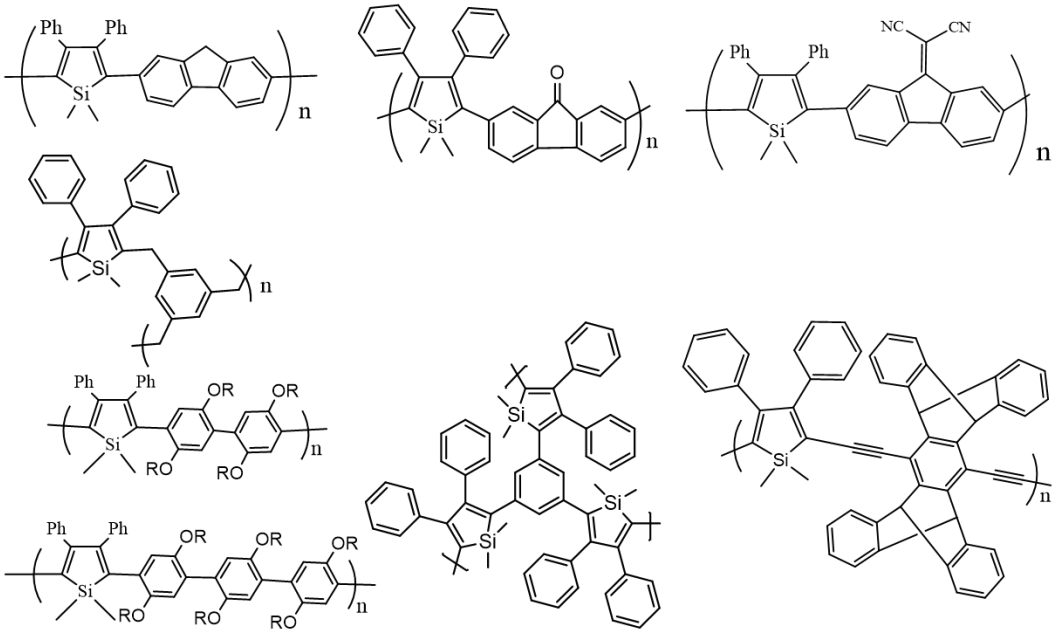

Figure 4: Different types of silole in 2,5-position conjugated through π-π* conjugation

1.3 Optical Property of Conjugated Silole

Silole exhibit unique optical characteristics as a novel π-electronic material and due to conjugation of σ*–π* between the silicon atom and the butadiene moiety [3]. Silole have another interesting optical property that it shows the aggregation-induced emission (AIE) behavior in solid state by restricting the free rotation of phenyl ring in 3,4 positions (figure 5). In solution, silole emit weak emission due to the intramolecular rotation of phenyl ring which brings the non-radiative decay. whereas in solid state, the non-radiative decay can be prevented by restricted the intramolecular rotation (RIR) and thus the emission has been enhanced [12,13]. In recent time, conjugated silole polymer possess advantages over their small-molecule counterparts and a huge number of efforts have been done based on photoluminescence (PL) and electroluminescence properties [14–19].

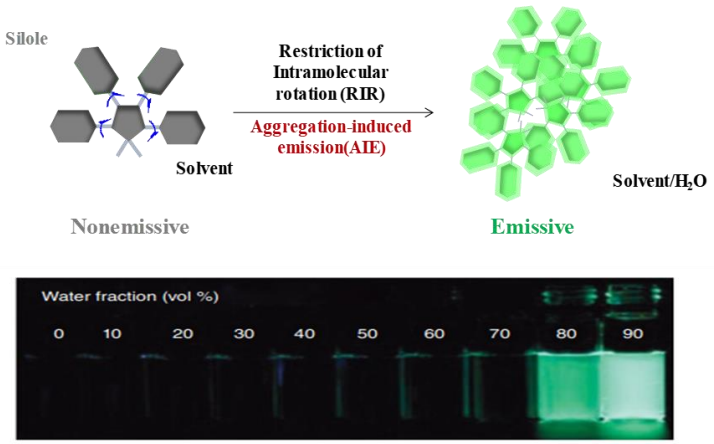

Figure 5: Schematic illustration for the AIE property of silole

1.4 Applications of Conjugated Siloles

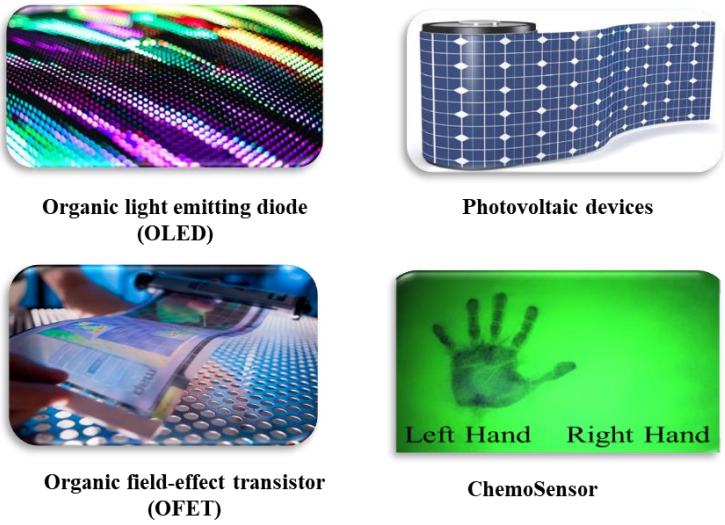

Figure 6: Various applications of silole

Due to the unique optical property of silole, many device applications incorporated with AIE-active siloles have been implemented in different field such as, electron transporting materials [20], memory storage [21], photovoltaic cells [22] and light-emitting diodes (LEDs) [10,23]. Figure 6 displays the various application in optoelectronics fields with siloles.

1.4.1 Introduction of Silole as Chemosensors

Detection of chemical explosives is essential for homeland security, mine removal, and forensic investigations. Detecting ultra-trace chemical analytes by sensors offers a new way to solve this problem. Siloles have shown their potentiality for sensing nitroaromatic compounds as chemo-sensors by transferring electron to analyte and used to detect chemical explosives by photoluminescence (PL) quenching. Figure 7

showed the use of chemical sensor in various form such as fluorescent polymer, metal-organic framework.

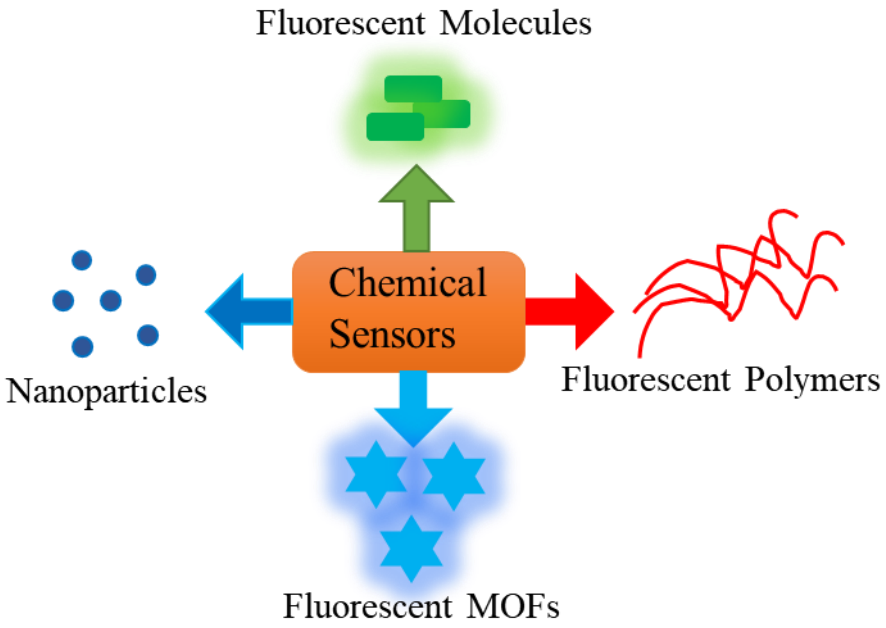

Figure 7: Schematic diagram of chemical sensor in different ways.

1.4.2 Sensing Mechanism

Silole are electron rich molecules, and the NACs are electron deficient. Fluorescence quenching for the detection of NACs involves electron transfer from electron rich silole to electron deficient NACs. As shown in Figure 8, the excited electron from the Lowest unoccupied molecular orbital (LUMO) of siloe fluorophore can transfer to the LUMO of NACs analyte. This process is known as photo-induced electron

transfer (PET) process which causes the fluorescence quenching [17,24]. The quenching is classified into two parts of static quenching and dynamic quenching which play an important role in sensing. Through the quenching process can be defined by time-resolved fluorescence decay. The dynamic quenching process involves the excited-state lifetime change of fluorophores, while it meets analyte without bonding each other. On the other hand, the lifetime does not change during the fluorescence quenching in the static quenching process. Poly(tetraphenyl)silole shows a linear Stern–Volmer relationship for NACs sensing and the excited-state lifetime does not decrease on addition of analytes. Thus, the polysilole exhibits static quenching processes [17]. In this study, the detection of NACs such as 2,4,6-trinitrotoluene (TNT), 2,4-dinitrotoluene (DNT) and 2,4,6-trinitrophenol (PA) with the silole derivatives were investigated. In addition, 1,2-dichlorobenzene (DCB), as an electron deficient aromatic molecule, was tested for an interference model compound. DCB has the higher LUMO level compared to LUMO of silole. Thus, the electron can nor transfer from silole to DCB. Although DCB is electron deficient molecules but due to the LUMO level, the quenching is not possible here.

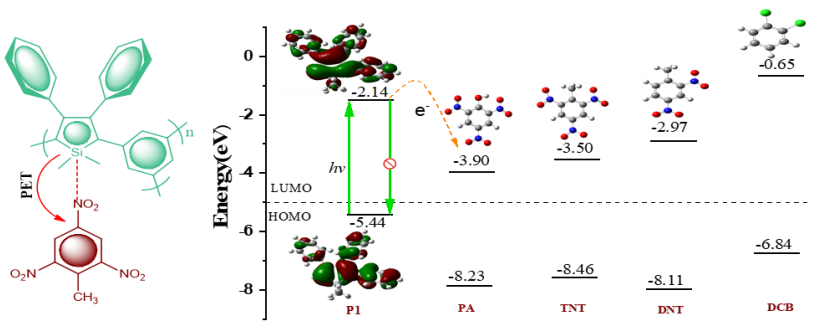

Figure 8: Schematic diagram of the interaction between silole with NACs and electron-transfer mechanism.

Chapter 2

Comparison of Aggregation-Induced Emission Enhancement Effect between π-σ and σ-σ* Conjugation on Silole and Application in Explosives Detection*

1. Introduction

Luminous materials are considered as promising candidate in optics and electronics field due to their structural versatility. Molecules which are non-emissive or weakly emissive in solution become more emissive in aggregate state by restricting intramolecular rotation (RIR) known as aggregation-induced emission (AIE) [9,13,25]. Whereas many luminophore molecules with planar structure in dilute solution, their emissions are often quenched in solid state due to intermolecular π-π stacking interaction or formation of excimer. This phenomenon called aggregation-caused emission quenching (ACQ) became huge problem in the development of various application field such as optoelectronics, chemo-sensors, biosensors, etc. [26–28]. This problem of quenching fluorescence in solid state can be improved effectively by restricting the π-π stacking and preventing the formation of excimer [29–31]. It is thus highly desirable to overcome this problem by developing aggregation-induced emission enhancement (AIEE) compounds where many AIEE active aromatic molecules have been already developed [32].

Detection of chemical explosives is essential for homeland security, mine removal, and forensic investigations. Detecting ultra-trace chemical analytes by sensors offers a new way to solve this problem. Siloles have shown their potentiality for sensing nitroaromatic compounds as chemo-sensors by transferring electron to analyte and used to detect chemical explosives by photoluminescence (PL) quenching. Excited electrons from silole can be transfer to the explosives as nitro aromatic compounds are electron deficient, thus the transmission results in emission quenching [17,33]. Siloles containing a five-membered ring have attracted much attention due to their unusual optical and electrical properties [34]. The silole molecule containing

butadiene moiety has the lowest LUMO energy level compared with that of other hetero-cyclic five membered ring compounds, such as pyrrole, furan, and thiophene [3]. Moreover, siloles showed AIE property in the aggregation states where rotation of the phenyl rings were restricted and the non-radiative decay pathways were blocked [35]. The AIE active sensor shows high sensitivity due to the strong light emission [36]. Therefore, many device applications incorporated with siloles have been demonstrated in various field such as, light-emitting diodes (LEDs) [11,12], chemical sensors [6,13], memory storage [21], electron transporting materials [20], and photovoltaic cells [22].

The luminescent characteristics of π conjugated compound can be altered by chemical modification through tuning of their energy level [38]. The fluorescent conjugated polymers have been of great interest to their capability to produce signal gain in response to interactions with analytes. Due to the highly efficient transportation of electrons or holes in electronic excited states, the fluorescent conjugated polymers exhibit the increased sensitivity in terms of fluorescence quenching [39–41]. On the other hand, siloles of silicon-carbon framework which are delocalized through σ-π hyper conjugation shown promise as a considerable candidate for optoelectronics applications [24,42,43].

We report herein the AIEE behaviors and sensitivity of two different types of hyper conjugated silole molecules, such as 1,4-bis(1-methyl-2,3,4,5-tetraphenyl-1-silacyclopentadien), bissilole, and 1,4-bis(1-methyl-2,3,4,5-tetraphenyl-1-silacyclopentadienyl)benzene, bissilole-benzene. Bissilole-benzene nanoaggregates showing π-σ* hyper conjugation via π orbitals of benzene bridge and σ* orbital of silole and σ-σ* hyper conjugation of bissilole indicating the

orbital overlap via σ orbitals of silicon in silole and σ* orbitals of adjacent silicon in silole. These nanoaggregates showed very weak fluorescence emission in solution but exhibited strong emission in aggregation states. AIEE active properties for silole nanoaggregates are examined and used in sensing for explosives detection. Previously we have reported the sensitivity of bissilole [44,45]. In this work we report the novel bissilole-benzene and would like to also investigate the main driving force between bissilole and bissilole-benzene for photoluminescence (PL) enhancement and sensitivity towards nitroaromatic compounds (NACs).

2. Results and Discussion

2.1. Synthesis and Characterization

The synthetic route of bissilole and bissilole-benzene was depicted in scheme 1 and the procedures are described in experimental section. Both the compounds were synthesized with 1-chloro-1-methyl-2,3,4,5-tetraphenyl-1-silacyclopentadiene and characterized by $^{1}H/^{13}C$ NMR spectroscopies and high-resolution mass spectrometry. (See Figs. S1-S4 in the Supporting Information).

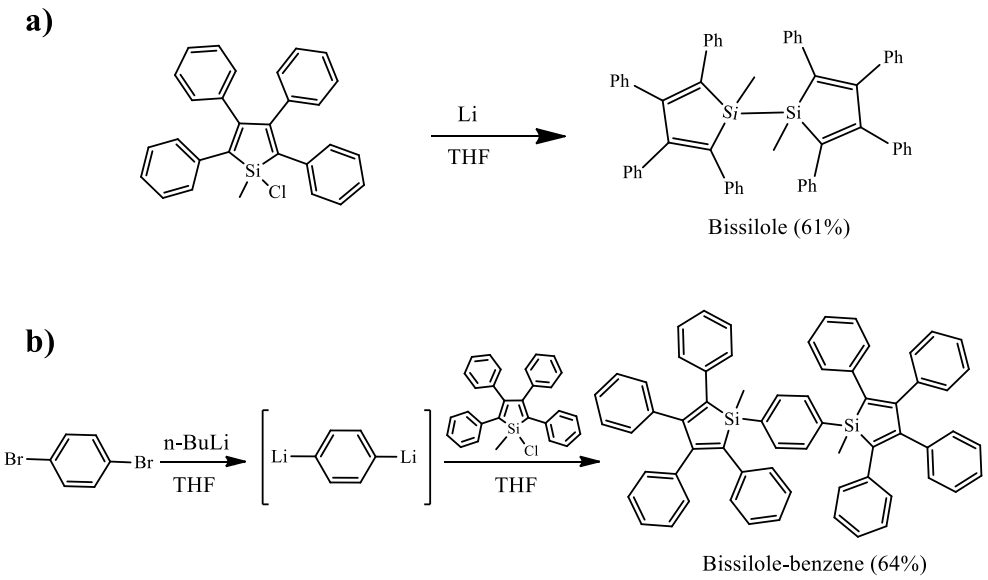

Scheme.1. Synthetic route of bissilole (a) and bissilole-benzene (b).

The absorption spectrum and fluorescence spectra of bissilole-benzene and bissilole were measured in pure THF solution and shown in Figure. 1.

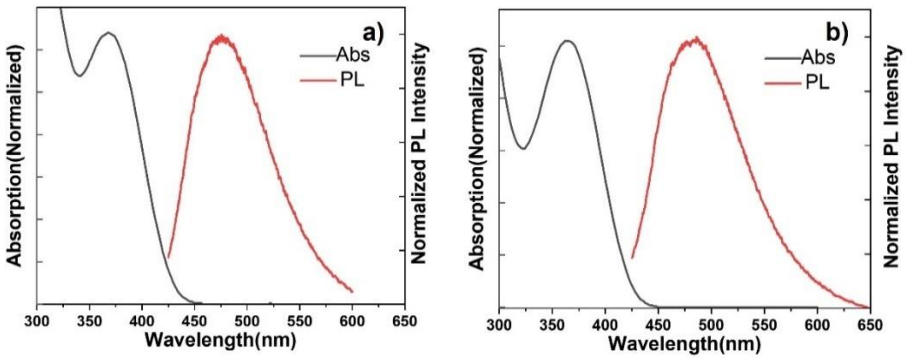

Figure 1. Absorption and emission spectra of bissilole-benzene (a) and bissilole (b)

2.2. Photophysical Properties

Siloles have an attractive optical property which is AIEE due to the peripheral phenyl rings. These peripheral phenyl rings caused nonplanar conformation as a result π-π stacking was prevented. Moreover, the weak PL emission in solution state becomes strong emitters in aggregate state, due to the restriction of intramolecular rotation via blocking the nonradiative decay. Different types of silole nanoaggregates having two distinct hyper conjugations were prepared in this study and investigated for their optical properties and sensitivity.

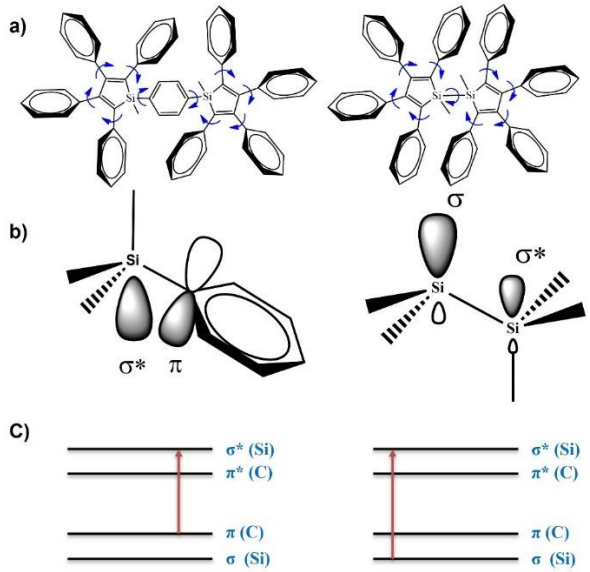

Figure 2. (a) Chemical structure of bissilole-benzene (left) and bissilole (right) and (b) Structural orientation of bissilole-benzene (left) and bissilole (right). Hydrogen atom and phenyl rings are omitted for the clarity. (c) Schematic energy-level diagram of bissilole-benzene (left) and bissilole (right).

Herein, we synthesized bissilole-benzene, which allows more flexible intramolecular rotation. Figure 2(a) showed the chemical structures of bissilole-benzene and bissilole, exhibiting the π-σ* and σ-σ* hyper conjugations, respectively. Figure 2(b) illustrates the π-σ* hyper conjugation indicating the orbital overlap between the benzene bridge and LUMO of the silole in bissilole-benzene and the σ-σ* hyper conjugation indicating the orbital overlap between the σ orbital of silicon in silole and σ* orbital of other silole in the bissilole, which might be more sterically hindered. Figure 2(c) displays the schematic energy-level diagram of both siloles which exhibit the absorption band. These are ascribed from π-σ* and σ-π* transition of silicon atom with phenyl ring in bissilole-benzene and σ-σ* transition between two silicon atoms of bissilole. The optical properties of bissilole and bissilole-benzene were determined by UV-Vis and PL spectrometer (Table 1).

Table 1. Summary of photoluminescence data for bissilole and bissilole-benzene

Compounds	λ_{abs} (nm)[a]	Solution λ_{flu} (nm)[a]	Aggregate λ_{flu} (nm)[b]	Φ_{flu}[c] (%) (Sol/Agg)
Bissilole	360	480	482	0.8/60
Bissilole-benzene	365	484	493	0.3/55

[a] UV–vis and fluorescence taken in THF. [b] fluorescence emission of nanoaggregates at f_w-99%. [c] Absolute quantum yield of fluorescence (In solution and aggregates state).

The bissilole-benzene exhibited a 5 nm and 4 nm red shift in λ_{abs} and λ_{flu} from the bissilole, respectively. Due to the long conjugation of bissilole-benzene compared to bissilole, this result might be obtained. This red shift indicates that

the π-σ* hyper conjugation is more effective than the σ-σ* hyper conjugation between monomer unit. The absolute quantum yield (QY) of bissilole-benzene and bissilole in THF solution were 0.3% and 0.8%, respectively.

2.3. Theoretical calculations and analysis:

To studied the energy level of bissilole-benzene and bissilole, we carried out the density functional theory (DFT) calculation on their energy levels with a B3LYP/6-31G(d) basis set using the Gaussian 09 package [46]. Figure 3 shows the calculated electronic structures of these two bissiloles 2and their molecular orbital distributions of HOMO and LUMO.

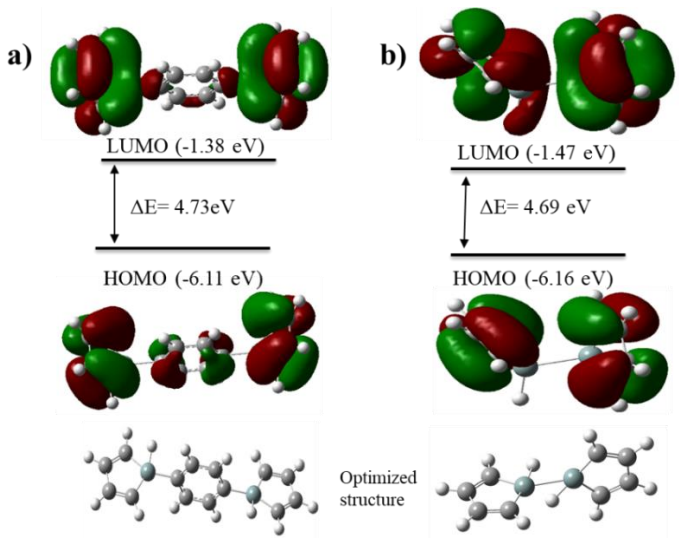

Figure 3. Density functional theory (DFT) optimized structures of (a) bissilole-benzene and (b) bissilole from the ab initio calculations at the B3LYP/6-31G(d) level. Phenyl rings and methyl are omitted for the clarity.

According to the calculation, the band gap of bissilole is smaller which might have more conjugation effect. The conjugation effect of bissilole is better than that of bissilole-benzene which causes the highly efficient transportation of electrons or holes in electronic excited states and gives the increased sensitivity. Since the σ-σ* hyper conjugation effect of Si-Si bond lowers the LUMO level of bissilole compared to the π-σ* hyper conjugation of bissilole-benzene. The σ-σ* hyper conjugation effect could be the predominant parameter which gives low band gap energy and increases sensitivity for detection nitroaromatic compounds (NACs).

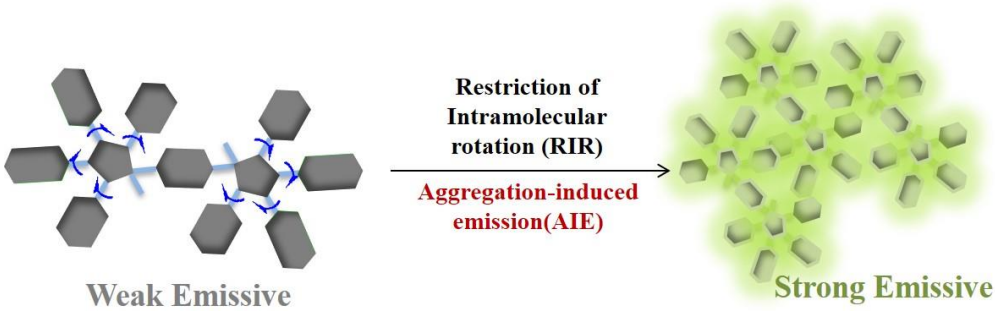

Figure 4. Schematic diagram for the preparation of bissilole-benzene nanoaggregates.

2.4. AIEE properties of bissilole-benzene and bissilole:

To investigate the AIEE property, the nanoaggregates with the concentration of 1 × 10^{-5} mol/L were prepared in different THF/water mixtures. PL intensity of silole aggregate is depending on the degree of aggregation [47]. Figure 4 illustrates that how the nanoaggregates is forming and enhancing the luminescence by restricting intramolecular rotation of phenyl rings. Since the water is nonsolvent for the silole, so in the high-water solvent mixtures siloles molecules become aggregate which blocks non-radiative decay and restricts the intramolecular rotation. Figure 5 shows the AIE enhancement upon adding water for the bissilole-benzene (a) and bissilole (c). As shown in Figure 5(a), the fluorescence emission intensity of bissilole-benzene remains almost same up to 70% of water fraction. On the further increasing of water fraction, intensity dramatically started to increase indicating that the colloid starts to form at 80% of water fraction. At f_w-99%, fluorescence emission increased along with 9 nm redshift. Figure 5(c) shows the AIE behavior of bissilole and PL intensity starts to increase from 60% water fraction. At 99% of water fraction, the PL intensity of bissilole-benzene increased by 180 times while the PL intensity of bissilole increased by 54 times (Fig. 5b and d).

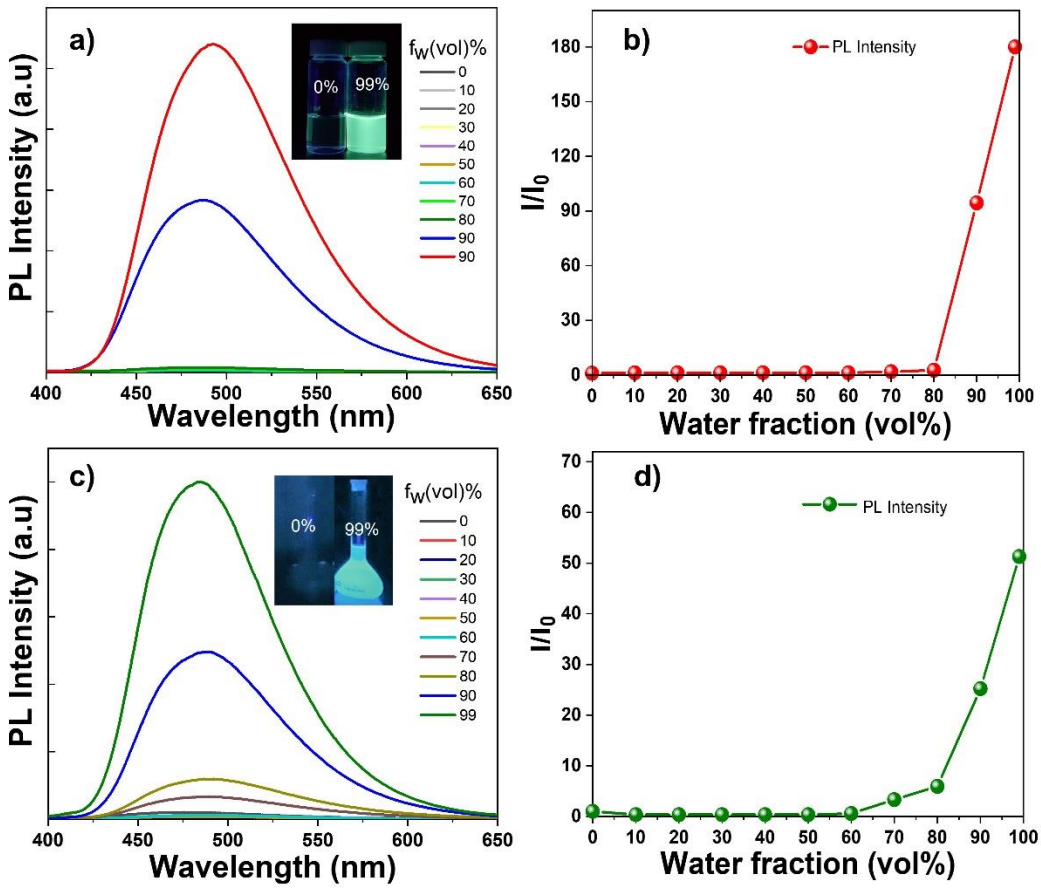

Figure 5. PL spectra of (a) bissilole-benzene and (c) bissilole in THF/water mixtures with different fraction of water. (b,d) Plots of I/I_0 versus different water fraction of bissilole-benzene and bissilole, respectively. I_0 is the PL intensity in Pure THF solution (concentration 10^{-5}M). (Inset: Fluorescence photograph of silole nanoaggregates at f_w-0% and 99%).

The photograph of two bissilole in different THF/water mixtures (0~ 99%) are captured under the UV lamp illumination at 365 nm (Fig. 6) indicating the color

changes upon adding water fraction which presenting the AIEE feature by changing color as well as enhancing the fluorescence intensity.

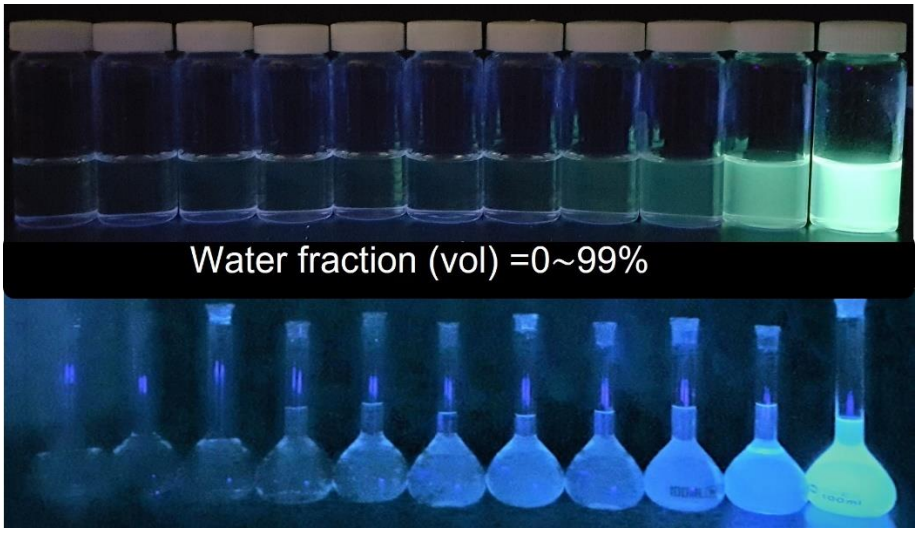

Figure 6. Fluorescence photograph of bissilole-benzene (top) and bissilole (bottom).

For the absolute quantum yield (QY), bissilole and bissilole-benzene nanoaggregate showed 60% and 55% at 99% water fraction, respectively. These results reveal that both compounds showed great AIEE property.

This result indicates that the σ-σ* hyper conjugation of Si-Si bond of bissilole might beless effective on AIEE compared to the π-σ* hyper conjugation of Si-C phenyl ring due to the higher non-radiative decay. As a result, bissilole-benzene reveals higher PL enhancement than bissilole by preventing non-radiative decay. Moreover, high steric hindrance between two silole unit of bissilole causes more strict intramolecular rotation and colloid forming faster because of less flexibility

in solution. Since the bissilole-benzene are connected by phenyl ring has less steric hindrance, which might allow more flexible intramolecular rotation and bissilole-benzene nanoaggregates are not formed up to 80% of water fraction. On the other hand, due to the more steric hindrance which gives rigid structure of bissilole could bring more PL enhancement as we expected. However, we get the reverse result from these two siloles compounds in case of AIEE property. In this case, the hyper conjugation effect might be the main driving force for enhancing PL. Thus, it indicates that the π-σ* hyper conjugation could be predominant effect for higher PL enhancement rather than steric hindrance. Furthermore, we carried out the dynamic light scattering measurements to measure the particle size and their distribution at different fraction of water to investigate AIEE characteristics.

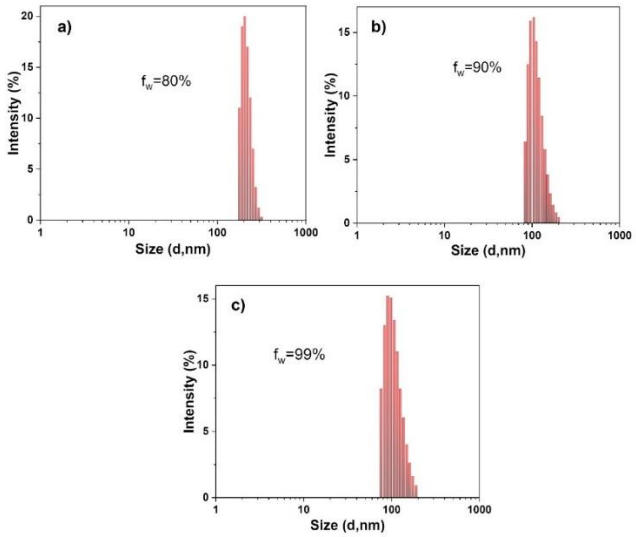

Figure 7. DLS data showing when the water fraction increases then the size bissilole-benzene nanoaggregate decreases to (a) 80%, (b) 90%, (c) 99%.

The particle size of the bissilole-benzene nanoaggregates decreased when the water fraction increased as expected (Fig. 7). Average particle size of the bissilole-benzene was about 215, 148 and 107 nm when water fraction increases from 80%, 90% and 99% respectively. This result is similar to the data of other silole nanoaggregates previously reported [44,48]. Hydrophobic molecules are prone to aggregate at higher hydrophilic environment, this could be a reason for decreasing particle size while water fractions increase [45].

2.5. Detection of nitro-explosives in aqueous solution:

Detection by fluorescence quenching involves electron transfer from electron rich silole to electron deficient NACs. As shown in Figure 8, the excited electron from the LUMO of bissilole-benzene fluorophore can transfer to the LUMO of NACs analyte. This process is known as photo-induced electron transfer (PET) process which causes the fluorescence quenching [17,24]. Basically, the fluorescence quenching is classified into two parts of static quenching and dynamic quenching which play a vital role in sensing. Through the time-resolved fluorescence decay, the quenching process can be defined. The dynamic quenching process involves the excited-state lifetime change of fluorophores, while it meets analyte without bonding each other. On the other hand, the lifetime does not change during the fluorescence quenching in the static quenching process. Poly(tetraphenyl)silole shows a linear Stern–Volmer relationship for NACs sensing and the excited-state lifetime does not decrease on addition of analytes. Thus, the polysilole exhibits static quenching processes [17]. Since the bissilole-benzene shows the linear Stern–Volmer relationship in sensing, the detection mechanism might be the static quenching. In this study, the detection of NACs such as 2,4,6-trinitrotoluene

(TNT), 2,4-dinitrotoluene (DNT) and 2,4,6-trinitrophenol (PA) with the bissilole-benzene nanoaggregates was investigated. In addition, 1,2-dichlorobenzene (DCB), as an electron deficient aromatic molecule, was tested for an interference model compound. The nanoaggregate (f_w-90%) used to investigate the fluorescence quenching behavior by adding of an identical volume-fraction of 90% water solution of NACs.

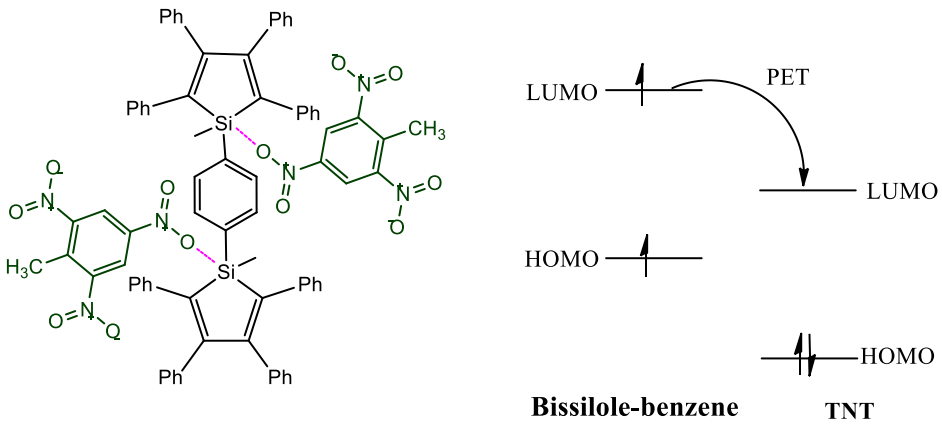

Figure 8. Schematic diagram of the interaction between bissilole-benzene with TNT (left) and electron-transfer mechanism for quenching photoluminescence by TNT (right).

Stern-Volmer equation: $I_0/I=K_{SV}$ [Q]+1 was used to analyze the quenching behavior, where K_{SV} is the Stern–Volmer constant, I is the fluorescence intensity at presence of quencher [Q] and I_0 represents the intensity while [Q]=0. Figure 9(a) and (b) display the quenching of PL spectra upon adding TNT and PA to the nanoaggregate solution, respectively. Bissilole-benzene exhibits the linear Stern–Volmer relationship for TNT and PA in μM concentration range (Fig. 7c). The

Stern-Volmer constant, $K_{SV,}$ for TNT and PA was 1.3×10^4 and 1.8×10^4 M^{-1}, respectively. This result is higher than those for linear conjugated poly(tetraphenylsilole-vinylene) and poly(tetraphenylsilole-silafluorene-vinylene) [42].

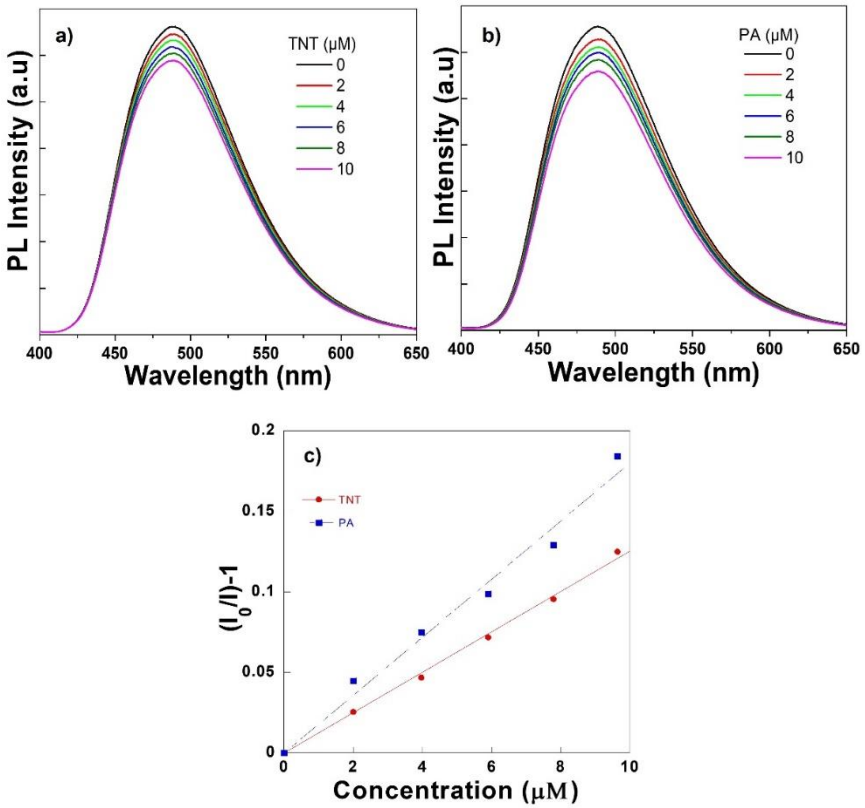

Figure 9. Quenching of PL spectra upon adding (a) TNT and (b) PA in bissilole-benzene nanoaggregates solution. (c) Stern–Volmer plot showing sensing efficiency for analytes in nanoaggregates.

Previously, we reported the K_{SV} of non-aggregate poly(tetraphenyl)siloles for the detection of PA, TNT, and DNT. Bissilole-benzene nanoaggregates showed much higher sensitivity to those NACs compared to polysiloles [17]. Moreover, the bissilole-benzene nanoaggregate showed 3 times higher sensitivity for TNT detection than oligo(tetraphenyl)silole nanoaggregate reported by Trogler et. al (ca. 4,100 M^{-1}) [33].

Moreover, it is also important to detect DNT because it is a precursor of TNT. DNT contains nitro groups and has high toxicity, which is also considered as a threatful material for our environmental issues. The sensitivity for DNT has been studied. As expected, the K_{SV} (6,000 M^{-1}) value for DNT in nanoaggregates is 2 times lower compared to TNT (Fig. 10).

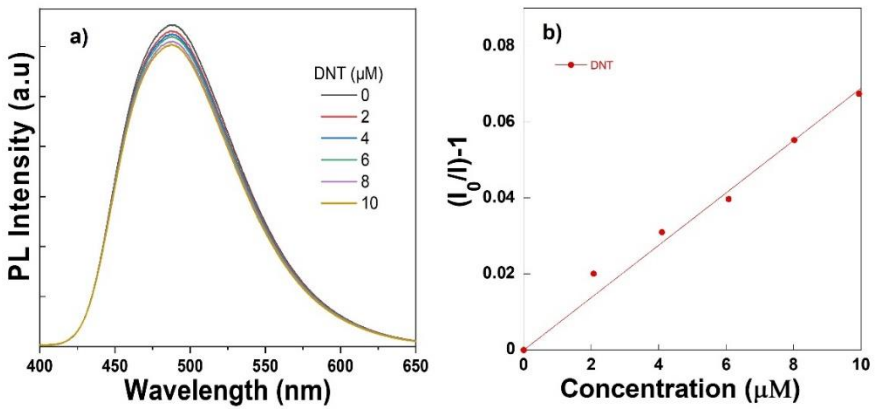

Figure 10. Quenching of PL spectra upon adding (a) DNT and (b) Stern–Volmer plot showing sensing efficiency for analytes in nanoaggregates.

For the interference test, the fluorescent measurement of bissilole-benzene also carried out in the presence of another electron deficient aromatic compound, such as DCB. Figure 11 clearly shows that the photoluminescence intensity does not quench upon adding DCB. Due to the high lying LUMO of DCB, the electron transfer between bissilole-benzene and DCB is unfavorable. This result indicates that bissilole-benzene exhibits less or no response to interferences, while it highly sensitive to NACs compared to the other reported chemosensors.

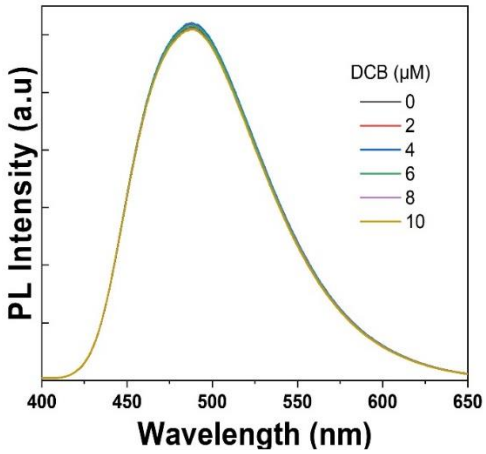

Figure 11. PL spectra upon adding DCB in bissilole-benzene nanoaggregates solution.

3. Conclusion

In conclusion, we investigated the AIEE property between π-σ* conjugated bissilole-benzene and σ-σ* conjugated bissilole nanoaggregate and their sensing efficiency for detection of DNT, TNT and PA. Bissilole-benzene nanoaggregate exhibited 180 times higher PL enhancement in THF/water mixtures. Due to the π-σ* hyper conjugation, bissilole-benzene reveals higher PL enhancement by preventing more non-radiative decay compared to σ-σ* conjugated bissilole. DFT calculation was also carried out to study orbital distribution of those two silole nanoaggregates through two types of conjugation. The bissilole-benzene nanoaggregates exhibit the existence of particle with average size of 148 nm and 107 nm for 90% and 99% fraction of water respectively. Higher fluorescence quenching was observed upon adding NACs into the nanoaggregates. The nanoaggregates of bissilole-benzene showed high Stern–Volmer constant for sensing PA, TNT and DNT compared to previously reported work. On the other hand, due to the low band gap energy, bissilole showed little high sensitivity towards explosives than bissilole-benzene. Thus, these results demonstrated that AIEE active bissilole-benzene nanoaggregates could be a considerable candidate to develop fluorescent sensor for detecting explosives.

Chapter 3

Detection of TNT Vapors by Real-time fluorescence Quenching with New Fluorescent Conjugated Silole Polymers

1. INTRODUCTION

The detection of nitroaromatic compounds (NACs), such as 2,4,6-trinitrotoluene (TNT) and picric acid (PA), has become an urgent need owing to rising international terrorism as well as environmental concerns. Many improvised explosive devices use impure TNT as a starting material [1-3]. Conjugated polymers are considered excellent materials for the detection of nitroaromatic explosives as chemosensors. Many studies reported the use of linear conjugated polymers as fluorescent chemosensors [2-8]. Conjugated polymers exhibit excellent fluorescence quenching on adding PA and TNT to the solutions or films owing to electron transfer [9]. When the energies of the energy bandgap of the polymer and the LUMO of the NAC analyte match, the electron in the excited state of the polymer can transfer into the analyte. This electron transfer causes the quenching of the emission intensity [10-12]. Charge-transfer (CT) occurs between the electron-deficient analyte and electron-rich conjugated polymer backbone, which is anticipated to be the reason for nitroaromatic analyte quenching [13]. The porous morphology or loose molecular packing of the polymer structure facilitates the binding of nitroaromatic compounds to the polymers by transferring energy [14]. Concurrently, the porous morphology imparts high permeability, which enables TNT analytes to rapidly penetrate the polymer films to accomplish greater and faster quenching responses [15]. Zhou et al. investigated the solid-state quenching behavior of TNT and discovered that the recovery process was much slower with pentiptycene-poly(phenylene ethynelene) [16]. TNT has a low vapor pressure, which makes practical applications challenging owing to the low sensitivity of the polymer [14,17]. The solid-state quenching depends on features such as the porous structure of materials, diffusion of the analyte into the material film, and

electrostatic interaction of the material with the analyte, which ensures favorable diffusion and analyte vapor release [18]. These properties enhance the sensitivity of a fluorescent sensor in the vapor phase.

We synthesized 1,1-polysiloles such as the poly(tetraphenyl)silole (PTPS) and two new 2,5-polysiloles to investigate their optical properties and sensing performance toward chemical explosives [11]. Owing to the helical structure of PTPS, there is no porous morphology where the analyte can intercalate into the solid state. In contrast, 2,5-polysilole polymer has a porous structure in the solid state, enabling it to readily attain the sensitivity toward TNT analyte. However, the discovery of aggregation-induced emission (AIE) active compound in 2001 by Tang et al. drew attention to the conjugated polymers with AIE properties [11]. Extensive research has been conducted on the development of novel AIE chromophores that are significantly more emissive in an aggregated state than in a dilute solution. Siloles are five-membered rings with σ^*–π^* conjugation between the silicon atom and butadiene moiety [20-21]. Owing to conjugation, the electron affinities increase while the LUMO energy level lowers [22]. Siloles exhibit AIE in the aggregate states by restricting the intramolecular rotations of the phenyl moiety, which is another appealing property of siloles [23]. Due to their unusual electronic and optical properties, siloles have attracted significant attention as potential novel π- electronic materials. In recent years, because of their excellent photoluminescence and electroluminescence properties [11,24-29], silole polymers have been used in many devices such as photovoltaic cells [25], light-emitting diodes (LEDs) [27-28], flexible memory storage [30], and chemical sensors [11,12,31]. Although PTPS exhibits AIE in 90 % water, these 1,1-polysiloles do not have porous structure. Furthermore, pentiptycene-poly(phenylene ethynylene) provides enough porous space for the TNT analyte but does not exhibit any AIE due to its structure.

The molecules with donor (D) and acceptor (A) moieties exhibiting AIE properties show advanced photoluminescence (PL) characteristics. The D–π–A interaction reveals emission color tunability in photophysical behaviors, which causes intramolecular charge transfer (ICT). Therefore, by assembling different types of donor–acceptor moieties, luminescence properties of various luminescent materials can be altered [32-34].

To investigate the structure-dependent aggregation behaviors, we synthesized and characterized two 2,5-tethered conjugated rigid type silole polymers (**P1** and **P2**) incorporating octyloxy benzene subunits based on the AIE and ICT dual active properties. Moreover, octyloxy moieties with both the rigid inter-polymers backbone can prevent excimer formation and π-stacking [35]. Furthermore, we demonstrated that the conjugated polymers, **P1** and **P2**, exhibit excellent optical properties and are fluorophore sensitive toward NACs in solutions, aggregations, and solid states. Although the Stern–Volmer constant, $K_{sv,}$ values for the two polymers were low in solution, they exhibit high sensitivity in solid-state sensing of TNT in practical applications. The larger the K_{sv}, the better may be the sensing in solutions; however, this may not be inevitably true for real-time sensing in the solid state. Additionally, **P1** is used as a fluorescent sensor in the detection of TNT in the vapor phase in real-time sensing. Because of the alkoxy sidechain attached to the primary silole, the polymers are thermally stable and soluble in common organic solvents, facilitating polymer synthesis and solution processing [16].

2. RESULTS AND DISCUSSION

2.1. Synthesis and Mechanism

The synthetic procedures of the two polymers (**P1** and **P2**) are depicted in Scheme 1. We investigated the properties of the phenyl rings in 5-membered siloles and PTPS. **P1** and **P2**, containing two or three octyloxy benzene units between the siloles, were obtained mainly by changing the catalyst amount with a slight modification due to the steric hindrance of phenyl rings at 3 and 4 positions of the silole. Intermediate compound **5** reacted with octaloxy benzene **4** to give compound **6**. Due to the one-pot reaction, compound **7** was produced from the reaction of compound **6** with excess $ZnCl_2$. Subsequently, the coupling of compound **7** with compounds **6** and **4** gives **P1** and **P2**, respectively. Compounds **3** and **4** were characterized by ^{1}H NMR and ^{13}C NMR spectroscopy. Both **P1** and **P2** polymers were characterized by ^{1}H NMR and GPC analyses, which showed reliable data based on their molecular structures. Due to a large number of free spaces within the polymer repeat units along with the octaloxy chains, the polymers were highly soluble in common organic solvents such as tetrahydrofuran (THF), toluene, CH_2Cl_2, and $CHCl_3$. The electronic absorption spectra of **P1** and **P2** peaked at 338 and 332 nm, respectively. The UV-Vis absorption and fluorescence spectra of the polymers in the aggregated state were also studied. Figure 1 shows the UV-Vis absorption (λ_{ab}) and photoluminescence (PL) spectra of the polymers in different states.

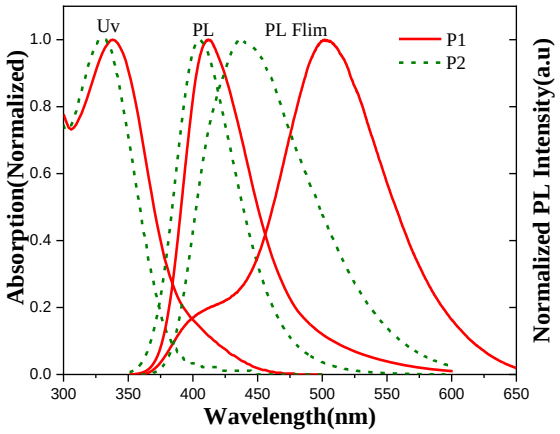

Figure 1. UV-absorption and photoluminescence spectra of **P1** and **P2**.

P1 in THF solution emits a blue PL at 410 nm, whereas **P2** emits at 405 nm. The slight blue shift for **P2** due to another phenyl linker presence slightly twists its structure in the excited state, which decreases the long conjugation interaction between the polymer and backbone [36-37]. Due to the same conformation of the polymers, the λ_{ab} behaviors remain the same in the film state as in the THF solution. The emission peak of **P1** was red-shifted by 93 nm in the solid state compared to the dilute solution in THF, and it shows a higher absolute quantum yield (QY) value of 44 % in the solid state than PTPS (31.9 %). Moreover, **P1** showed a higher QY value in both solid and aggregate states. **P2** was red-shifted by 30 nm in the solid state. This was because of the enhancement in the inter-molecular interactions between the polymer molecules. The fluorescence colors of **P1** and **P2** with π-conjugated systems are greenish-yellow and green, respectively. The corresponding changes in the two polymers in different states are depicted in Table 1 and Figure 2.

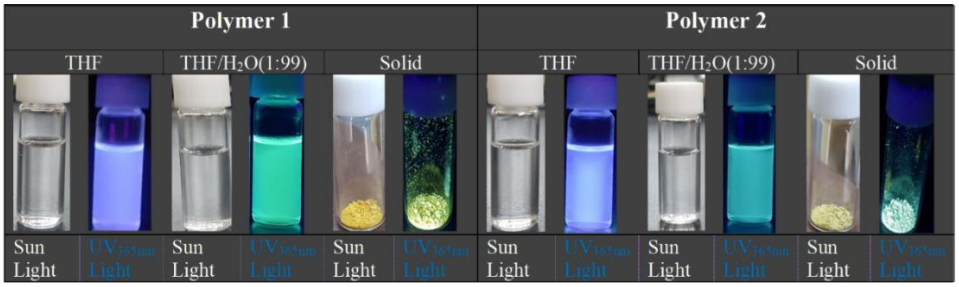

Figure 2. The photographs of **P1** and **P2** in THF, H_2O/THF and solid state under sun light and UV 365 nm lamp.

The UV absorption spectra of the two aggregated polymer molecules in different water fractions (f_w) were studied. **P2** showed little absorption changes with the 60 % and 80 % water fractions, while **P1** showed no changes at f_w-60 % (Figure 3).

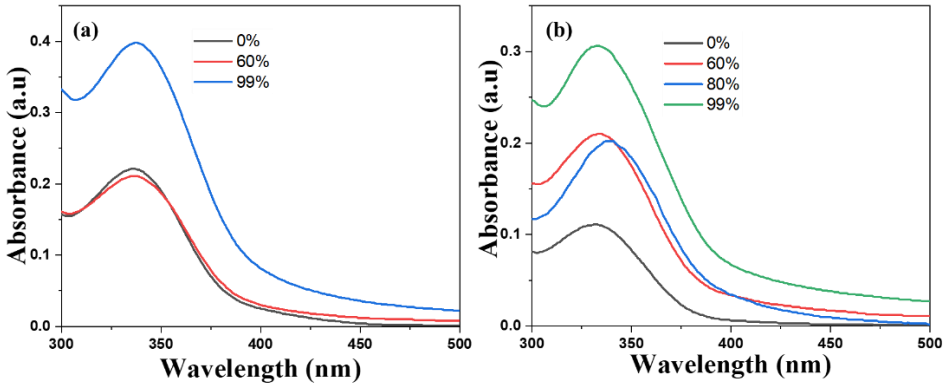

Figure 3. UV-Vis spectra of (a) **P1** in THF with (i) 0%, (ii) 60%, and (iii) 99% water and (b) **P2** in THF with (i) 0%, (ii) 60%, (iii) 80% (iv) 99%. Inset photographs represent the color changes with different water fractions.

Furthermore, when the f_w was changed to 99 %, the intensity of the absorption spectra of both the polymers uplifted with no change in the absorption value. These results prove that both the two polymers are highly stable in different aqueous environments [38]. The difference in the dielectric constants of pure THF and THF/H_2O solvent mixtures has an impact on the changing absorbance value in fluorophore solubility in the two media [39-40]. The spectral differences of the polymers depend on the aggregation formation with decreasing solubility in various water fractions and the structures.

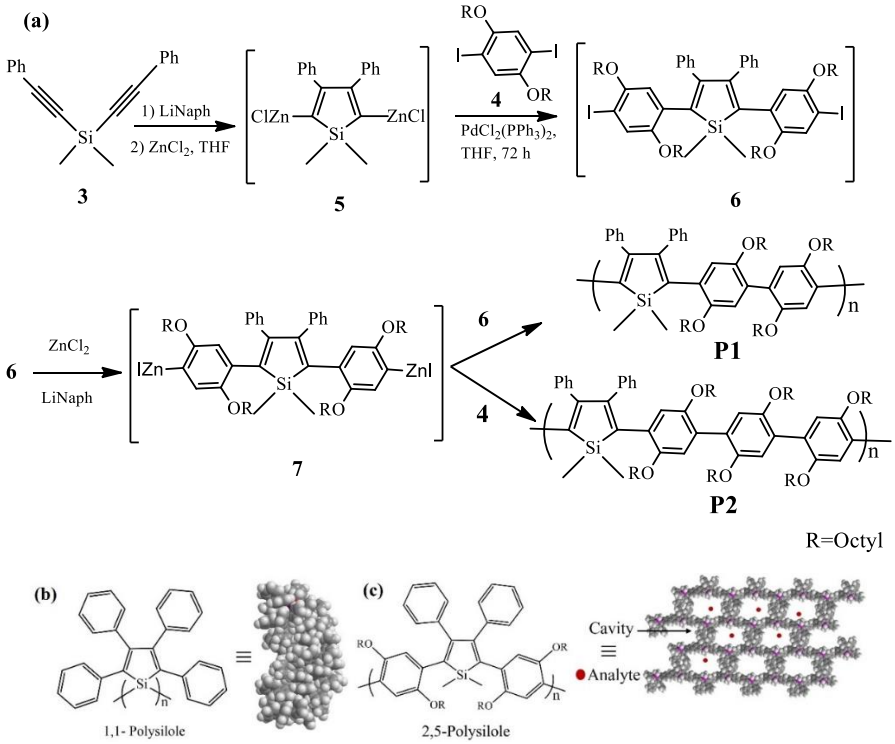

Scheme 1. (a) Synthetic route of 2,5-tethered conjugated silole polymers. space-filling model of (b) PTPS, and (c) 2,5-polymer stacks interacting with analyte on their porous spaces. n-Bu group has been omitted for clarity.

2.2. AIE and ICT Properties :

For further investigation, the emission spectra of **P1** and **P2** were recorded in various THF/H_2O mixtures (Figure 4).

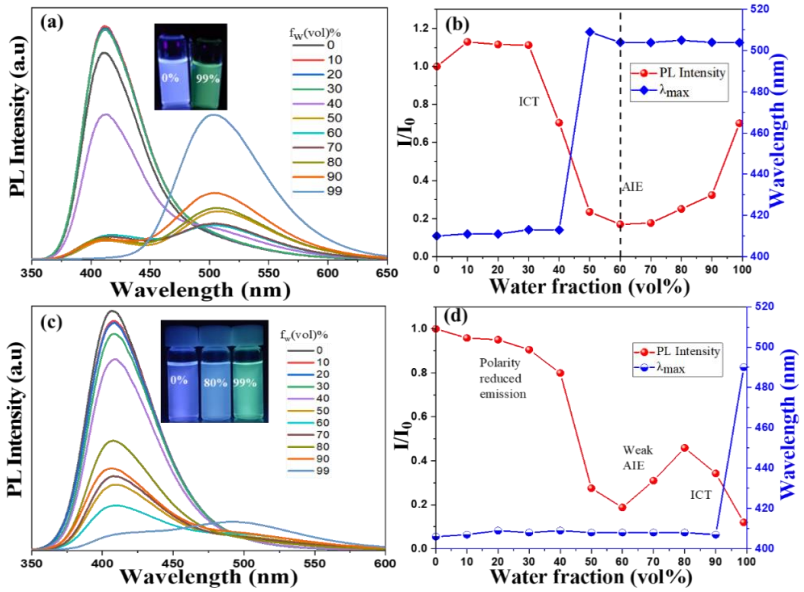

Figure 4. PL spectra of (a) P1 and (c) P2 in THF–water mixtures with different water fractions (f_w). (b and d) Change in the relative PL intensity (I/I_0) with the composition of the aqueous mixtures for polymers 1 and 2, respectively. Insets: Fluorescence photograph of the aqueous mixtures taken under a 365 nm UV lamp with different f_w values.

On adding water to the THF solution of the polymer, the emission intensity of **P1** slightly increased at f_w -10 % and almost remained the same up to 30 % f_w. Subsequently, the intensity declined drastically up to 50 % f_w due to the polarity of the solvent and strong ICT character of the molecules.[49] The molecules did not

form colloids because they are not consistent up to 50 % of f_w. Gradually increasing water in the solution increased the solvent polarity and improved the ICT effect on the molecules [42].

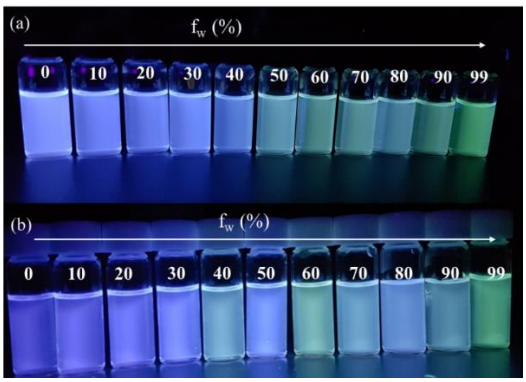

Figure 5. Fluorescence photograph of the **P1** (a) and **P2** (b) with THF/water mixtures with different volumetric fraction of water.

Figure 5 depicts the change in color on adding water to the polymer solutions. As water is more polar than THF, the emission behavior is dominated by the ICT effect. When f_w increased, the intensity decreased, and red shifting occurred. When $f_w \geq 50$ %, nanoparticles of the **P1** formed and blocked the ICT channel by triggering its AIE nature. Concurrently, the emission started to increase and **P1** mostly exhibited the AIE effect [5]. In a 99 % water solvent mixture, the PL intensity increased 7 times compared to that when f_w at 60%. Moreover, the emission intensity gradually shifted from 415 (f_w -0%) to 504 nm (f_w -99%). Clearly, for **P1,** aggregate formation enhanced the PL intensity of the mixture above 60%. However, **P2** exhibited an aggregation-caused quenching (ACQ) behavior due to the strong π–π interaction, on adding water up to 60%.

Table 1. UV-Vis absorption and fluorescence properties of **P1**, **P2**, and **PTPS** in different states

Compound	λ_{ab}[nm][a]	λ_{em}[nm][b]			Φ_F[%][c]		
Polymer	Solution	Solution	Film	Aggregate[d]	Solution	Solid	Aggregate[d]
P1	338	410	503	504	35.1	44	39.5
P2	332	405	435	407	33.9	15.8	19.2
PTPS	368	513	513	513	2.3	31.9	30.7

[a] UV-Vis absorption maximum; [b] emission maximum; [c] absolute PL quantum yield; [d] in a THF/water mixture (f_w = 99 % for P1 and PTPS and f_w = 80 % for **P2**). The film was prepared by spin-coating a solution of pure polymers in THF.

Up to f_w = 80 %, **P2** has a slightly higher emission wavelength of 408 nm. The PL intensity peak of **P2** red-shifted from 408 to 494 nm for the 99 % water mixtures with decreased intensity due to the formation of excimer at longer wavelengths. Both the polymers showed ICT because of the electron-donating and electron-accepting units in their molecular structures. By increasing water fractions from 60 to 99% for **P1** and 60 to 80% for **P2,** both the polymers exhibited AIE due to the presence of(octyloxy) benzene group, which helped in preventing unfavorable π–π stacking interaction between the molecule in the aggregate state. The weak emitters became strong emitters in the aggregate form because the restriction of intramolecular rotations (RIR) which blocked the non-radiative decay [43-44].

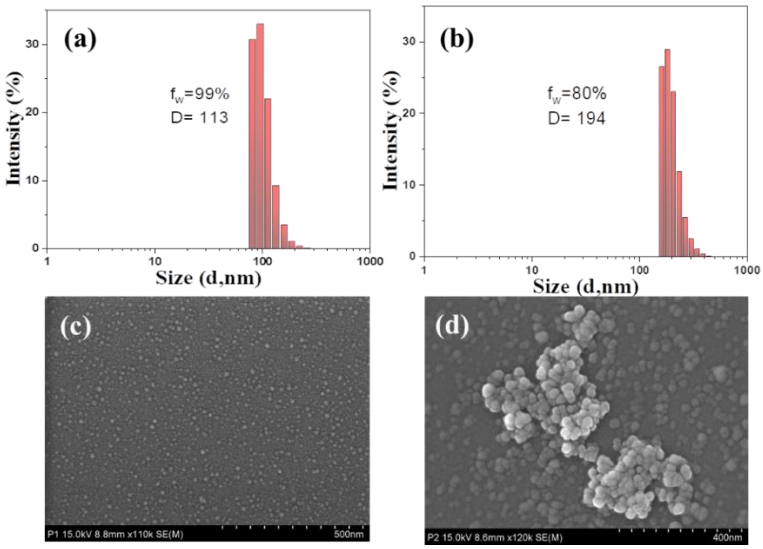

Figure 6. Dynamic light scattering results of P1 (a) aggregates in H_2O/THF (H_2O fraction: 99 %) and P2 (b) aggregates in H_2O/THF (H_2O fraction: 80 %), Concentration: 10 μg/mL; Scanning electron microscope (SEM) images of P1 (c) aggregates in H_2O/THF (H_2O fraction: 99 %), and P2 (d) aggregates in H_2O/THF (H_2O fraction: 80 %).

The molecules of the polymer aggregated in the presence of a large amount of water due to their water insolubility. However, all aqueous mixtures were homogenous without precipitates, which suggested that all the molecules were aggregated [45]. The absolute quantum (Φ_F) values in pure THF solution for **P1** and **P2** were 35.1% and 33.9%, respectively (Table 1). At a water fraction of 60%, the Φ_F values for **P1** and **P2** were 16% and 14.7%, respectively. The water fractions were increased gradually. At 99% and 80% for **P1** and **P2**, respectively, the Φ_F values increased progressively and reached the maxima of 39.5% and 19.4%, respectively, where **P1**

showed a 2.4 times higher Φ_F value than that in 60 vol%, demonstrating a remarkable AIE. However, **P2** showed a 1.3 times higher Φ_F value when the water fraction reached 80% (Φ_F = 19.4). To demonstrate the aggregation formation and the morphology of the polymers in THF/water mixtures, we investigated the dynamic light scattering (DLS) and scanning electron microscope (SEM) measurements. According to the DLS result, as shown in Figure 6(a, b), the average diameters of the particles were about 113 nm for **P1** in f_w = 99% and 194 nm for **P2** in f_w = 80%, respectively. When the water fraction increased, the particle size of polymers decreased (Figure 7). This phenomenon is similar to other AIE active silole compounds [46]. Both the polymers formed well-dispersed spherical nanoparticles in various aqueous solutions (Figures 6c and 6d).

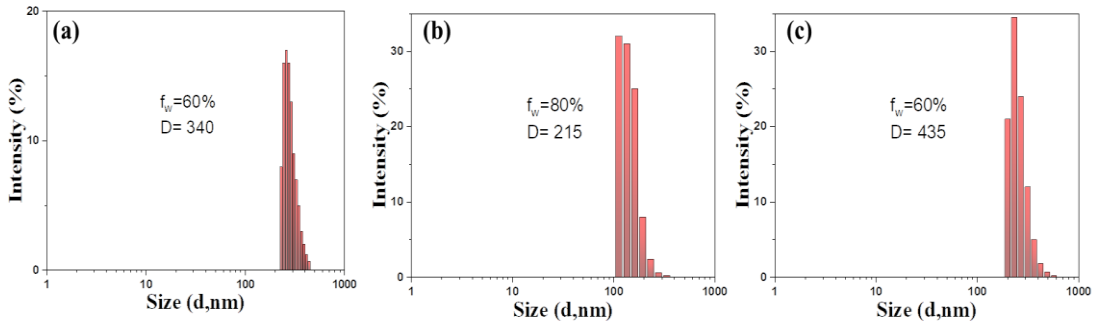

Figure 7. Dynamic light scattering results in H_2O/THF of **P1** (a,b) and **P2** (c).

Furthermore, we used DFT calculations to observe the molecular orbitals of the two polymers using B3LYP/6-31G(d). The corresponding results are presented in Figure 8, which shows the local distributions of the highest occupied molecular orbital (HOMO) and lowest unoccupied molecular orbital (LUMO) levels of polymers [47].

These results demonstrate that the electron density is distributed around the octyloxy benzene ring in HOMO. LUMO is a π* orbital and the electron density extent throughout the molecule. This behavior indicates the ICT character based on the D-A moieties of the molecule [48].

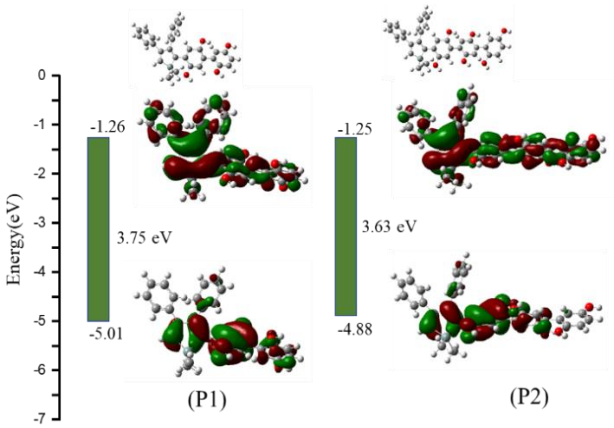

Figure 8. HOMO (Bottom) and LUMO (Top) of the polymers P1 and P2 from the *ab initio* calculations at the B3LYP/6-31G(d) level.

2.3. Solvatochromic Effect of P1 and P2

The DFT-optimized structures of **P1** and **P2** demonstrated that both the polymers are favorable for active intramolecular rotations of D or A moieties in various solutions. This depicted the possibility of solvent-dependent emission effects for **P1** and **P2**. As a representative example, the absorbance spectra of the two polymers in different solvents were also investigated (Figure 9), and the fluorescence images of **P1** and **P2** under 365 nm UV light and sunlight in different solvents are demonstrated in Figure 10.

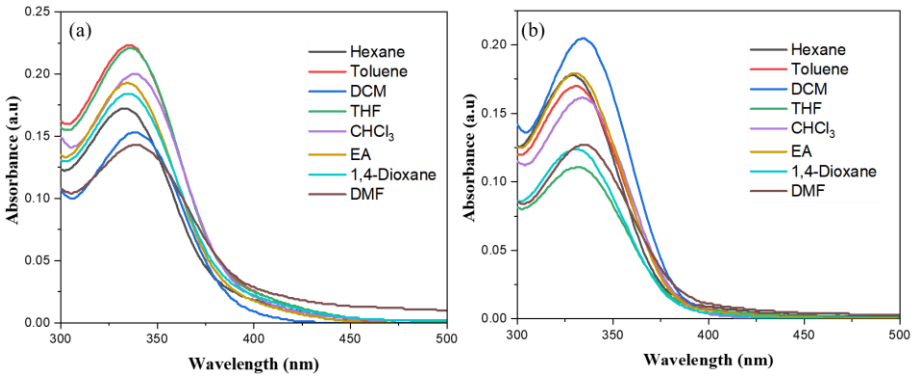

Figure 9. Absorption spectra of **P1** (a) and **P2** (b) in different solvents

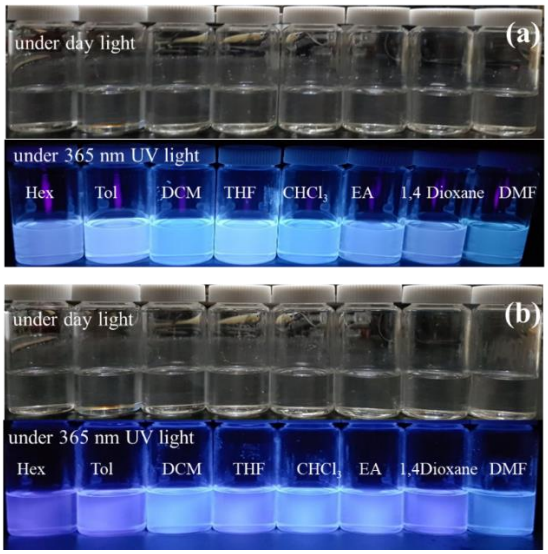

Figure 10. Images of **P1**(a) and **P2** (b) in various solvents under day and 365 nm UV light.

P1 and **P2** emit at 400 and 398 nm, respectively, in hexane. Whereas in moderately polar solvents like DCM, **P1** and **P2** emit at 425 and 413 nm, respectively. Moreover, on increasing the solvent polarities to high polar solvents like DMF, the emission peak of **P1** and **P2** further shifted to 424 and 418 nm, respectively. Fluorophore with D-A moiety gives a bathochromic shift when the solvent polarity changes from low to high. The quantum efficiency and emission intensity also decrease [49]. The excited state of ICT-based polymer in highly polar solvent is more stable compared to that in the non-polar solvent and a bathochromic shift was observed due to the lower excitation energy in the polar solvents [50].

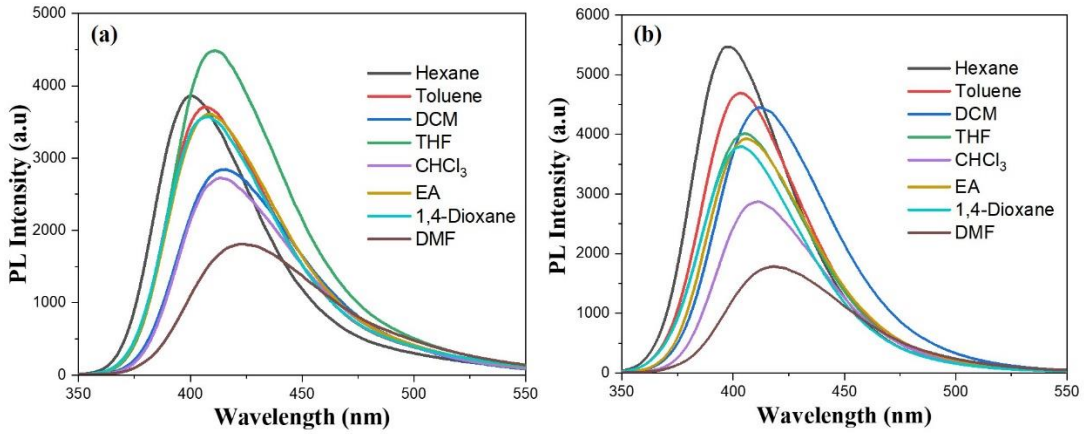

Figure 11. PL spectra of (a) polymer 1 and (b) polymer 2 in different solvents.

The emission spectra and absolute fluorescence QYs of the two polymers in various solvents with different polarities were recorded to investigate their solvatochromism behaviors (Figure 11 and Table 2).

Table 2. Optical properties of P1 and P2 in different solvents

Polymer 1					**Polymer 2**				
State	λ_{ab} [a]	λ_{em} [b]	Φ_F [c]	Stokes Shift (nm)[d]	State	λ_{ab} [a]	λ_{em} [b]	Φ_F [c]	Stokes Shift (nm) [d]
Hexane	334	400	25.7	66	Hexane	329	398	29.4	69
Toluene	336	407	28.8	71	Toluene	331	404	31.5	73
DCM	339	415	32.3	76	DCM	335	412	28.6	77
THF	338	412	35.1	74	THF	332	405	33.9	73
$CHCl_3$	338	413	26.3	75	$CHCl_3$	334	412	26	78
EA	335	409	23.8	74	EA	331	406	27.4	75
1,4 Dioxane	336	408	22.5	72	1,4 Dioxane	330	404	19.8	74
DMF	340	424	27.8	84	DMF	336	418	23.1	82

Notes: [a] UV-vis absorption spectra; [b] FL emission spectra; [c] Fluorescence quantum yield; [d] stokes shift calculated by ($\lambda_{em, max} - \lambda_{abs, max}$)

The absolute fluorescence QYs in various solvents were also calculated and discussed. In hexane, **P1** and **P2** exhibited QY of 25.7% and 29.4%, respectively. QY of **P1** gradually increased in DCM to 32.3%, but **P2** slightly decreased to 28.6%. In $CHCl_3$, both the polymers showed similar QYs of 26%. In strong polar solvents such as DMF, **P1** exhibited a QY of 27.8%, which was slightly higher compared to that of **P2**. Generally, by studying the D-A structure, the emission ($\lambda_{em, max}$) of **P1** can be said to be highly dependent on the solvent nature, known by the ICT behavior. We observed a difference in the QY values for the polymers in non-polar and moderate polarity solvents like toluene and THF and more polar solvents like DMF. The strong bulky effect of the alkoxy group in the 2,5-positions of polymers could be the reason behind these changes, where the molecule cannot freely rotate and reduces the non-radiative

process as the QY enhances [51]. The energy gap between the first excited state and ground state of the fluorophore can be obtained from the Stokes shift. The changing value of the Stokes shift is considered a noticeable change in the dipole moment of the fluorophore in their excited state due to charge transfer to the D-A moieties by solvent relaxation [8,52].

2.4. Fluorescent Quenching and Recovery Cycles at Real-Time Sensing:

Impure 2,4-DNT is used as a starting material to synthesize TNT, which is mainly used for fabricating various improvised explosive devices. Moreover, it is very important to detect TNT in the air as it has a vapor pressure of 10 ppb [53]. Thus, we were interested in real-time sensing of TNT vapors in the solid state by fluorescence quenching. Figure 12 demonstrates the fluorescence quenching and recovery processes by "real-time sensing". We selected polymer **P1** for investigating the TNT vapor sensing. The absorption band of the polymer film is similar to its solution value at 340 nm and the fluorescence of 45 nm red shifted (λ_{em} = 497 nm). This can be explained by the existence of interchain aggregates in the polymer films [54]. Nevertheless, when a UV lamp illuminated the film, fluorescence from the polymer film can be easily observed by the naked eyes (Figure 12a). The conceptual models of PTPS and **P1** demonstrated that the helical structure of PTPS is not likely to have cavities or be porous for the analyte interaction (Scheme 1b and 1c). However, rigid polymers such as **P1**, which have octyloxy benzene groups in the 2,5-positions of the polymer backbone may create porous structure in the solid state. Porous morphology of the polymer films is possibly the origin of the significant responses of TNT analyte in vapor-phase sensing. As a result, film **P1** is likely to facilitate the penetration of the analyte vapor.

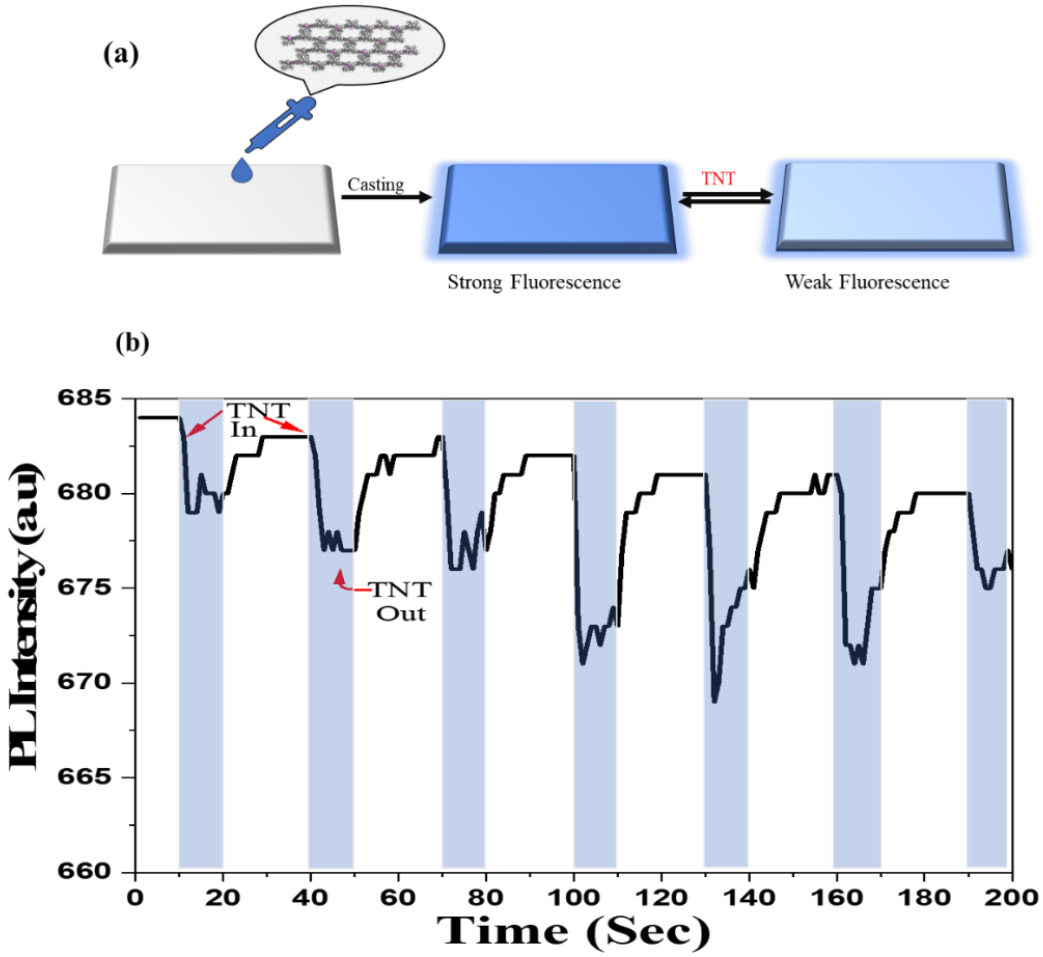

Figure 12. (a) Fabrication of polymer film and sensing performance of TNT. (b) Real-time fluorescence intensity profiles (quenching followed by recovery) of P1 in response to TNT vapors. The arrows indicate the points when quencher vapor was introduced and removed.

The sensing procedure was followed. TNT was placed in a glass box for 1 day at room temperature for saturation. The device with a sensor was then inserted into the box for 10 s and the fluorescence intensity was recorded. After that, the sensor device was removed for 20 s from the box and the emission intensity was recorded again. These quenching and recovery processes were repeated several times. The results are displayed in Figure 12(b), and they show that after removing the analyte, the polymer sensor was capable of detecting the TNT analyte by fluorescence quenching and fast self-recovery.

2.5. Detection of Explosive Compounds in Solution and Aggregate State:

We studied the changing behavior of the emission intensities of the polymers toward PA and TNT at different concentration in THF solution and aggregated states. In the presence of analytes, the polymers exhibited PL quenching characteristics in all states. The fluorescent quenching data is consistent through the Stern–Volmer equation:

$$(I_0/I) - 1 = K_{sv}[A] \quad (1)$$

where I_0 and I are fluorescence intensities in the absence and presence of the analyte [A] respectively, K_{sv} is the Stern–Volmer constant. The emission efficiencies of the two polymers in solution and aggregate media appealed an examination of chemical sensors to detect the TNT and PA. The quenching efficiencies and Stern–Volmer plots of **P1** and **P2** in solution and aggregate states are shown in Figures 13 and 14, respectively.

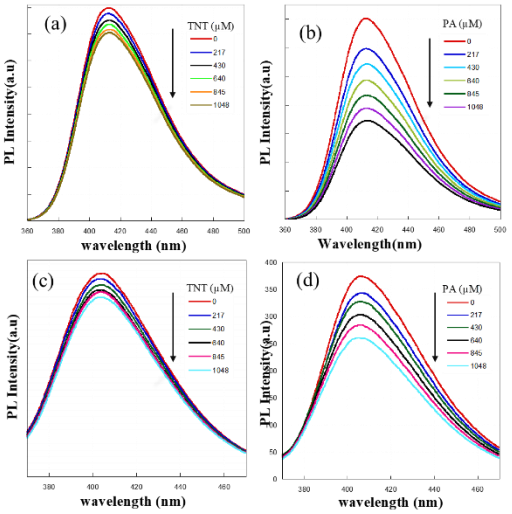

Figure 13. Quenching PL spectra of increasing fraction by each concentration of TNT (a) and PA (b) in THF solution for **P1**; TNT (c) and PA (d) for **P2**.

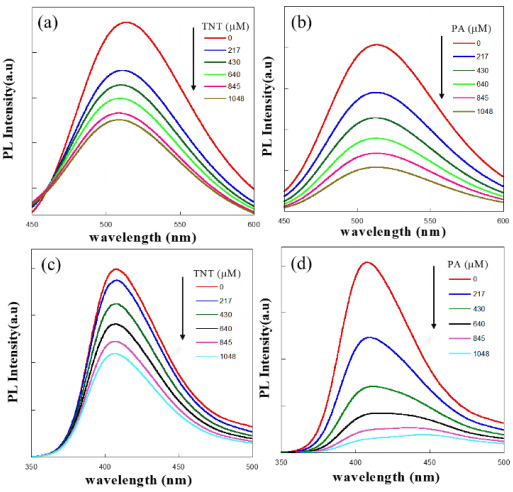

Figure 14. Quenching PL spectra of increasing fraction by each concentration in polymer nanoaggregates solution of TNT (a) and PA (b) for **P1**; TNT (c) and PA (d) for **P2**.

The polymers were affected by the analytes. The quenching constants of PA and TNT for **P1** in THF solution are 686 and 127 M^{-1}, respectively. **P2** exhibited similar data for TNT, while for PA, K_{sv} was found to be lower compared to that in **P1** (Figure 15). The emissions of the nanoaggregates were also quenched when PA and TNT in THF/water mixtures with f_w values of 99% and 90%, respectively, were added. The nanoaggregates of **P1** and **P2** with f_w values of 99% and 80%, respectively, were used as the fluorescent sensors. The PL intensity of each polymer aggregates progressively, quenching with the gradual addition of PA and TNT. The Stern–Volmer plots were linear and gave the quenching constants of 2344 M^{-1} and 800 M^{-1}, respectively, for PA and TNT of **P1** in aggregate states. We used f_w of 80% for the nanoaggregates of **P2** to investigate the quenching behavior of PA and TNT. Stern–Volmer constant of **P2** was similar to that of **P1** for TNT in aggregation, while for PA was twice as high as that of **P1** (Figure 6).

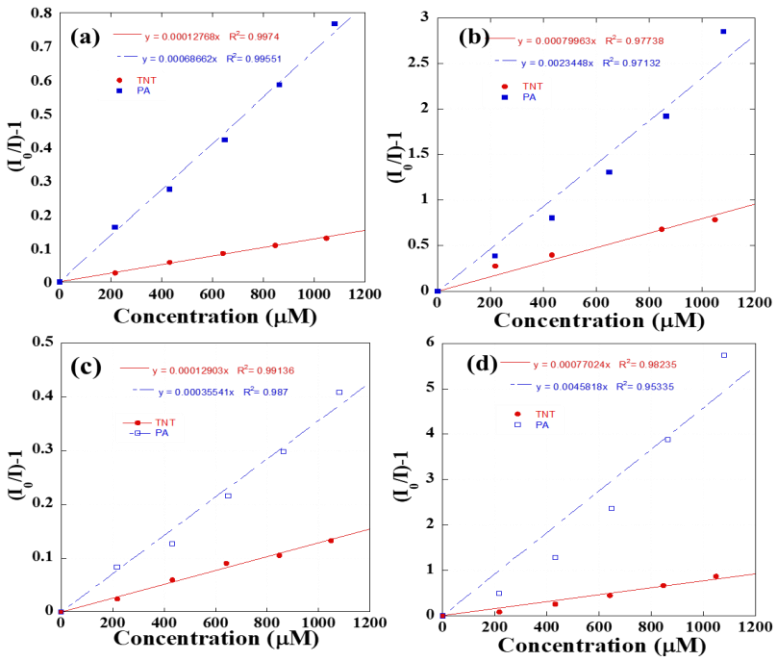

Figure 15. Stern–Volmer plot showing sensing efficiencies for TNT and PA in THF solution (a) P1, (c) P2, and in polymer nanoaggregate solutions (b) P1 and (d) P2.

Both the polymers showed low K_{sv} in THF solution which is similar to that reported by Williams et al [13]. The quenching constants toward PA and TNT for **P1** and **P2** in aggregate were several times higher than that in solution. We studied the sensing application of PTPS in the presence of TNT analyte for comparison in solution and aggregated state. Molecules of PTPS were found to be more flexible in this medium due to the molecular structure. As a result, the analyte can easily intercalate with the molecule, which gives more PL quenching and exhibited a greater K_{sv} constant value compared to that in **P1** and **P2**. The lower K_{sv} values of **P1** and **P2** may be the reason behind the fewer intercalations with explosive analytes in solution and aggregation

phases. The poor sensing results in the solution and aggregation phases may be because the two polymers are not flexible in those states like PTPS (Schemes 1b and 1c). Moreover, the lifetime measurements were also measured to investigate the electron quenching process in sensing for the PTPS and rigid type polymers such as **P1**.

2.6. Studies Electron Transfer Quenching:

An electron–hole pair is delocalized through the silole polymer, which was produced by optical excitation. NACs, such as TNT, are electron-deficient molecules. When TNT is present, the electron from the excited state of the polysilole transfers to the LUMO of TNT (Figure 16). Thus, the electron-transfer quenching occurs. The LUMO of polymers is higher than the analytes, which accelerates the driving forces for electron transfer (Figure 16b). To utilize the AIE properties for chemosensor applications, the PL lifetimes were measured for **P1** with different concentrations of PA to confirm the electron transfer processes (Figure 17). The fluorescence lifetime of **P1** in THF solution and aggregate state upon adding PA was the same, which indicates that the polymer can act as a receptor and PA can intercalate between the phenyl substituents of the silole moieties. This result confirms that the quenching of AIE-active **P1** by PA is purely static [11]. Moreover, static quenching was also observed for the analyte sensing by the PTPS polymer.

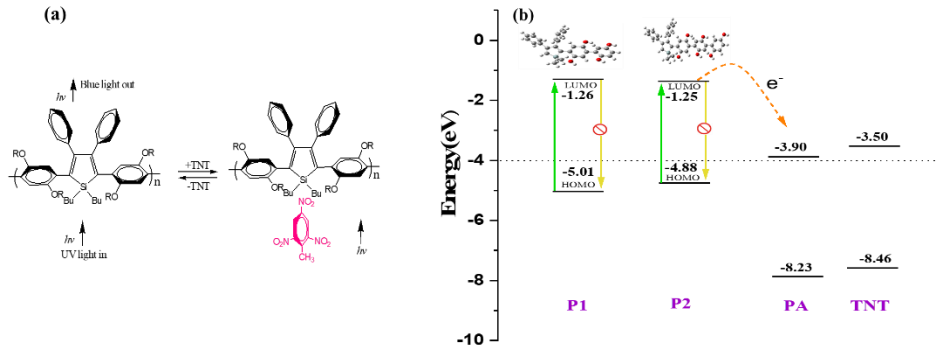

Figure 16. The interaction between the polymers in the presence of analytes. (a) Schematic diagram of electron-transfer mechanism for photoluminescence quenching and (b) HOMO–LUMO energy profiles of polymers, PA and TNT from the *ab initio* calculations at the B3LYP/6-31G(d) level.

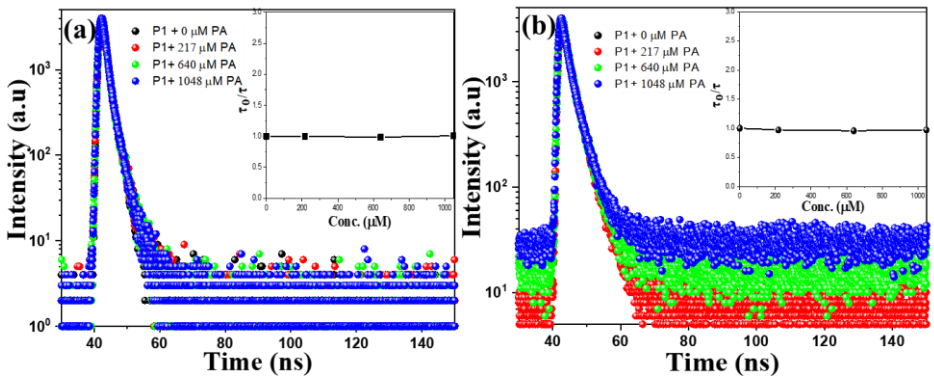

Figure 17. Fluorescence lifetime decay profile of P1 a) in THF solution and b) in H_2O/THF (H_2O fraction: 99%) with an increasing amount of PA (λ_{ex} = 379 nm). Inset: Fluorescence lifetime (τ_o/τ) are independent of added PA.

2.7. XRD Analyses

We investigated the powder X-ray diffraction (PXRD) spectra of both the polymers in the solid state, which is displayed in Figure 18. The strong and sharp peaks in the PXRD spectra indicate that the two polymers have semi-crystalline structures due to the regular repeated units in the polymer structures. The XRD patterns of both the polymers also showed broad peaks. The broadness of the peaks might be due to the amorphous structure of these polymers [55].

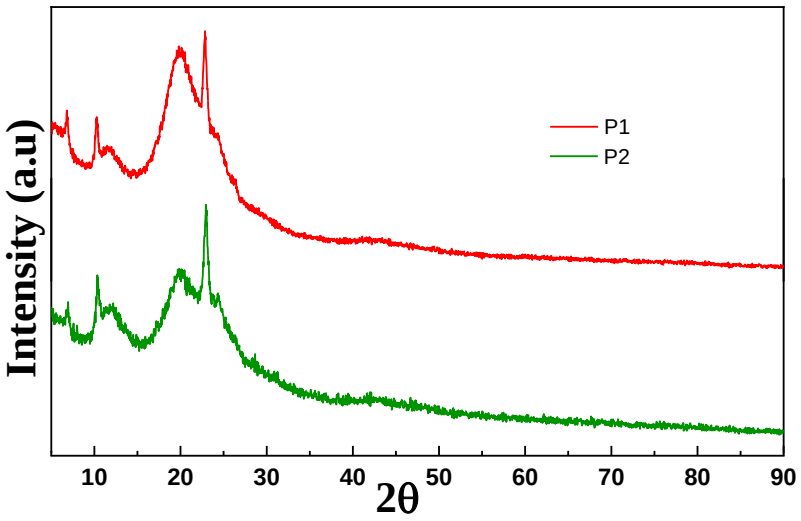

Figure 18. X-ray diffraction (XRD) patterns of polymer powders **P1**–**P2** in solid states.

2.8. Thermal Properties

TGA was used to demonstrate the thermal stabilities of **P1** and **P2**, which are depicted in Figure 19. When the two polymers were heated to a temperature of approximately 300 °C, almost no weight was lost. At temperatures of 348°C and 370°C, a 5% weight loss was observed for **P1** and **P2**, respectively, which indicates that the two polymers are thermally stable. Based on their initial weights, **P1** lost 66% of its weight, while **P2** lost 81% of its weight at the temperature of 600°C. These results indicate that the polymers may be used in various luminescent devices [56]. The thermal behavior is well-known to have a significant impact on the stability and lifetimes of various luminescent devices [4].

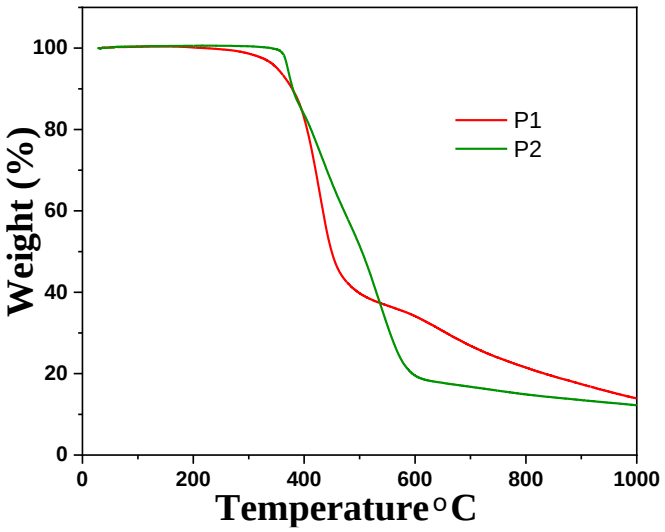

Figure 19. The TGA curves for **P1** and **P2**

3. CONCLUSIONS

Two new conjugated polymers were successfully synthesized, investigated, and characterized for the detection of chemical explosives. Although the quenching constants in PA and TNT for the polymers **P1** and **P2** in solution and aggregate media were low, this is the first time that 2,5 silole polymers showed a significant response to real-time fluorescence quenching and PL recovery processes toward TNT vapors in real-time sensing. The polymers revealed emerging photophysical properties because of their ACQ/AIE and ICT effects. These results depend on the aggregate state of the polymers in the types of stacking. We also studied the solvent behavior of the two polymers along with their ICT properties using DFT calculations, which arise from conjugated π-systems. The fluorescence and sensing properties for TNT and PA of the polymers have been studied in pure THF solution, films, and aggregated states. The quenching effects for both the polymers were not similar in the solution and solid state, which also drew attention to the differences in sensitivity. Moreover, these two polymers revealed high fluorescence efficiencies in all three states. In conclusion, this study explains that the unique combination of properties displayed by the rigid polymers with strong fluorescence makes these materials a promising candidate for detecting explosives by improving the fluorescent properties of sensors in films.

Chapter 4

AIE-active Conjugated Polyphenylsilole for Higher Sensitivity of Explosives Detection

1. INTRODUCTION

Detection of nitroaromatic compounds (NACs) effectively is become a global challenge. Nitroaromatic explosives such as 2,4,6-trinitrotoluene (TNT), 2,4-dinitrotoluene (DNT), and picric acid (PA) are not only threat for national security and humans but also consider as very threaten compounds for environment due to their high toxicity. Recently, a lot of sophisticated sensing methods have been developed commercially to detect the explosives. Raman spectroscopy (SERS), gas chromatography, plasma desorption mass spectrometry (PDMS), and energy-dispersive X-ray diffraction (EDXRD) are some conventional laboratory methods [50–52]. For the on-site detection it is very important that the mentioned techniques should be cost-effective, good portability and less time consuming. Interestingly fluorescent sensor have taken much attention due the aforementioned qualities [53].

On the other hand, most of the fluorophores emit less or weak emission in pure solution as they show planar structure and in solid state, they are non-emissive due to the π-π stacking. These interactions allow the non-radiative decay which causes the emission quenching as known the aggregation-caused quenching (ACQ). In numerous fields such as organic light emitting devices (OLEDs), organic solid lasers, and chemo or biosensors have faced some difficulties due to ACQ [47]. A lot of conjugated polymers show ACQ nature in solid state which is a big limitation for the practical applications. To overcome this problem, Tang and co-workers discovered the unique and novel phenomenon of aggregation induced emission (AIE) which reveals opposite behavior of ACQ [9,54].

Silole possess unique optical characteristics which is a novel π-electronic material

and show σ*–π* conjugation between the silicon atom and the butadiene moiety [3]. This conjugation increases the electron affinity by lowering their lowest unoccupied molecular orbital (LUMO) energy levels. Moreover, silole have another interesting optical property that it shows the AIE behavior in solid state by restricting the free rotation of phenyl ring in 3,4 positions. In solution, silole emit weak emission due to the intramolecular rotation of phenyl ring which brings the non-radiative decay. whereas in solid state, the non-radiative decay can be prevented by restricted the intramolecular rotation (RIR) and thus the emission has been enhanced [12,13]. In recent time, conjugated silole polymer possess advantages over their small-molecule counterparts and a huge number of efforts have been done based on photoluminescence (PL) and electroluminescence properties [14–19]. Therefore, many device applications incorporated with AIE-active siloles have been implemented in different field such as, electron transporting materials [20], memory storage [21], photovoltaic cells [22] and light-emitting diodes (LEDs) [10,23].

Besides in above mentioned applications, silole derivatives have found as chemosensor for the detection NACs due to their unique AIE characteristics. Trogler and co-workers successfully applied poly(1,1-2,3,4,5-tetraphenylsilole)s, which are conjugated through silicon atom for the detection of chemical explosives [17,37]. Tang and co-workers reported the hyperbranched poly(2,5-silole)s, which showed excellent fluorescence and used as chemosensors for the detection of explosives by emission quenching of polymer nanoaggregates [41]. A series of linear poly(2,5-silole)s which were linked at their 2,5-positions through vinylene bridges were synthesized and investigated as chemosensor by

Qiao Lai and co-workers [55]. Another hyperbranched polysiloles incorporating arylene ethynylene subunits were synthesized for the detection of NACs [40]. Generally, conjugated polymer with luminescence and the delocalization of excitons can increase sensing performance by effectively reducing background interference during detection. However, these hyperbranched polymers showed very weak AIE features with the sensing performance. Thus, we were interested to investigate the conjugated hyperbranched polymer containing phenyl unit which are directly linked to 2,5-position of silole.

In this work, we have synthesized a strong AIE-active hyperbranched poly(2,5-silole) incorporating phenyl ring which are linked with silole core at 2,5-positions thorough π-conjugation. At high water fraction (f_w), the polymer emits strong luminescence with high quantum yield (QY). The obtain polymer showed excellent sensing performance for the detection of chemical explosives and a linear Stern-Volmer constant was observed. Furthermore, the polymer was also investigated in solid state sensors for detecting NACs for the practical applications and polymer greatly responded towards analytes.

2. RESULTS AND DISCUSSION

Scheme 1 shows the synthetic prosses of **P1** and represents the schematic illustration of enhancing the fluorescence intensity while the water fraction (f_w) has been increased. **P1** reveals the AIE nature by restricting the rotation of phenyl ring and we were interested to check the sensing performance towards NACs in aggregate phase.

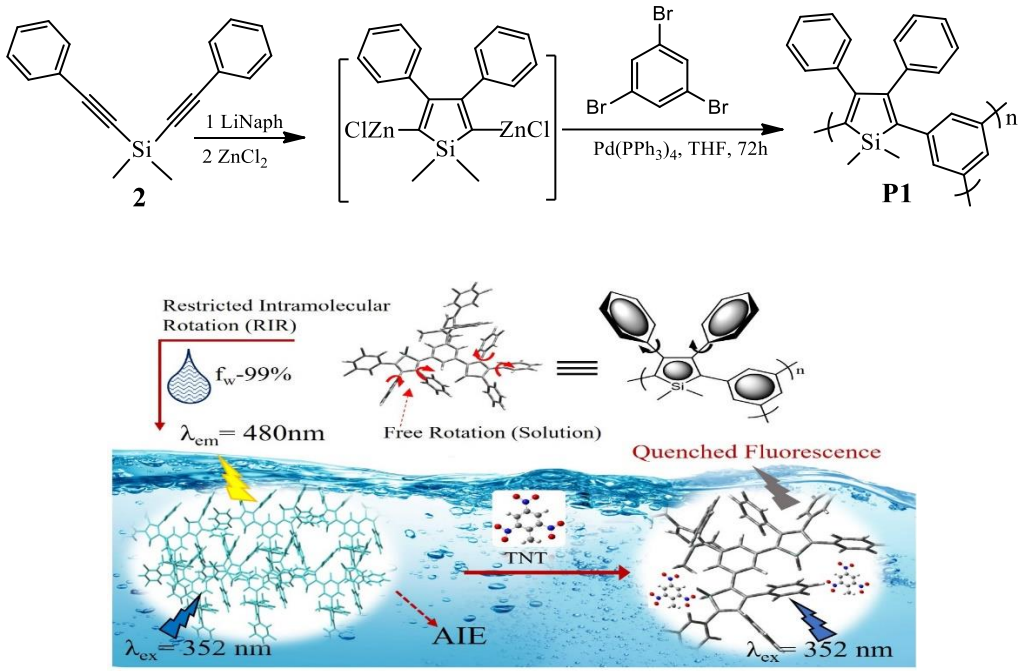

Scheme 1. Synthetic route of polymer (**P1**) and the schematic illustration for the preparation of polymer nanoaggregates and quenching fluorescence with explosives.

Both the compounds of monomer (2) and **P1** were synthesized according to the previous literature which are described in experimental section and characterized by ^{1}H NMR spectroscopy and GPC (Fig. S1-S2). Due to the phenyl ring in polymer backbone, the polymer was highly soluble in common organic solvents, such as tetrahydrofuran (THF), toluene, CH_2Cl_2, and $CHCl_3$. The UV-Vis absorption spectra of **P1** peaked at 352 nm and fluorescence spectra was recorded at 480 nm .

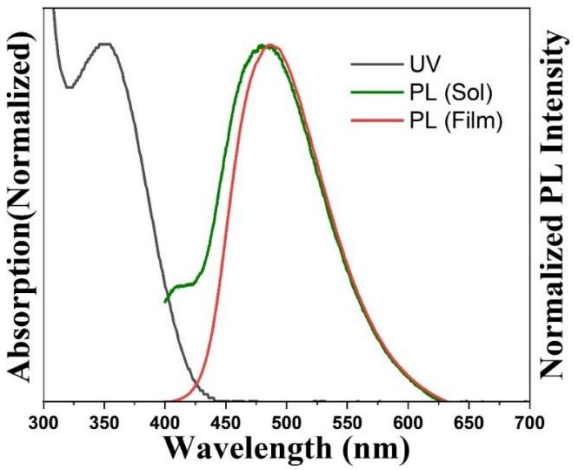

Figure 1. Absorption and photoluminescence spectra of **P1** in pure THF solution.

Figure 1 shows the absorption and photoluminescence (PL) spectra of the polymer in pure THF solution. The absorption peak locating in around 352 nm can be attributed to the combined contribution of silole core with phenyl ring in 2,5 positions and as a result this combination brings the π-π* conjugation between them. The quantum yield (QY) of **P1** in pure THF solution has been calculated to be 1.2%. Weakly emitting in solution emitted strong PL emission in 99% of water fraction and solid state and the QY were 13.4 and 14.2% respectively (table.1). The QY in solid state exhibit around 11 times higher PL emission which demonstrates the distinct AIE phenomenon. These AIE effect could come out due to the phenyl ring attached in silole core and the polymer side chain.

Table 1. Summary of photophysical property for **P1**

Compounds	λ_{abs} (nm)[a]	λ_{flu} (nm)[a]	λ_{flu} (nm)[b]	Film λ_{flu} (nm)[b]	Φ_{flu}[d](%)
P1	352	480	480	487	1.2/13.4/14.2

[a] UV–vis and fluorescence spectra are taken in THF. [b] fluorescence emission of nanoaggregates at f_w-99% and in solid (spin coating in film). [d] Absolute quantum yield of fluorescence (In solution, at f_w-99% and solid state).

1.1. AIE Properties of P1:

To further study of AIE property of **P1**, a series of PL spectra were obtained in different THF/ water fraction mixtures. Figure. 2a shows upon increasing of water fraction into the mixture, the PL intensity is also increasing.

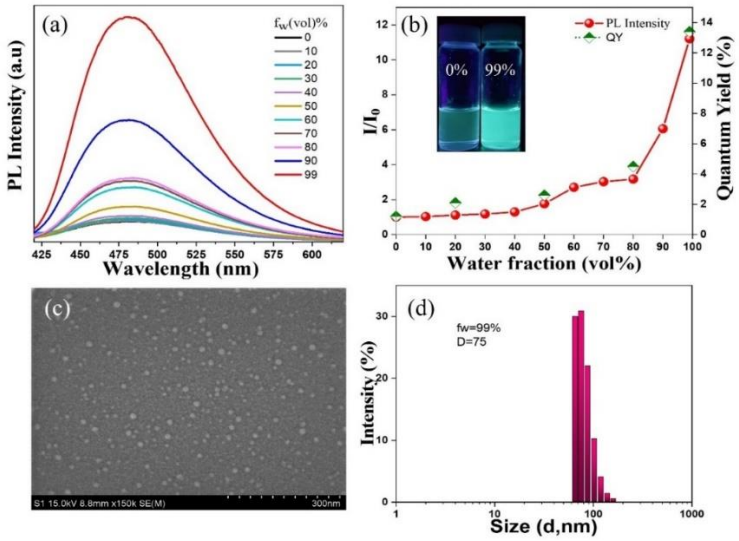

Figure. 2. PL spectra of (a) **P1** in THF/water mixtures with different fraction of water. (b) Plots of I/I_0 and quantum yields versus different water fraction of **P1**,

I_0 is the PL intensity in Pure THF solution (concentration 10^{-5}M) an. (Inset: Fluorescence photograph of polymer nanoaggregates at f_w-0% and 99%). (c) SEM image and (d) Average particle size distribution of **P1**.

When f_w was (0-40%), the PL intensities were slightly increased. Water is non-solvent for the polymer, molecules start to aggregate at a certain water level. Thus, PL intensity dramatically enhanced from 50-99% of water content due to the onset aggregation. Due to the restricted rotation of multiple phenyl ring on silole which prevents the non-radiative decay and the PL intensity (f_w -99%) is 12 times higher compared to its non-aggregated pure THF solution (Fig. 2b). Moreover, QY also increases upon increasing water fraction. These effects confirm the AIE characteristics of **P1**. Weak fluorescence become strong during the increasing of water fraction which is also noticeable in photograph under UV light (Fig. 3).

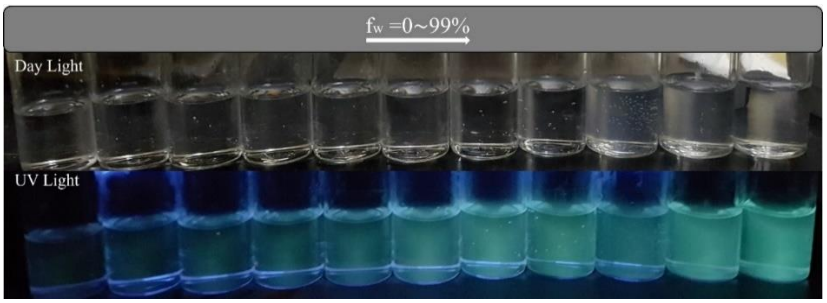

Figure 3. Fluorescence photograph of the **P1** in different volumetric fraction of water.

Figure 2(c,d) demonstrates the aggregation formation, morphology and the aggregated particle size which were checked by the scanning electron microscope (SEM) and dynamic light scattering (DLS) measurements. The average size of the particle is 75, 174 and 213 nm when water fraction was 99%, 90% and 80%

respectively (Fig. 2d and 4). Particle size is decreasing when the water fraction is increasing. These results are similar to others silole nanoaggregates. This phenomenon reveal that hydrophobic organic molecules are prone to aggregate in hydrophilic environment when the water fraction is high [11,12,26]. On the other hand, hyperbranched silole polymer which are linked with vinylene bridges or arylene ethynylene subunits showed very weak AIE. Due to the formation of excimer might be the reason for this weak AIE. Whereas **P1** is directly linked with silole which prevents the excimer formation and enhanced the PL intensity with high QY at f_w-99%. Thus, directly conjugated silole polymer incorporated with phenyl subunits reveals that **P1** is more effective on AIE feature.

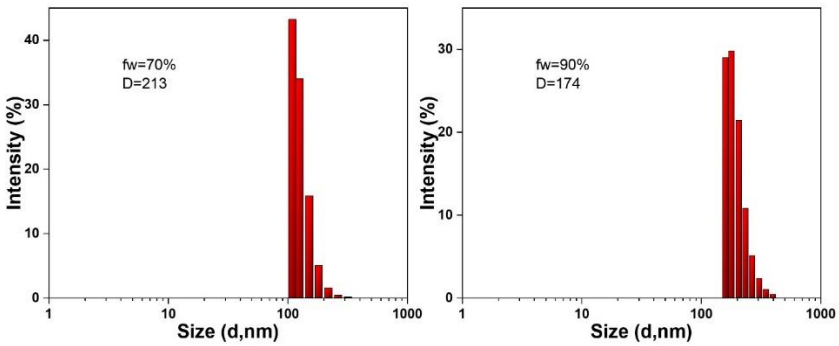

Figure 4. DLS data showing when the water fraction increases then the size **P1** nanoaggregate decreases.

1.2. *Sensing Mechanism of Nitro-explosives:*

The detection mechanism of **P1** to NACs was illustrated in figure 5. The optimized structures of polymer and NACs were analyzed by density functional theory (DFT) calculation using Gaussian 09 package [56]. Detection by fluorescence quenching involves electron transfer from electron rich molecules to electron deficient molecules.

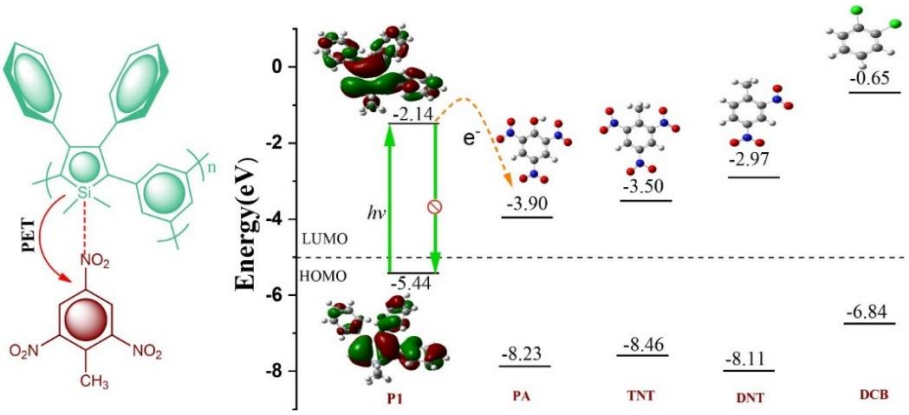

Figure 5. Schematic illustration for the interaction of polymer with analytes and optimized structures of **P1** and NACs by density functional theory (DFT) from the ab initio calculations at the B3LYP/6-31G(d) level.

NACs are known as electron deficient molecules and siloles are electron rich molecules. Figure 5 demonstrated that when NACs interact with silole, the electron from the LUMO of silole can transfer to the LUMO of analytes and thus the fluorescence is quenched which is known as photo-induced electron transfer process [17,24].

1.3. *Detection of Nitro-explosives in Aqueous Solution:*

We investigated the change of the emission intensity of the polymer responding to NACs with different quantities in THF/Water (1:99) solution. As expected in presence of analytes, **P1** exhibits attractive fluorescence quenching behavior. Figure 6 depicts the fluorescence emission spectra of **P1** at various NACs concentrations in aqueous phase. More than 50% of the emission is quenched when the analyte reaches at 2 μM.

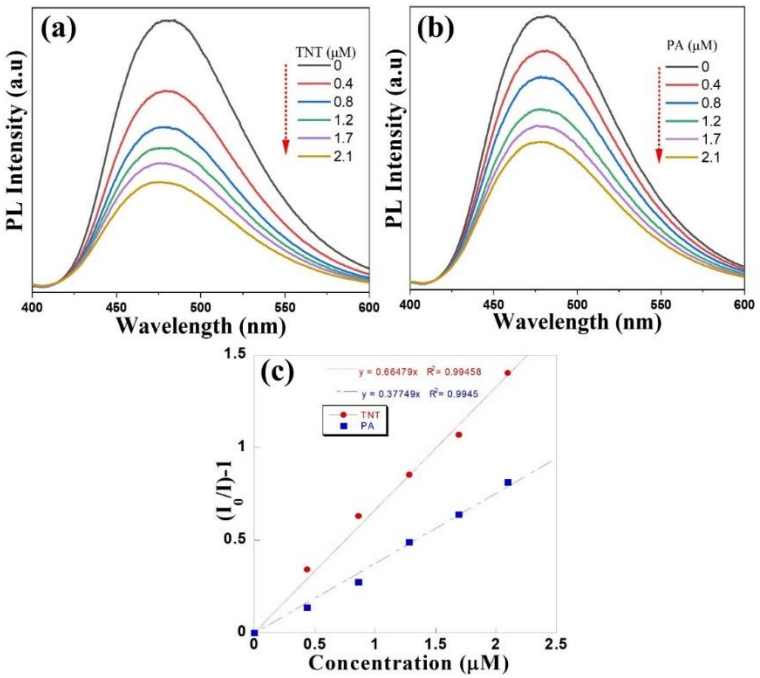

Figure 6. Quenching of PL spectra upon adding (a) TNT and (b) PA in polymer nanoaggregates solution. (c) Stern–Volmer plot showing sensing efficiency for analytes in nanoaggregates.

To evaluate the quenching differences, we used Stern-Volmer equation for various analytes. I_0 represents the fluorescence intensity without analyte [Q] and I is the intensity of **P1** in presence of analytes, and K_{sv} is the Stern-Volmer constant [57].

$$\frac{I_0}{I} - 1 = K_{sv}\,[Q] \qquad (1)$$

With the increase of NACs concentrations, the PL intensity of **P1** decrease progressively. This result demonstrates the sensitive interaction between polymer and analytes. A linear Stern-Volmer relationship is observed for both the analytes of TNT and PA. The quenching constants about TNT and PA for the nanoaggregates of **P1** is 6.67×10^5 M^{-1} and 3.77×10^5 M^{-1}, respectively. These values are much higher than the values of reported in the literature [14,15,17,33,45,55].

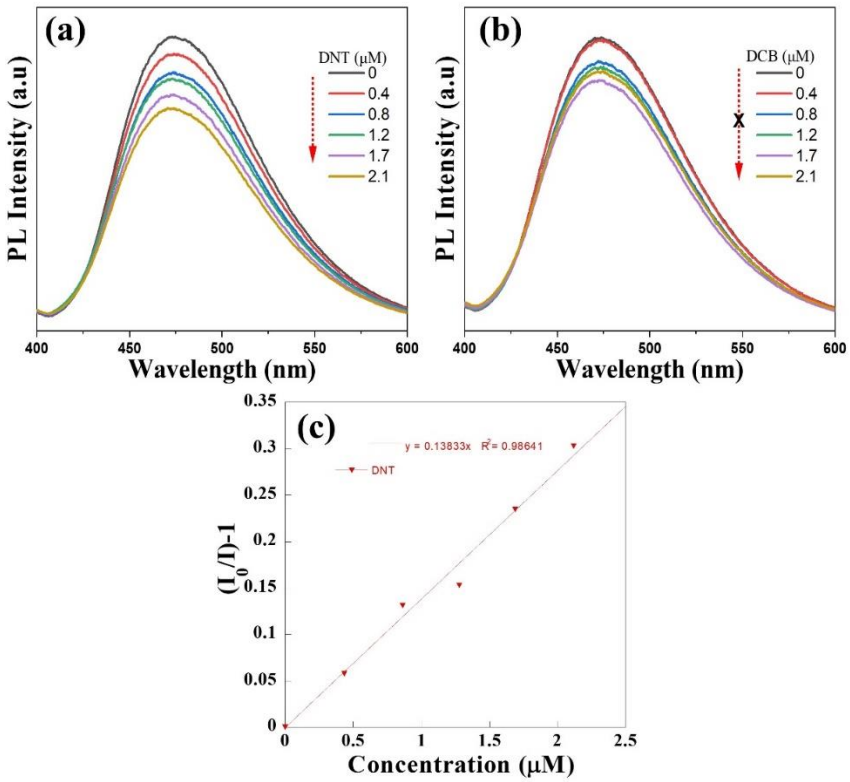

Figure 7. Quenching of PL spectra upon adding (a) DNT (b) DCB and (c) Stern–Volmer plot showing sensing efficiency for DNT analytes in nanoaggregates.

Moreover, DNT is also needed to detect as it is the precursor of TNT and consider as a threatful material for our environmental issues due to having nitro groups. In this work, the sensitivity for DNT and another electron deficient aromatic compound, such as 1,2-dichlorobenzene (DCB) have been studied for the interference. DNT contains one less nitro group and as expected, the K_{SV} (1.38×10^5 M^{-1}) value for DNT. The fluorescent quenching measurement of **P1**

nanoaggregates also carried out for DCB and it shows that the PL intensity does not quench continuously upon adding DCB (Figure 7).

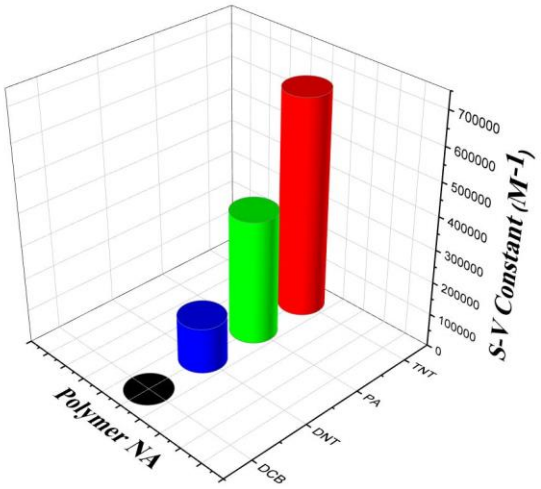

Figure 8. Comparison of quenching constant (Stern-Volmer plots) of **P1** with various NACs analytes at the same concentration.

As expected DNT showed 5 times lower data compared to TNT due to having one less of nitro group (Fig. 8). Due to the high lying LUMO of DCB, the electron transfer between polymer and DCB is unfavorable (Figure. 5). This result indicates that **P1** exhibits less or no response to interference, while it highly sensitive to NACs compared to the other reported chemosensors.

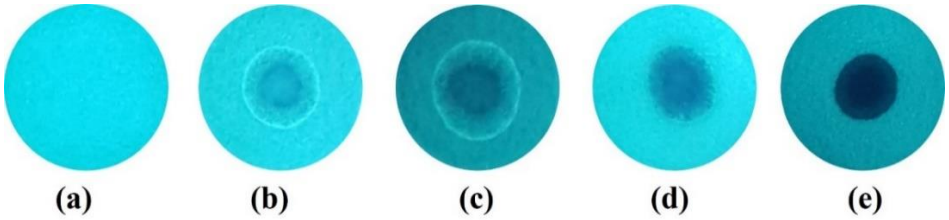

Figure 9. Before and after dropping TNT solution in THF with impregnated paper strips of **P1**. Concentration: (a) Blank (b) 4×10^{-5} (c) 4×10^{-4} (d) 1×10^{-3} (e) 2×10^{-3} M.

Furthermore, solid state sensors will be play an important role to detect NACs for the practical applications. Towards this aid, we choose TNT as sample to check the solid-state sensing performance with impregnated paper of **P1**. Paper strips were prepared by drop-coating polymer solutions onto the filter papers and dried them under air stream. Figure 9 showed the color changes of paper strips before and after TNT interaction with **P1**. The blank paper is more bright green which indicates the original PL emission. When different concentrations of TNT are dropped on to the paper, the PL emissions are quenched progressively. The results demonstrate that the P1 could be a considerable material for the detection of TNT in solid state sensor devices.

3. CONCLUSION

In summary, the high luminescent hyperbranched polymer with AIE feature was successfully synthesized by one spot reaction. The polymer exhibits unique strong AIE phenomenon by enhancing the PL intensity by 12 times at 99% faction of water compared to THF solution and high QY at 99% also confirms the AIE nature. Compared to previously reported work for sensing NACs, the synthesized polymer nanoaggregates showed very high Stern–Volmer constant. Moreover, for solid state sensing, polymer responded very well towards explosives by paper strips experiments. Thus, to develop selective and sensitive fluorescent sensor for detecting explosives, the AIE active hyperbranched polysilole nanoaggregates could be a considerable candidate.

Chapter 5

Dual Mode Colorimetric and Fluorescent Sensing of TNT by Conjugated Fluorenone-Substituted 2,5-Silole Polymer

1. INTRODUCTION

On-spot detection of nitroaromatic compounds (NACs) are immense important and desirable to protect homeland and environment from terrorist activities. NACs in military munitions and landmines can release heat and potential energy by self-oxidation which makes sudden outburst.[58] 2,4,6-trinitrotoluene (TNT) is consider one of the most dangerous and hazardous aromatic explosives among all NACs which is a threat for environment and human beings for causing many types of diseases including cancer [59–61]. Therefore, it is highly desirable to employed *'onsite'* sensor which would be cost effective, selective, and sensitive for the trace level of TNT. In this case of detection, many attempts have been successfully applied such as, gas chromatography, Raman and mass spectrometry, ion mobility and sensor based colorimetry and fluorometry [39,62–66]. These sensory methods are costly, bulky, complex to operate and prevents the on-spot detection of TNT. Interestingly, colorimetric and fluorometric-based sensor have taken more attention for detection TNT due to the easy visualization, low cost, short response time and high sensitivity [67–70].

On the other hand, organic conjugated molecules having luminescent properties with well-defined morphology have taken much attention to synthesis. Due to the tunable photoluminescent behavior in aggregation, these materials induced to emit intensity on aggregation while they were weakly emissive or might be non-emissive in solution is well known by aggregation induced emission enhancement (AIEE) or aggregation-enhanced emission (AEE) through the restricting intramolecular motions (RIM) and restricting intramolecular rotation (RIR)

[71,72]. Whereas the typical planar polymers exhibit very low or no emission in solid state because of strong π-π stacking. This phenomenon is called aggregation-caused emission (ACQ) which allow nonradiative decay by forming excimer, excitonic coupling, and excitation energy migration [73–75]. Therefore, it is very hard to understand detail mechanism of AIEE and design novel fluorescent molecules with AIEE properties [76]. To understand the AIE in deeply, enormous research has been reported based on AIEE active compounds. AIEE is considered an alternative option by preventing the intramolecular rotation of fluorescence molecules in many applications to overcome the problem of ACQ in solid state [32,45]. Therefore, to develop the optoelectronic and biomedical applications it is necessary to design new organic luminescent molecules having AIEE.

Silole or silacyclopentadiene conjugated molecules are become more emissive in aggregated or solid state where they are weakly or non-emissive in solution due to the intramolecular rotation of phenyl ring [77]. Siloles contain Si atom in 5-membered cyclic ring with π electron that shows an AIEE properties having lowest LUMO level incorporated with σ*-π* conjugation [9]. Due to the remarkable phenomenon of silole, these molecules could be applied in chemical sensor [17,37], organic light-emitting diodes (OLED) [78], electron transporting materials [20], and memory storage [21]. Thus, our focus was to study the structural behavior of fluorenone containing silole-conjugated polymer based on AIEE and their sensing properties for TNT by colorimetric and fluorescence quenching.

Herein, we investigate dual mode, colorimetric and fluorometric sensing of TNT by 2,5-conjugated silole polymer. The obtained polymer demonstrated unique

AIEE properties, vapochromic behavior towards solvent and TNT vapor. The morphology and particle size were confirmed by scanning electron microscope (SEM) and density functional theory (DLS) experiment, respectively. We also investigate thermal properties of polymer to check their thermal stability. Thus, we demonstrated the molecular structure and aggregation emission enhancement properties. The novel AIEE active polymer might be a promising material for applications in optics, electronics, environmental and biological field.

2. RESULTS AND DISSCUSION

2.1. Synthesis and characterization:

Scheme 1 shows the synthetic process of the **P1** and the schematic diagram of fluorescence quenching upon adding TNT vapor. **P1** was characterized by ^{1}H NMR and GPC analysis and details were given in experimental part. Syntheses of the monomers **2** and **3** were followed by previous reported articles and characterized by NMR spectroscopy. Briefly, the new silole-fluorenone alternating copolymer was synthesized *via* endo-endo intramolecular reductive cyclization of di(phenylethynyl)silanes (**2**) followed by the treatment with bis(phenylethynyl)dimethylsilane and LiNaph, to afford target **P1** in moderate yields using a slightly modified method of the literature [28,30]. We want to investigate the properties of fluorenone in between 5-membered silole. **P1** containing two fluorenone unit between silole, were obtained mainly due to the steric hindrance of phenyl rings at 3 and 4 positions of silole. Due to the one pot reaction, intermediate compound 7,7'-(1,1-dimethyl-3,4-diphenyl-1H-silole-2,5-diyl)bis(2-bromo-9H-fluoren-9-one) reacted with excess $ZnCl_2$ and later react

with another unit of monomer **3** and gives product of **P1**. The polymer was soluble in common solvents like toluene, tetrahydrofuran THF and chloroform.

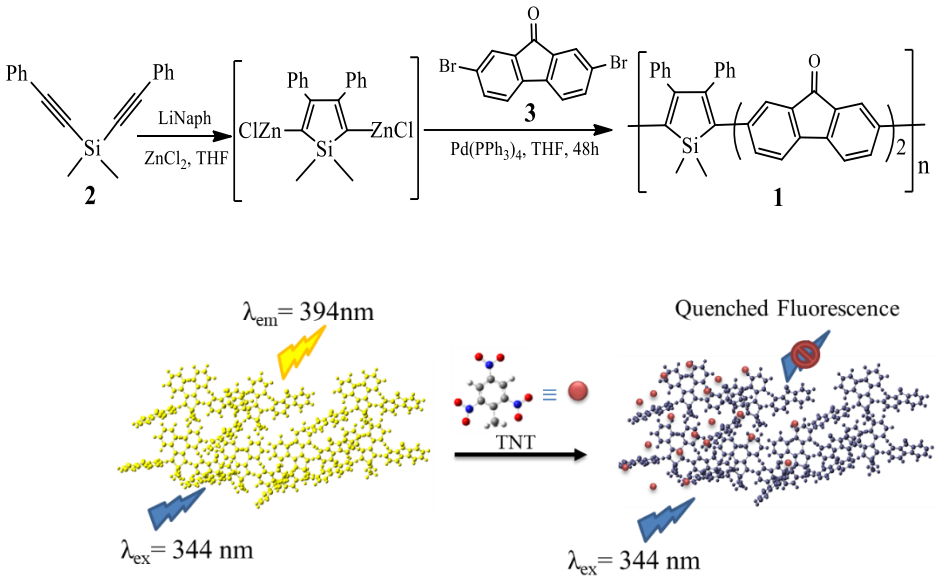

Scheme 1. The synthetic route of P1 and schematic of its fluorescence response to TNT vapor.

The UV absorption band was found at 344 nm in THF solution and emission bands of **P1** at 394 nm having two small shoulders due to monomeric fluorenone emission which might be formed during relaxation of singlet excited fluorenone groups (Figure. 1).

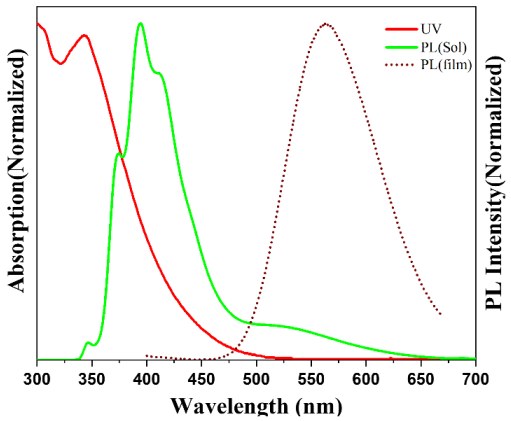

Figure 1. Absorption and photoluminescence spectra in solution and film (λ_{ex} = 344 nm) of P1. The film was prepared by drop-casting from a solution in toluene.

The small shoulder near 550 nm comes from silole unit due to the π-π* conjugation between silole core and fluorenone unit. The absolute quantum yield (QY) of **P1** in THF solution and in aggregation at f_w-50% were 15.6% and 23.2%, respectively. Whereas **P1** shows low QY of 2.7% in solid state (table 1).

Table 1. Optical properties of the **P1** in different states

	λ_{abs} (nm)[a]	Solution λ_{flu} (nm)[b]			Φ_{flu}[c] (%)		
State	Sol	Sol	Film	Agg[e]	Sol	Solid	Agg[d]
P1	344	394	563	563	15.6	2.7	23.2

[a] UV absorption maximum; [b] emission maximum; [c] Absolute PL quantum yield. [d] in 50% and [e] 99% THF/water mixture. Film was prepared by spin-coating a solution of pure polymers in THF.

2.2. *Vapochromic Behavior in Solvent and Detection of TNT:*

Fluorescent conjugated polymer has taken much attention as chemosensors for detecting explosives, such as TNT due to their potentiality in national security. We were interested to study TNT sensing in solid states and investigate the colorimetric visualization. Vapocromism effect has been studied upon the diffusion of solvents into the solid state of polymer and acetone was peaked to check as shown in figure 2. The stamp with the letters 'PNL' was dipped in acetone solution of **P1** and stamped on filter paper which was not visible at day light. After removing solvent, it displays yellow color under uv light. Furthermore, diffusion of acetone on it, as the original yellow color changes to blue which indicate the largest vapochromic characteristics of **P1** [80]. Upon exposing to acetone vapor to polymer, it takes less than 1 min to change the color from yellow to blue while the vapor exposure was stopped, a few minutes needed to back the original color from blue.

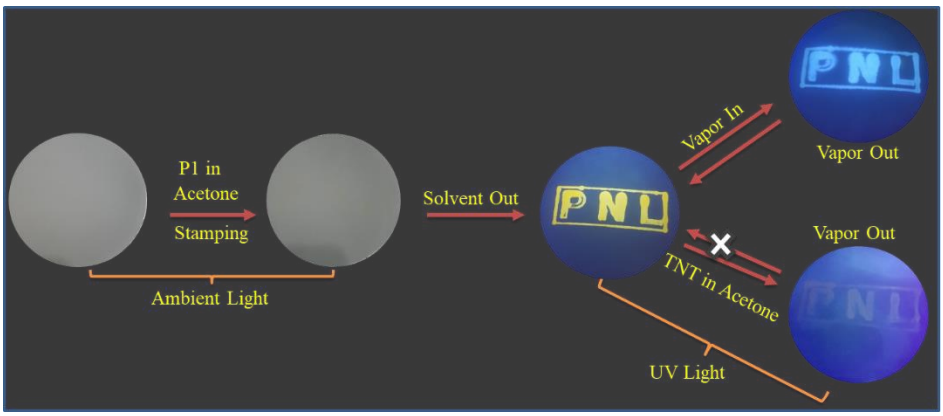

Figure 2. Procedures and effect of solvent vapor in solid state and colorimetric TNT sensing method by P1. Stamping into filter paper with P1 in acetone

we carried out detection of TNT in solid states on filter paper through solvent. Same as acetone process, the letter "PNL" with **P1** was stamped on filter paper and yellow color showed in UV-lamp light. When TNT in acetone diffused, the yellow emission quenched due to the interaction of polymer with analyte in solid states and become slight crimson color which does not return to yellow after completely drying. Due to the electron transfer and fluorescence intensity quenching are the main reason for color changing of **P1** in solid state. Amplified PL quenching used to detect nitroaromatic compounds by transferring electron to LUMO of the analyte from polymer fluorophore [17]. These results indicate that the electron from **P1** transferred to the LUMO of TNT by quenching PL intensity and changing color which appeared that it might have great potentiality to detect TNT in real world samples (figure 3).

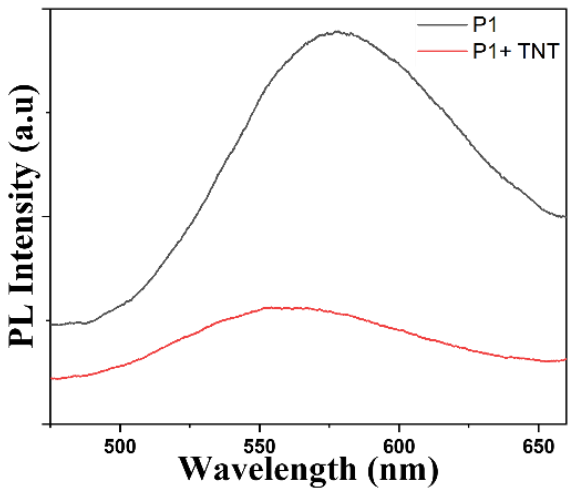

Figure 3. Photluminescence quenching of P1 in the presence of TNT analyte.

NACs compounds such as TNT are electron deficient. Detection of analytes by fluorescence quenching involves electron transfer from electron rich silole to electron deficient NACs. Figure 3 shows the interaction between silole and TNT. The excited electron from the LUMO of **P1** fluorophore can transfer to the LUMO of NACs analyte. This fluorescence quenching process is known as photoinduced electron transfer (PET) [14,17].

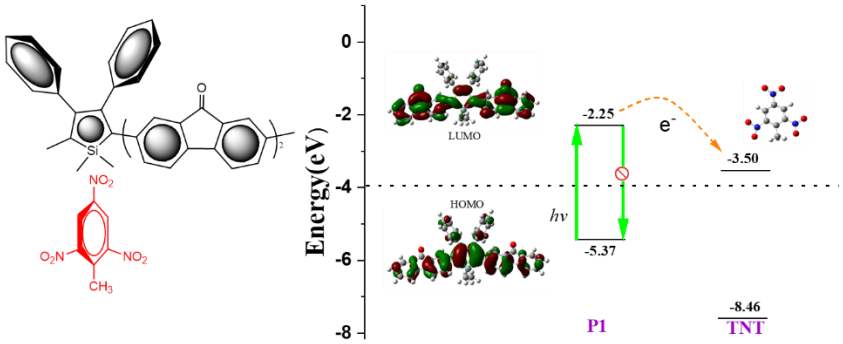

Figure 4. The interaction between polymers in presence of TNT. Schematic diagram of electron-transfer mechanism for photoluminescence quenching. HOMO-LUMO energy profiles of **P1** and TNT calculated from the ab initio at the B3LYP/6-31G(d) level

2.3. *Theoretical calculations and analysis:*

Moreover, density functional theory (DFT) was used to study the photophysical properties of the silole polymer and to demonstrate the molecular calculation, we used B3LYP/6-31G(d) as basis set from gaussian view 09 [56]. In **P1** except silicon atom with methyl, the highest occupied molecular orbitals (HOMO) are extended almost all the molecules (figure 4). Whereas, in the lowest unoccupied molecular orbital (LUMO), where the orbitals of the silole core and its 2,5-

substituents dominated the polymer. The electron density from the silole core moiety and the 3,4-substituted phenyl rings were slightly reduced and vanish while the electron clouds of the 2,5-substituted of **P1** groups increase. This verifies that the 2,5-fluorenone groups have a strong effect on the energy band gap of the silole polymer. Such an orbital distribution demonstrated that might be possible reason to induce the emission quenching of **P1** in at f_w-99% [81].

2.4. *Photophysical properties:*

In order to investigate, the aggregation behavior of P1, THF/water was performed in different mixers to study AIEE or AIE where THF is good solvent and water is poor solvent for **P1**. The photoluminescence spectra were recorded and depicted in figure 5 displaying that the weak PL are changing from single isolated molecule to strong fluorescent nanoaggregates up to 50% water fraction [82,83]**.** On increasing water fraction from 0% to 50% the fluorescence intensity was increased due to the aggregation-induced enhanced emission properties compared to pure solution in THF. At 50% of water mixers, PL intensity was increased by 2.4 times compared to 0% (figure 5a-4b).

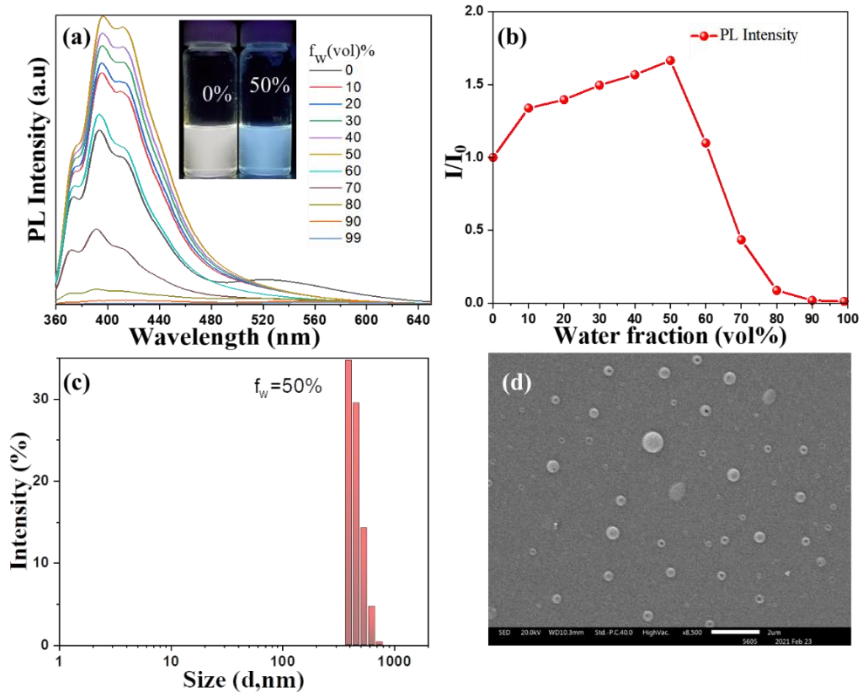

Figure 5. a) PL spectra of P1 in the THF/H_2O mixture with different H_2O fractions. b) Plots of maximum emission intensity and wavelength of P1 versus the water fraction in the THF/H_2O mixture c) DLS data shows the particle size of P1 at f_w-50% (d)SEM images of P1 prepared from spin-coating from 50% water fraction. Inset: images of P1 with different H_2O fractions under UV light at 365 nm.

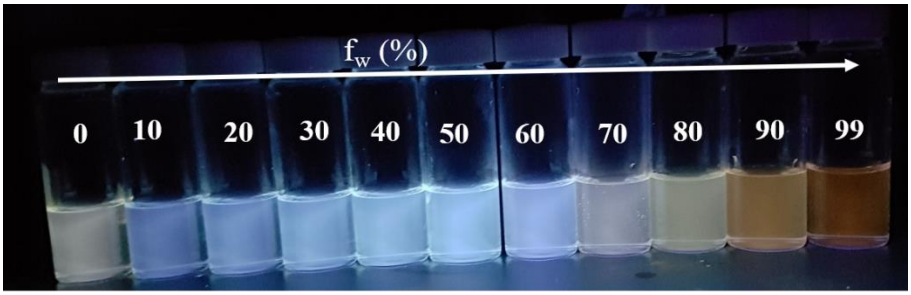

Figure 6. Fluorescence photograph of the P1 in different volumetric fraction of water.

The inset photograph in figure 5a showed the emission picture in pure THF solution and f_w-50% aggregation. After 50%, intensities were started to decrease in solution due to precipitation in aggregation state. From 60-99% the molecules return to ground state and exhibit weak luminescence via non-radiative processes and these aggregated molecules also brings steric effect between the neighboring segments [84]**.** Moreover, a very weak peak appeared at 563 nm while water fraction increased to 90%-99% due to the formation of amorphous aggregates (figure 6). The emission shifting at higher wavelength upon adding water at higher fraction can be attributed to the ACQ effect. The thin film of **P1** had similar peak at 563 nm which was red shift. Due to becoming more integrate sphere in those media which greatly enhanced compare to solution [85]**.** Figure 5(b,c) shows DLS and SEM results which studied to examine the morphology and the size of aggregates.

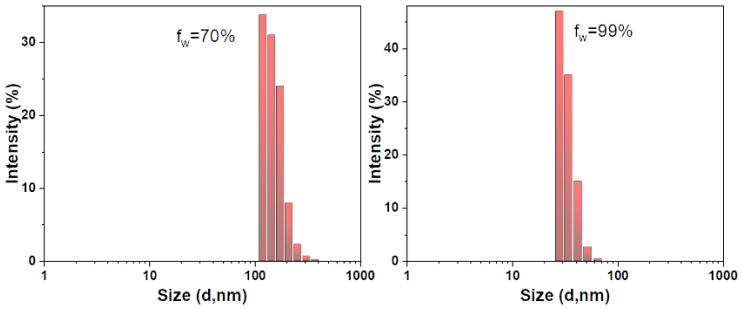

Figure 7. DLS data showing when the water fraction increases then the particle size of P1 nanoaggregate were decreased.

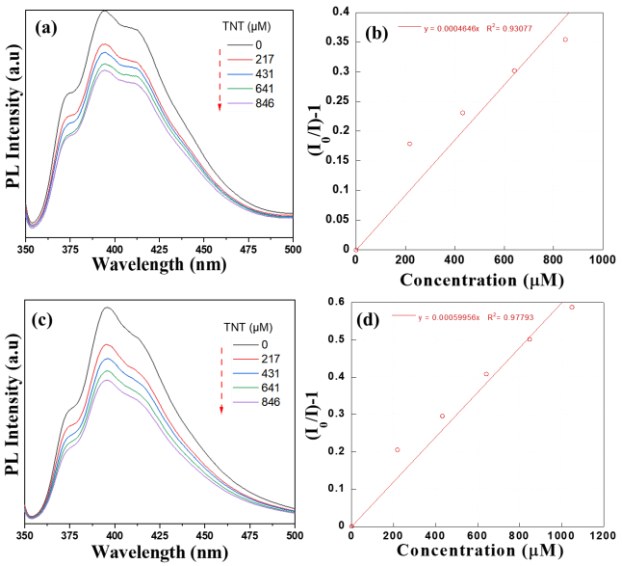

Figure. 8. (a) Quenching PL spectra and (b) Stern–Volmer plot showing sensing efficiency by increasing in THF solution for **P1** (c) Quenching PL spectra and (d) Stern–Volmer plot showing sensing efficiency by increasing TNT in THF/water solution (50% water) for **P1**.

At f_w-50%, the particle size was observed an average 425 nm . The diameter of the particle decreases upon increases of water fraction. The particle size was observed at f_w-70% and 99% with an average 250 and 45 nm respectively (figure 7). This behavior is similar with some other silole molecules [14,15]. Furthermore, **P1** in THF solution and THF/water mixture with 50% water (v/v) were used to investigate the fluorescence quenching of TNT where Stern-Volmer plot was carried out to display the study. In presence of TNT in solution and aggregate states with P1 are shown in figure 8. To analyze the quenching behavior, Stern-Volmer equation: $I_0/I=K_{SV}$ [Q]+1 was used. I_0 represents the intensity without analyte at [Q] = 0 and I is the fluorescence intensity at presence of analyte [Q]. K_{SV} represents the Stern–Volmer constant. The quenching constant K_{SV} for TNT in solution and aggregate states at water fraction of 50% were 464 $M^{-1}$and 600 M^{-1} respectively which are higher than published literature about linear conjugated polymer [40].

2.5. *Physical property analysis:*

We have examined the thermogravimetric analysis (TGA) and powder X-ray diffraction (PXRD) to study thermal property and crystallinity of **P1**. The TGA analysis and it exhibits good thermal stability where below 5% weight loss measured at 270℃ (figure 9). Heating rate of 10℃/min under N_2 atmosphere the experiment was carried out. From room temperature to 245℃, the weight loss was below 5% corresponding to solvent molecules releasing (obsd. 1.4%). Then the polymer began to decompose at 425℃ where anhydrous polymer destructed from 245 to 425℃ (obsd. 22.2%) and from 425 to 545℃ (obsd. 11.1%) respectively. The polymer would consider of making amorphous emissive layer of different photoelectric layer due to the great thermal stability.

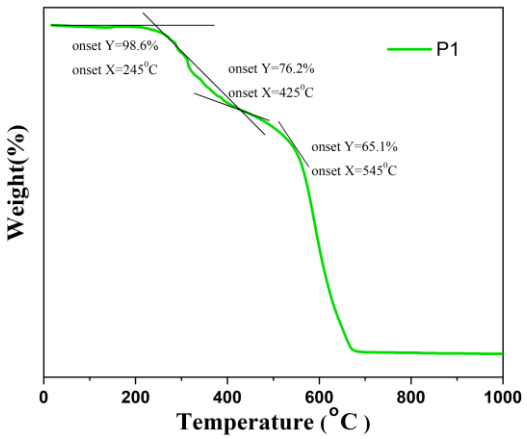

Figure 9. The TGA curve of P1

The polymer demonstrated a narrow peak at 4.6 Å in XRD patterns. The difference of polymers backbones and distance between the chains could be explained by d-spacing results [87]**.** The lower d-spacing suggests shorter distance between the chains which indicate the polymer might be more ordered (figure 10). The PXRD displays the packing arrangements differences of the polymer chains, which brings separate interpenetrations of another polymer chains.

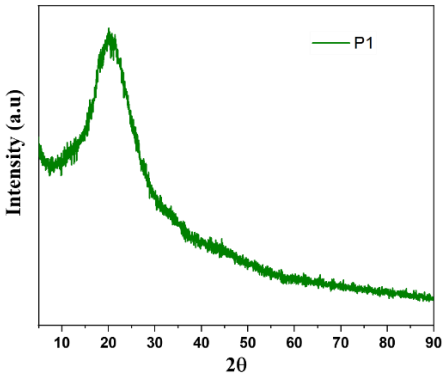

Figure 10. X-ray diffraction (XRD) patterns of polymer powders P1 in solid states.

3. CONCLUSION

In conclusion, the conjugated polymer of silole substituted on 2,5-positions with fluorenone moiety was synthesized and investigated for dual mode of detection TNT by fluorescence quenching and colorimetric. The polymer displays reversible vapochromic properties during the solvent diffusion in solid state while presence of TNT, it responded well by quenching emission and color changed which was irreversible. Thus, this polymer can be used as chemosensor for detection of TNT as it is highly sensitive. In addition, the polymer showed emission intensity enhancement during increasing of water fraction up to 50%, which demonstrated the AIEE characteristics. The polymer shows linear Stern-Volmer constant by fluorescence quenching for TNT in solution and aggregate medium. Besides, polymer showed great thermal stability by losing below 5% weight at 270℃ (obsd. 3.4%). From overall study, this research suggest that the obtained conjugated polymer may enrich the luminescent materials and could provide a convenient platform for NACs sensing.

Chapter 6 - Experimental Section

6.1. Measurements and Instruments

All synthetic methods were carried out under dry argon atmosphere using standard Schlenk technique. According to standard literature methods all solvents were purified and degassed before use. All the chemicals and reagents purchased from commercially available company. Tetrahydrofuran (THF), n-hexane, diethyl ether, and ethanol were purchased from Aldrich Chemical Co. Inc and distilled before using by sodium/benzophenone ketyl. All other reagents such as 1,4-dibromobenzene, 1,3,5-tribromobenzene, dibutyldichlorosilane, methyltrichlorosilane, lithium wire, *n*-butyllithium, naphthalene, palladium-tetrakis(triphenylphosphine) and diphenylacetylene purchased from available company and used without any purification.

^{1}H NMR (300 MHz) and ^{13}C NMR (75 MHz) spectra were recorded on a Bruker Avance-400 spectrometer. JMS-T200GC-TOF mass spectrometer was used to obtain high-resolution mass spectral analyses. A Nikon Eclipse LV100 optical polarized microscope (POM) equipped with a Linkam TMS 94 heating system was used to measure the melting point. Absorption measurements were obtained from a Shimadzu UV-1650 PC spectrometer (Kyoto, Japan) and fluorescence emission spectrum were recorded using Hitachi F-7000 spectrometer (Tokyo, Japan). The absolute PL quantum yield (QY) data was recorded from Quantaurus (QY) absolute PL quantum yield spectrometer C11347-11 (Hamamatsu, Japan) with of 150 W xenon monochromatic light source, multichannel Czerny-Turner type spectroscope, and 3.3 inch spectral on integrating sphere. Dynamic light scattering (DLS) measurement was obtained by using a DLS-8000HL (Otsuka

Electronics, Japan) with 10 mW He–Ne Laser (Max 30 mW), photomultiplier tube detector, and silicon photodiode monitor detector. Time-resolved fluorescence measurements were performed on Fluorolog3 (Horiba) Fluorescence Spectrometers. Thermal gravimetric analysis (TGA) measurements were recorded with an SDT-Q600 Build 95 thermal analysis system at a heating rate of 10° C/ min under a N2 atmosphere. The molecular weights measurement was obtained by gel permeation chromatography (GPC) using THF as the eluent and polystyrene as the standard. Scanning electron microscopic (SEM) images were conducted with a (JEOL JSM-6700F, Japan) scanning electron microscopy.

6.2. Synthesis of Materials

6.2.1. Synthesis of 1,4-bis(1-methyl-2,3,4,5-tetraphenyl-1-silacyclopentadien), bissilole.

1,4-Bis(1-methyl-2,3,4,5-tetraphenyl-1-silacyclopentadien) was synthesized and the analytical data was identified with an authentic sample [[88]. 1-Chloro-1-methyl-2,3,4,5-tetraphenyl-1- silacyclopentadiene (3.92 g, 9 mmol) and lithium (0.06 g, 9 mmol) in THF (150 mL) were stirring at room temperature for overnight. After removing THF from mixture, the remaining solid was extracted water with DCM several times. Then the DCM was removed in reduced pressure. The solid was washed with ether and hexane for purification to give the product (2.2 g, 61%) as a pale green solid. M.p. 310 °C, (lit. [30] m.p. >300 °C); ^{1}H NMR (300 MHz, $CDCl_3$): δ 0.19 (s, 6H), 6.65-7.10 (m, 40H). ^{13}C NMR (75 MHz, $CDCl_3$): δ 154.6, 143.4, 139.9, 138.7, 130.3, 129.4, 127.9, 127.4, 126.3, 125.6, -6.2 ppm. HRMS (ESI-TOF, m/z) $C_{58}H_{46}Si_2$: $[M+H]^+$ Calcd: 798.3132, Found: 798.3138.

6.2.2. Synthesis of 1,4-bis(1-methyl-2,3,4,5-tetraphenyl-1-silacyclopentadienyl)benzene, bissilole-benzene.

Under dry nitrogen atmosphere, *n*-butyllithium solution (3.26 mmol, 1.6 M in hexane) was added dropwise into a solution of 1,4-dibromobenzene (0.35 g 1.48 mmol) in dry THF at -78 °C. After the addition the mixture was stirred for 30 min and then a solution of (1.42 g, 3.26 mmol) of 1-chloro-1-methyl-2,3,4,5-tetraphenyl-1-silacyclopentadiene in freshly distilled THF (20 mL) was added dropwise. Then the mixture was allowed to warm at room temperature. Then distilled water was poured into the mixture and extracted with dichloromethane and dried over $MgSO_4$. After removing the solvents under reduced pressure, the solid was washed with ethanol for purification to give the product of 1,4-bis(1-methyl-2,3,4,5-tetraphenyl-1-silacyclopentadienyl)benzene (0.92 g, 64%) as a light green solid. M.p. 275 °C; ^{1}H NMR (300 MHz, $CDCl_3$): δ 0.79 (m, 6H), 6.80-7.04 (m, 40H), and 7.50 (s, 4H). ^{13}C NMR (75 MHz, $CDCl_3$): δ 155.9, 138.6, 136.1, 131.5, 129.9,128.9, 128.9, 127.9, 127.8, 127.5, 127.4, 126.4, 125.7, -6.7 ppm. HRMS (ESI-TOF, m/z) $C_{64}H_{50}Si_2$: $[M+H]^+$ Calcd: 874.3445, Found: 874.3486.

6.2.3. Synthesis of bis(phenylethynyl)dibutylsilane

We followed with modification from the literature [89]. Briefly, a solution of phenylacetylene (10.21g, 100mmol) in diethylether (180 mL) was added a solution of n-Butyllithium (1.6 M in hexane, 62.5 mL, 100mmol) dropwise slowly at 0^0C. The mixture was stirred at the same condition overnight. A solution of dibutyldichlorosilane (10.6g, 50mmol) in Ether (50 mL) was added at the temperature over 30 min. The mixture was allowed to warm to room temperature.

After stirred for another 6 h, the mixture was terminated with a saturated NH_4Cl aqueous solution, and the mixture was extracted by Et_2O.After dried over $MgSO_4$ the solution was filtered and concentrated under reduced pressure. After that obtained product was in 16.6g in 96% yield as a redish liquid and purity was 99.2%. ^{1}H NMR (300 MHz, CDCl3, δ): 7.51 (m, 4H), 7.32 (m, 6H), 1.61-1.38 (m, 8H), 1.50-1.20 (m, 12H), 0.85-1.05 (m, 10H); ^{13}C NMR (75 MHz, CDCl3, δ): 132.3, 128.9, 128.3, 123.04, 106.7, 89.5, 26.1, 25.9, 14.6, 13.6.

6.2.4. Synthesis of 1,4-diioodo-2,5-bis(octyloxy)benzene

Compound **3** was prepared by following with modification from the literature[90]. (Yield 91%), ^{1}H NMR (300 MHz, CDCl3, δ): 7.17 (s, 2H), 3.93 (t, 4 H), 1.85-1.76 (m, 4 H), 1.55-1.30 (m, 20 H), 0.92-0.87 (m, 6 H); ^{13}C NMR (75 MHz, CDCl3, δ): 152.9, 122.8, 86.3, 70.3, 31.7, 29.21, 29.20, 29.1, 26.0, 22.6, 14.08.

6.2.5. Synthesis of polymer (P1 and P2)

P1: Lithium granular (0.40 g, 58mmol, 4eq) and naphthalene (7.44 g, 58mmol, 4eq) in THF (50 mL) was stirred at room temperature (RT) under an argon atmosphere for 6h to form a deep-green solution of lithium naphthalenide (LiNaph). A solution of bis(phenylethynyl)dibutylsilane (5g, 14.51 mmol) in THF (50mL) was added to the solution of LiNaph dropwise over 10 min at RT. After stirring for 40min, the mixture was cooled to 0℃. The addition of $ZnCl_2$ (7.9g, 58mmol) to the mixture, followed by dilution with THF (30 mL), gave a black suspension. After stirring for 40 min at RT, 1,4-bis(octyloxy)-2,5-diiodobenzene (8.5g, 14.51mmol) and $Pd(PPh_3)_2Cl_2$ (102 mg, 1 mol%) were added successively with 30ml THF. The mixture was stirred at 80℃ for 72 h. MeOH (10 mL) was added and the mixture was extracted thrice with Et_2O

(10 mL). The combined Et_2O solution was washed with brine, dried over $MgSO_4$ and concentrated under vacuum and precipitated with methanol. The precipitate was collected by filtration and washed with MeOH. This procedure was repeated three times to remove low molecular weight oligomers. A yellow solid was collected by vacuum filtration (3.98g, yield 28.2%). ^{1}H NMR (300 MHz, $CDCl_3$, δ): 7.56-6.23 (m, 14H, Ph-H), 4.0-3.42 (m, 8H, OCH_2), 1.80-0.86 (m, 78H, CH_2, CH_3, Si $(CH_2)_2$), GPC (THF): M_w =9862, M_n=6237, PDI=1.58.

P2: The synthetic procedure is similar to that for the preparation of P1, instead of 1 mol% of $Pd(PPh_3)_2Cl_2$ we use 0.1 mol% for **P2** and a grenish solid was collected by vacuum filtration. (3.86g, yield 21.5%) ^{1}H NMR (300 MHz, $CDCl_3$, δ): 7.56-6.23 (m, 16H, Ph-H), 4.0-3.42 (m, 12H, OCH_2), 1.80-0.86 (m, 108H, CH_2, CH_3, Si $(CH_2)_2$), GPC (THF): M_w=4970, M_n= 3764, PDI=1.32.

6.2.6. Synthesis of Dimethyl bis(phenylethynyl) Silane

Dimethyl Bis(phenylethynyl) Silane was prepared by following literature methods with little modification [91]. (Yield 85%), ^{1}H NMR (300 MHz, $CDCl_3$, δ): 7.52 (dt, 4H), 7.33 (m, 6H), 0.49 (m, 6H).

6.2.7. Synthesis of Hyperbranched Polymer

Polymer 1 (**P1**) was synthesized with slightly modification from reported publication [20,79]. At the room temperature (RT), bis(phenylethynyl)dimethylsilane (1g, 3.84 mmol) in THF (5mL) was added into the solution of LiNaph dropwise over 10 min and stirred for 40min before cooled to 0°C. After the addition of solid [$ZnCl_2$, 2.09g, 15.36mmol,4eq] followed by dilution with THF (10 mL) into the solution, the suspension become black. After

stirring another 40 min 1,3,5- tribromobenzene (1.2g, 3.84mmol) and Pd (PPh_3)$_4$, (0.09 g) were added successively at RT. Then the mixture was allowed to stir at 100°C for 3 days. The mixture was extracted thrice with DCM (10 mL) after adding Water (10 mL). Then the solution was washed with aqueous $NaHCO_3$ and brine, dried over $MgSO_4$ and concentrated under vacuum and precipitated with MeOH. To remove low molecular weight oligomers this procedure was repeated three times and a yellowish solid was collected by vacuum filtration (0.72g, yield 49%). ^{1}H NMR (300 MHz, $CDCl_3$, δ): 7.12-6.21 (m, Ph-H), 0.6-0.20 (m, -CH_3), GPC (THF): M_w =3457, M_n=2531, PDI=1.3.

6.2.8. Synthesis 2,7-Dibromo-9-fluorenone

2,7-Dibromo-9-fluorenone (**3**) was prepared by following with modification from the literature [92]. (Yield, 95%), ^{1}H NMR (300 MHz, $CDCl_3$): δ= 7.77 (d, 2H; COCCH), 7.63 (dd, 2H; CBrCHCH), 7.39ppm (d, 2H; CBrCHCH).

6.2.9. Synthesis of polymer (P1)

Under dry nitrogen Lithium granular (0.106 g, 15.36 mmol, 4 eq.) and naphthalene (1.96 g, 15.36 mmol, 4 eq.) in THF (10 mL) was stirred at room temperature (RT) under an argon atmosphere for 6h to form a deep-green solution of lithium naphthalenide (LiNaph). A solution of bis(phenylethynyl)dimethylsilane (1 g, 3.84 mmol) in THF (5 mL) was added to the solution of LiNaph dropwise over 10 min at RT. After stirring for 40min, the mixture was cooled to 0°C. The addition of solid [$ZnCl_2$, 2.09 g, 15.36 mmol, 4 eq.] to the mixture, followed by dilution with THF (10 mL), gave a black suspension. After stirring for 40 min at RT, 2,7-dibromo-9-fluorenone (1.29 g,

3.84 mmol) and $Pd(PPh_3)_4$, (177 mg, 4 mol%) were added successively with 20 mL THF. The mixture was stirred at 100℃ for 48 h. Distilled water (10 mL) was added to the reaction mixture and the mixture was extracted three times using dichloromethane (DCM, 10 mL). The combined solution was washed with $NaHCO_3$ and brine, dried over $MgSO_4$ and concentrated under vacuum and precipitated with hexane. This procedure was repeated three times to remove low molecular weight oligomers. A redish orange solid of polymer (**P1**) was collected by vacuum filtration (0.78 g, yield 35%). ^{1}H NMR (300 MHz, $CDCl_3$): δ= 7.19-6.80 (m, 10H; Ph-H), 7.87-7.40 (m, 12H; COCH, CBrCH), 0.6-0.20 ppm (m, 6H; Si $(CH_3)_2$), GPC (THF): M_w =2356, M_n=2253, PDI=1.04.

6.3. Experimental Spectra.

NMR Spectra:

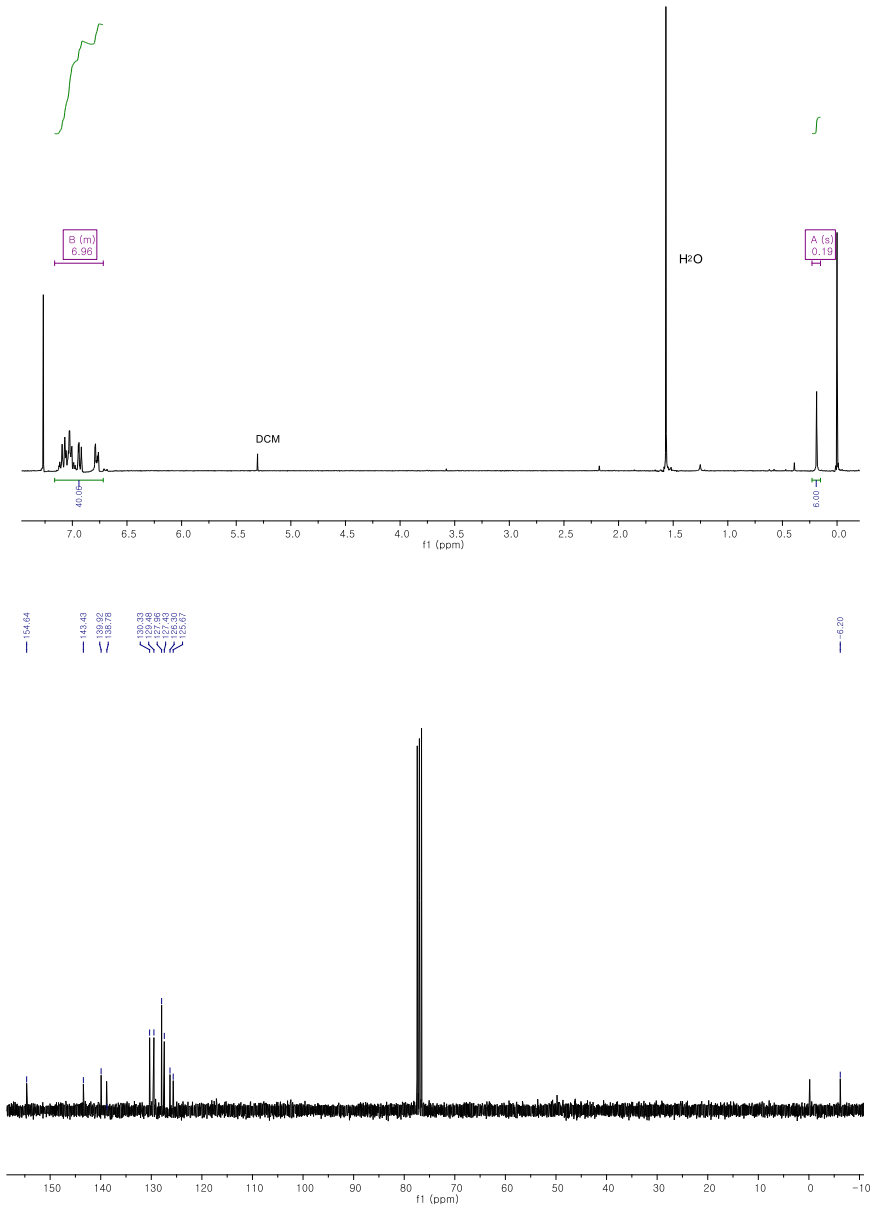

^{1}H and ^{13}C NMR spectra of 1,4-bis(1-methyl-2,3,4,5-tetraphenyl-1-silacyclopentadien), bissilole

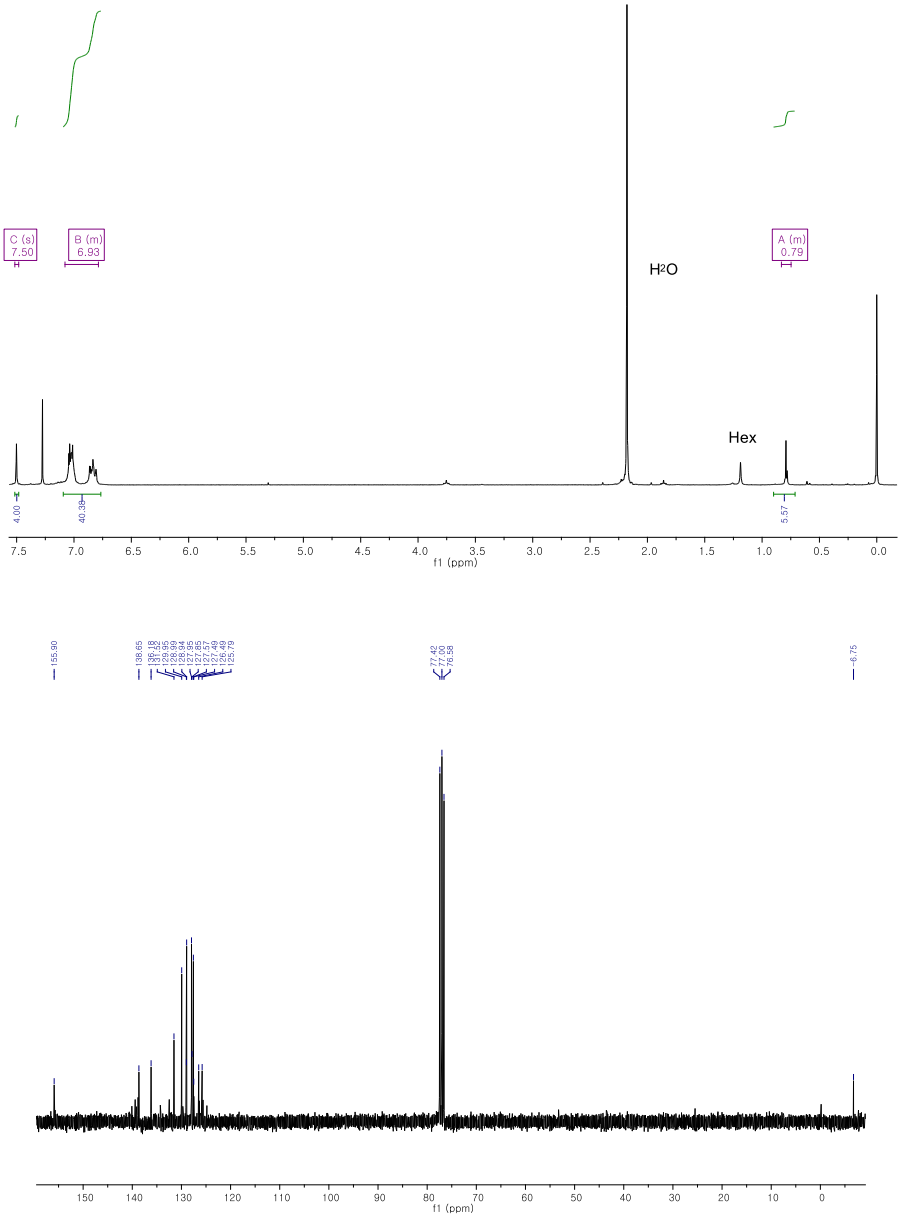

^{1}H and ^{13}C NMR spectra of 1,4-bis(1-methyl-2,3,4,5-tetraphenyl-1-silacyclopentadienyl)benzene, bissilole-benzene

High-resolution Mass Spectroscopy (HRMS)

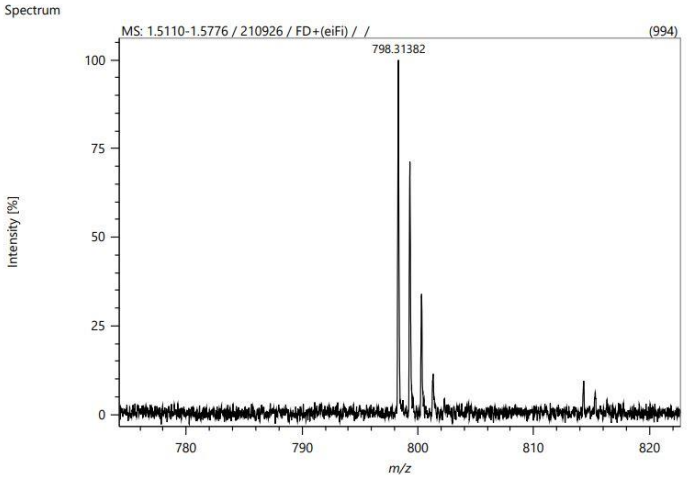

Mass spectrum of bissilole

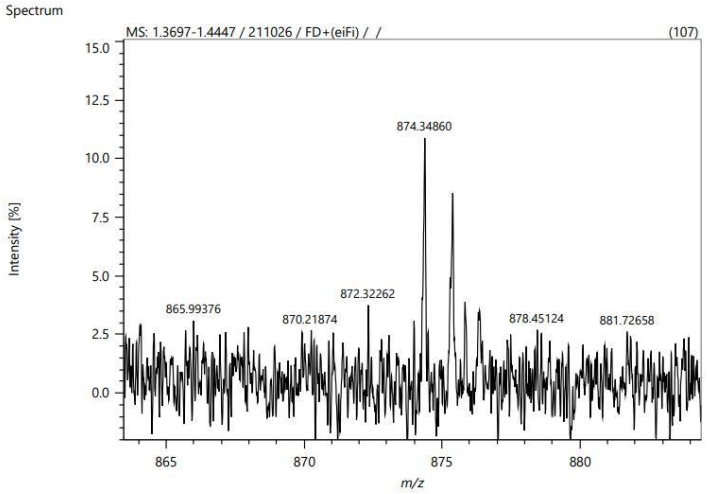

Mass spectrum of bissilole-benzene

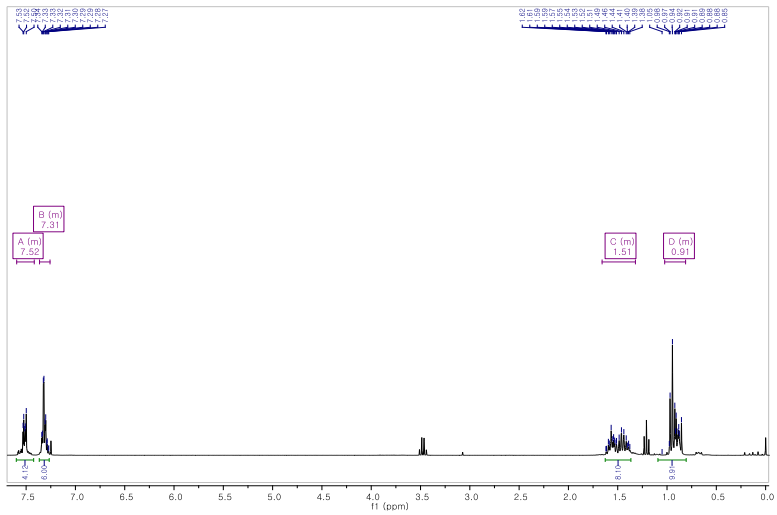

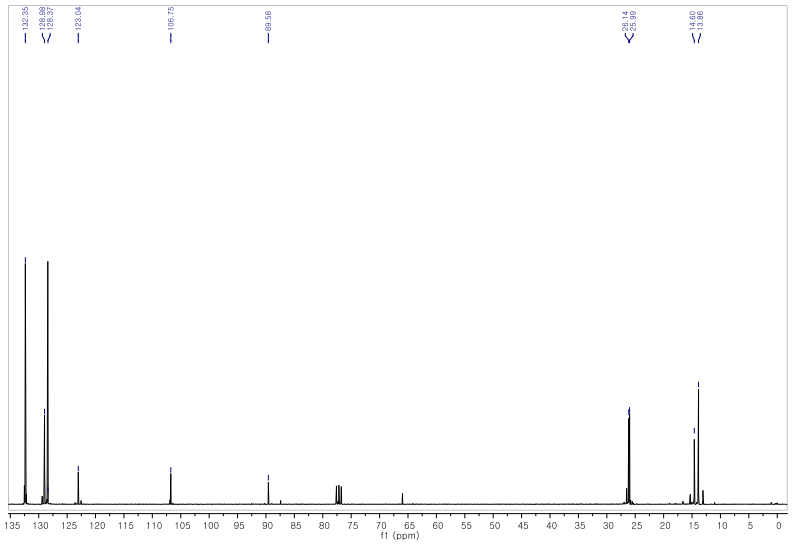

^{1}H and ^{13}C NMR spectra of bis(phenylethynyl)dibutylsilane

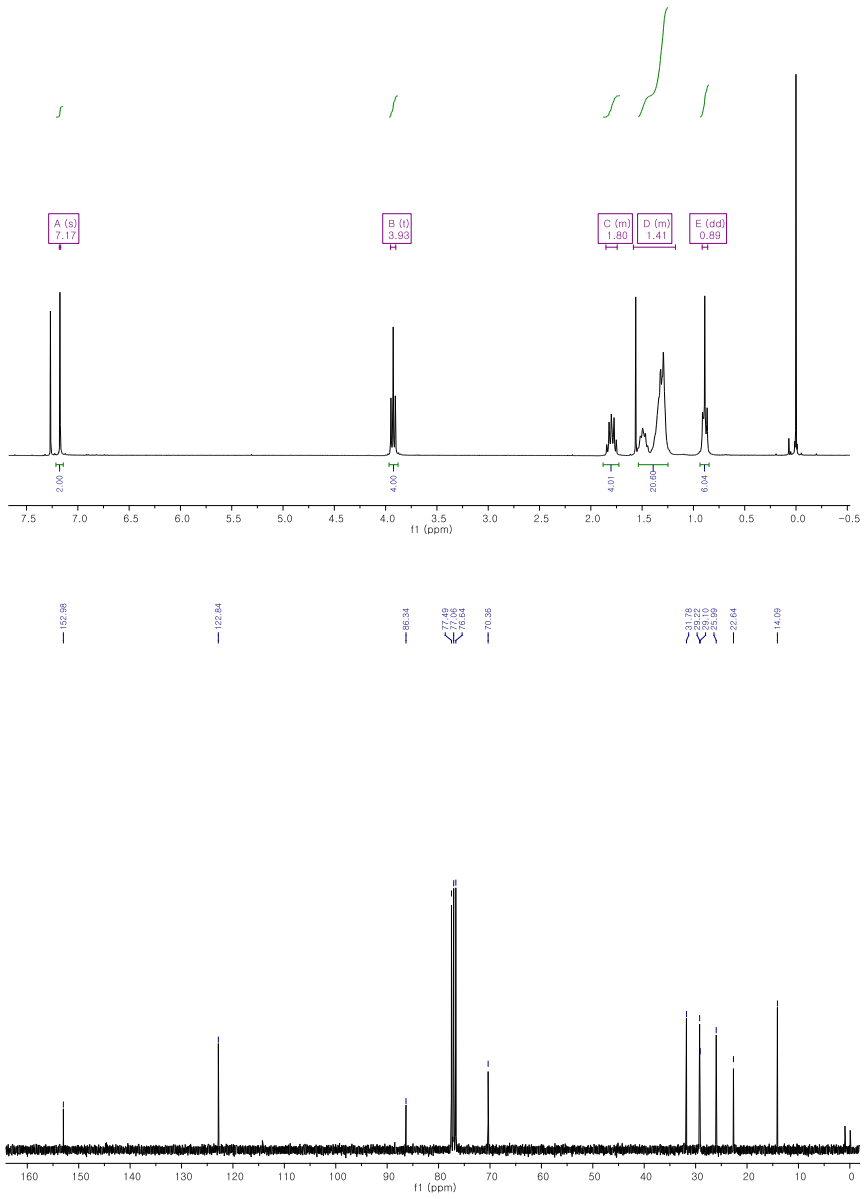

^{1}H and ^{13}C NMR spectra of 1,4-diioodo-2,5-bis(octyloxy) benzene

P1

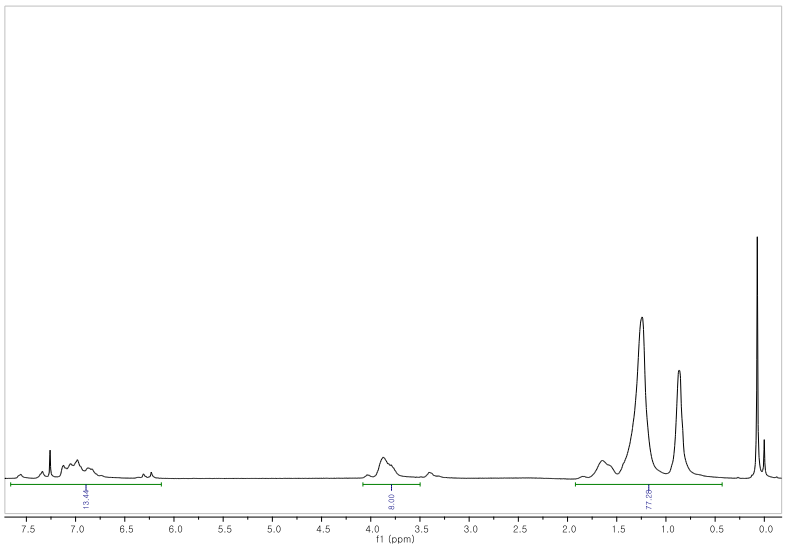

P2

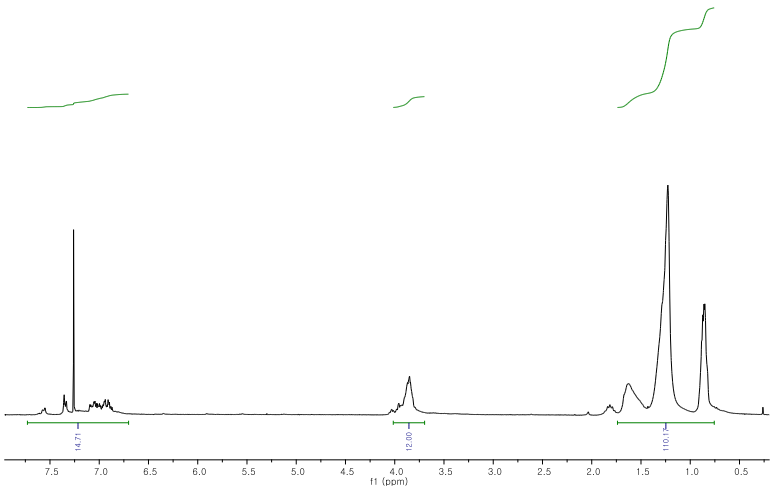

^{1}H-NMR spectrum of polymer **P1** and **P2** (Chapter-3)

P1

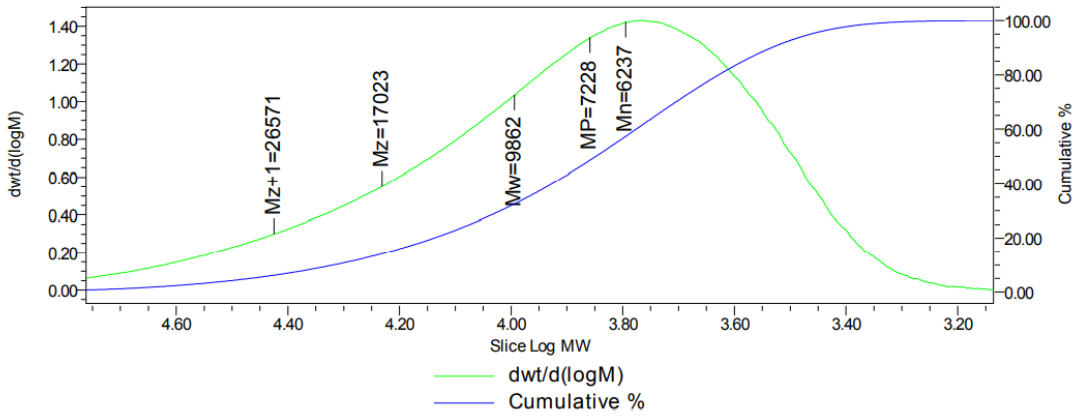

P2

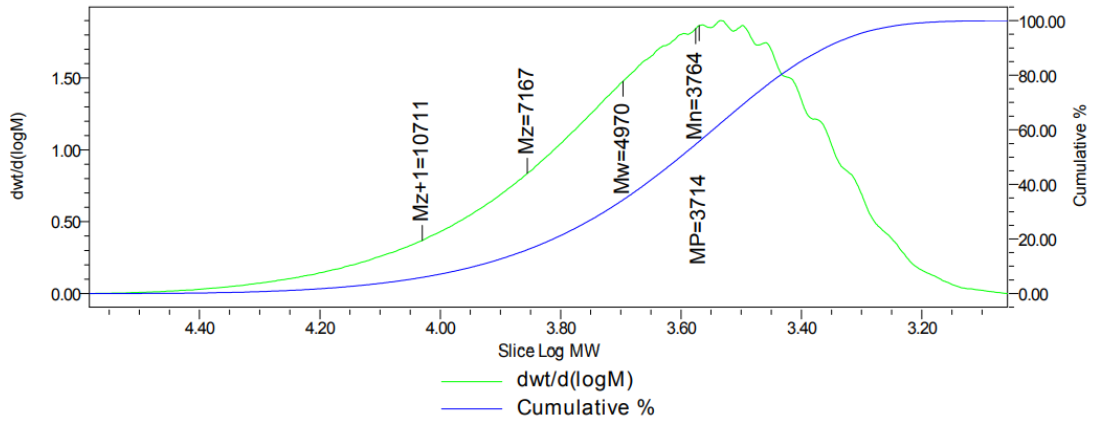

GPC chromatographs for polymer **P1** and **P2** (Chaper-3)

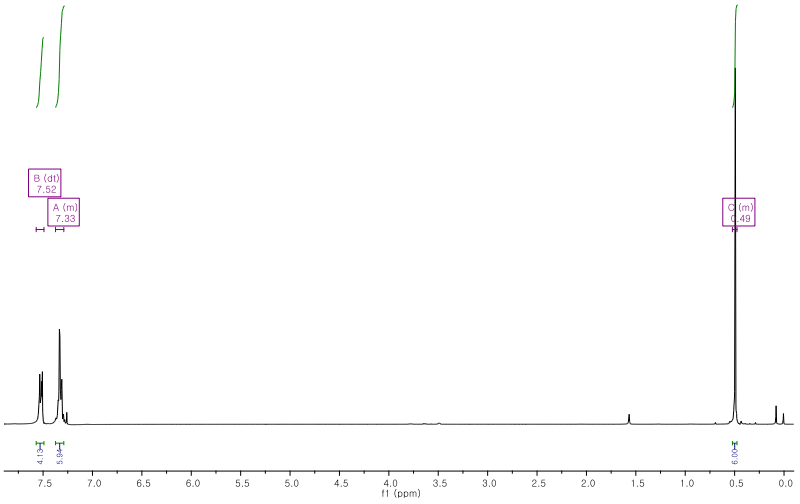

^{1}H NMR spectra of Dimethyl bis(phenylethynyl) Silane

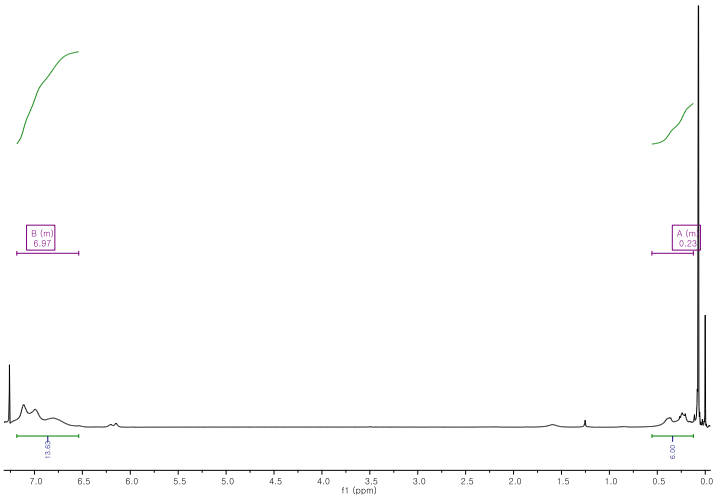

^{1}H-NMR spectrum of polymer (Chapter-4)

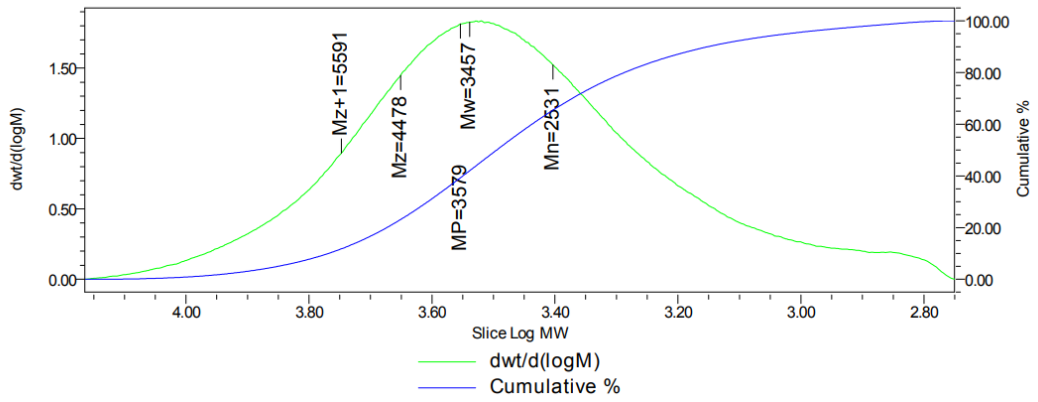

GPC chromatograph for polymer (Chaper-4)

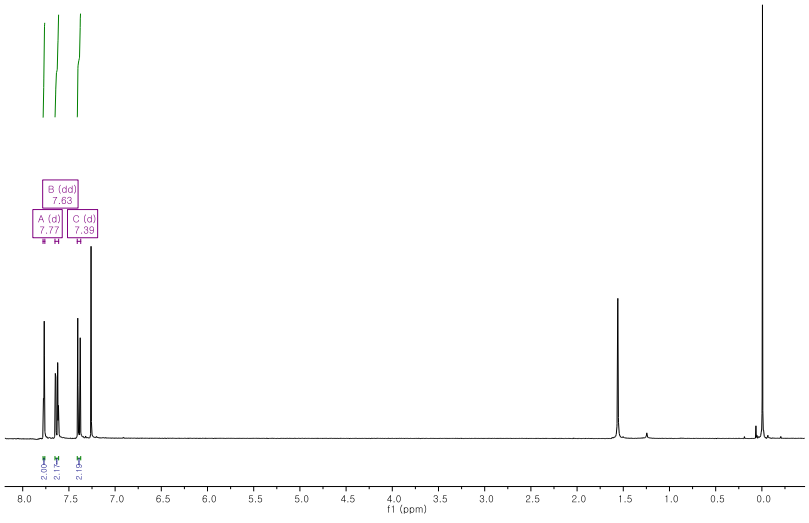

^{1}H NMR spectra of 2,7-Dibromo-9-fluorenone

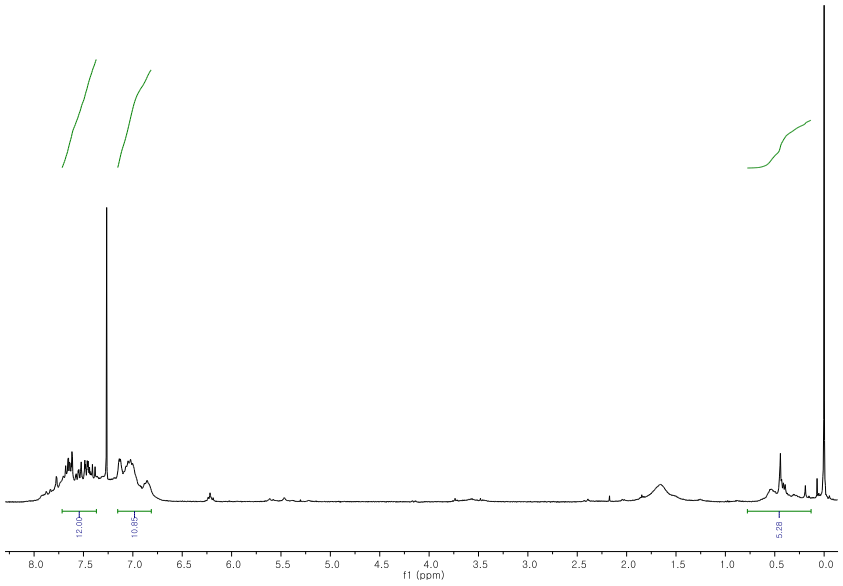

^{1}H-NMR spectrum of polymer (Chapter-5)

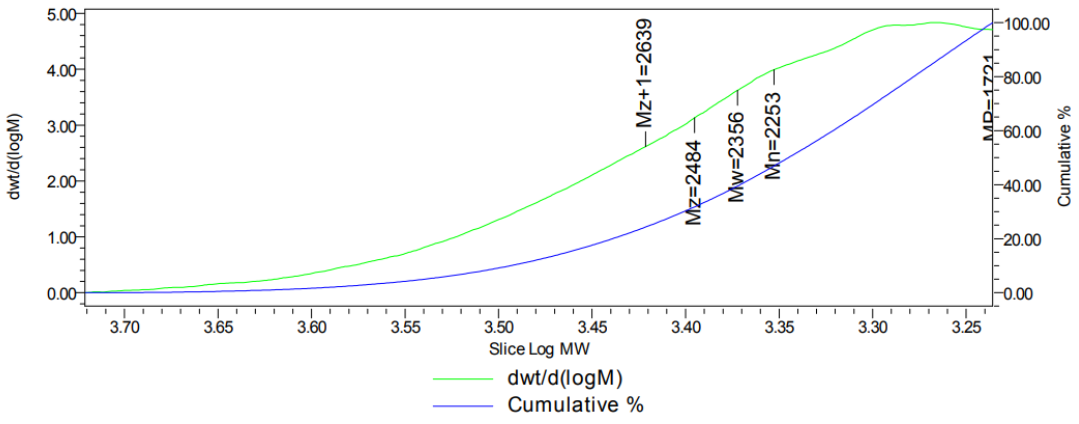

GPC chromatograph for polymer (Chaper-5)

Chapter 7

Conclusion of the Study

In summary, A series of conjugated polymers were successfully synthesized, investigated, and characterized for the detection of chemical explosives. The obtained siloles revealed emerging photophysical properties because of their ACQ/AIE and ICT effects at different fraction water. We also studied the solvent behavior of the two polymers along with their ICT properties using DFT calculations, which arise from conjugated π-systems. The fluorescence and sensing properties for NACs of siloles have been studied in pure THF solution, films, and aggregated states. Due to the π-σ* hyper conjugation, bissilole-benzene reveals higher PL enhancement by preventing more non-radiative decay compared to σ-σ* conjugated bissilole. The nanoaggregates of bissilole-benzene showed high Stern–Volmer constant for sensing PA, TNT and DNT compared to previously reported work. On the other hand, due to the low band gap energy, bissilole showed little high sensitivity towards explosives than bissilole-benzene. The high luminescent hyperbranched polymer exhibits unique strong AIE phenomenon by enhancing the PL intensity by 12 times at 99% faction of water. Compared to previously reported work for sensing NACs, the synthesized polymer nanoaggregates showed very high Stern–Volmer constant. Moreover, for solid state sensing, polymer responded very well towards explosives by paper strips experiments. 2,5 silole polymers containing octyloxy benzene showed a significant response to real-time fluorescence quenching and PL recovery processes toward TNT vapors in real-time sensing. Moreover, silole exhibited high fluorescence efficiencies in all three states. Moreover, the conjugated polymer of silole substituted on 2,5-positions with fluorenone moiety revealed dual mode of detection TNT by fluorescence

quenching and colorimetric. The polymer displays reversible vapochromic properties during the solvent diffusion in solid state while presence of TNT, it responded well by quenching emission and color changed which was irreversible. From overall study, this research suggest that the obtained conjugated polymer may enrich the luminescent materials and could provide a convenient platform for NACs sensing.

In conclusion, this study explains that the unique combination of properties displayed by silole with strong fluorescence makes these materials a promising candidate to develop selective and sensitive fluorescent sensor for detecting explosives by improving the fluorescent properties of sensors in all states.

References

1. Hermanns, J.; Schmidt, B. Five-and six-membered silicon–carbon heterocycles. Part 2. Synthetic modifications and applications of silacycles. *J. Chem. Soc. Perkin Trans. 1* **1999**, 81–102.

2. Lee, V.Y.; Sekiguchi, A.; Ichinohe, M.; Fukaya, N. Stable aromatic compounds containing heavier group 14 elements. *J. Organomet. Chem.* **2000**, *611*, 228–235.

3. Yamaguchi, S.; Tamao, K. Silole-containing σ-and π-conjugated compounds. *J. Chem. Soc.-dalt. Trans.* **1998**, 3693–3702.

4. Yamaguchi, S.; Jin, R.-Z.; Tamao, K. Modification of the electronic structure of silole by the substituents on the ring silicon. *J. Organomet. Chem.* **1998**, *559*, 73–80.

5. Boydston, A.J.; Yin, Y.; Pagenkopf, B.L. Synthesis and Electronic Properties of Donor− Acceptor π-Conjugated Siloles. *J. Am. Chem. Soc.* **2004**, *126*, 3724–3725.

6. Boydston, A.J.; Pagenkopf, B.L. Improving Quantum Efficiencies of Siloles and Silole-Derived Butadiene Chromophores through Structural Tuning. *Angew. Chemie Int. Ed.* **2004**, *43*, 6336–6338.

7. Yamaguchi, S.; Endo, T.; Uchida, M.; Izumizawa, T.; Furukawa, K.; Tamao, K. Toward new materials for organic electroluminescent devices: synthesis, structures, and properties of a series of 2, 5-diaryl-3, 4-diphenylsiloles. *Chem. Eur. J.* **2000**, *6*, 1683–1692.

8. Lee, J.; Liu, Q.-D.; Motala, M.; Dane, J.; Gao, J.; Kang, Y.; Wang, S. Photoluminescence, Electroluminescence, and Complex Formation of Novel N-7-Azaindolyl-and 2, 2 '-Dipyridylamino-Functionalized Siloles. *Chem. Mater.* **2004**, *16*, 1869–1877.

9. Luo, J.; Xie, Z.; Lam, J.W.Y.; Cheng, L.; Chen, H.; Qiu, C.; Kwok, H.S.; Zhan, X.; Liu, Y.; Zhu, D.; et al. Aggregation-induced emission of 1-methyl-1, 2, 3, 4, 5-pentaphenylsilole. *Chem. Commun.* **2001**, 1740–1741.

10. Chen, J.; Xie, Z.; Lam, J.W.Y.; Law, C.C.W.; Tang, B.Z. Silole-containing polyacetylenes. Synthesis, thermal stability, light emission, nanodimensional aggregation, and restricted intramolecular rotation. *Macromolecules* **2003**, *36*, 1108–1117.

11. Zhan, X.; Barlow, S.; Marder, S.R. Substituent effects on the electronic structure of siloles. *Chem. Commun.* **2009**, 1948–1955.

12. Chen, J.; Law, C.C.W.; Lam, J.W.Y.; Dong, Y.; Lo, S.M.F.; Williams, I.D.; Zhu, D.; Tang, B.Z. Synthesis, light emission, nanoaggregation, and restricted intramolecular rotation of 1, 1-substituted 2, 3, 4, 5-tetraphenylsiloles. *Chem. Mat.* **2003**, *15*, 1535–1546.

13. Chen, J.; Kwok, H.S.; Tang, B.Z. Silole-containing poly (diphenylacetylene): Synthesis, characterization, and light emission. *J. Polym. Sci. Pol. Chem.* **2006**, *44*, 2487–2498.

14. Haque, M.H.; Sohn, H. Comparison of aggregation-induced emission enhancement effect between π-σ* and σ-σ* conjugation on silole and

application in explosives detection. *Dye. Pigment.* **2022**, *201*, 110175.

15. Haque, M.H.; Sohn, H. Aggregation-induced emission enhancement of fluorene-substituted 2, 5-silole polymer and application as chemosensor. *J. Korean Phys. Soc.* **2022**, *80*, 1060–1064.

16. Sanji, T.; Sakai, T.; Kabuto, C.; Sakurai, H. Silole-Incorporated Polysilanes1a. *J. Am. Chem. Soc.* **1998**, *120*, 4552–4553.

17. Sohn, H.; Sailor, M.J.; Magde, D.; Trogler, W.C. Detection of nitroaromatic explosives based on photoluminescent polymers containing metalloles. *J. Am. Chem. Soc.* **2003**, *125*, 3821–3830.

18. Yamaguchi, S.; Goto, T.; Tamao, K. Silole–Thiophene Alternating Copolymers with Narrow Band Gaps. *Angew. Chemie* **2000**, *112*, 1761–1763.

19. Yamaguchi, S.; Jin, R.-Z.; Itami, Y.; Goto, T.; Tamao, K. The first synthesis of well-defined poly (2, 5-silole). *J. Am. Chem. Soc.* **1999**, *121*, 10420–10421.

20. Tamao, K.; Uchida, M.; Izumizawa, T.; Furukawa, K.; Yamaguchi, S. Silole derivatives as efficient electron transporting materials. *J. Am. Chem. Soc.* **1996**, *118*, 11974–11975.

21. Choi, J.-K.; Jang, S.; Kim, K.-J.; Sohn, H.; Jeong, H.-D. Observation of Negative Charge Trapping and Investigation of Its Physicochemical Origin in Newly Synthesized Poly (tetraphenyl) silole Siloxane Thin Films. *J. Am. Chem. Soc.* **2011**, *133*, 7764–7785.

22. Wang, F.; Luo, J.; Yang, K.; Chen, J.; Huang, F.; Cao, Y. Conjugated fluorene

and silole copolymers: synthesis, characterization, electronic transition, light emission, photovoltaic cell, and field effect hole mobility. *Macromolecules* **2005**, *38*, 2253–2260.

23. Sohn, H.; Huddleston, R.R.; Powell, D.R.; West, R.; Oka, K.; Yonghua, X. An electroluminescent polysilole and some dichlorooligosiloles. *J Am Chem Soc* **1999**, *121*, 2935–2936.

24. Sanchez, J.C.; Urbas, S.A.; Toal, S.J.; DiPasquale, A.G.; Rheingold, A.L.; Trogler, W.C. Catalytic hydrosilylation routes to divinylbenzene bridged silole and silafluorene polymers. Applications to surface imaging of explosive particulates. *Macromolecules* **2008**, *41*, 1237–1245.

25. Reddy, T.S.; Shin, S.; Choi, M. Effects of molecular flexibility/rigidity on the AIE/AIEE properties of aromatic thiols–substituted 1, 8–naphthalimides. *Dye. Pigment.* **2019**, *160*, 483–491.

26. Grimsdale, A.C.; Leok Chan, K.; Martin, R.E.; Jokisz, P.G.; Holmes, A.B. Synthesis of light-emitting conjugated polymers for applications in electroluminescent devices. *Chem Rev* **2009**, *109*, 897–1091.

27. Feng, X.; Tong, B.; Shen, J.; Shi, J.; Han, T.; Chen, L.; Zhi, J.; Lu, P.; Ma, Y.; Dong, Y. Aggregation-induced emission enhancement of aryl-substituted pyrrole derivatives. *J Phys Chem B* **2010**, *114*, 16731–16736.

28. Kalva, N.; Tran, C.H.; Lee, M.W.; Augustine, R.; Lee, S.J.; Kim, I. Aggregation-induced emission-active hyperbranched polymers conjugated with tetraphenylethylene for nitroaromatic explosive detection. *Dye. Pigment.*

2021, *194*, 109617.

29. Toal, S.J.; Trogler, W.C. Polymer sensors for nitroaromatic explosives detection. *J. Mater. Chem.* **2006**, *16*, 2871–2883.

30. Ma, X.; Tao, F.; Zhang, Y.; Li, T.; Raymo, F.M.; Cui, Y. Detection of nitroaromatic explosives by a 3D hyperbranched σ–π conjugated polymer based on a POSS scaffold. *J Mater Chem A* **2017**, *5*, 14343–14354.

31. Wang, C.-Z.; Yu, Z.-D.; Zhao, W.-X.; Yang, K.; Noda, Y.; Zhao, Y.; Feng, X.; Elsegood, M.R.J.; Teat, S.J.; Redshaw, C. Pyrene-fused hexaarylbenzene luminogens: Synthesis, characterization, and aggregation-induced emission enhancement. *Dye. Pigment.* **2021**, *192*, 109452.

32. Mei, J.; Hong, Y.; Lam, J.W.Y.; Qin, A.; Tang, Y.; Tang, B.Z. Aggregation-induced emission: the whole is more brilliant than the parts. *Adv Mater* **2014**, *26*, 5429–5479.

33. Toal, S.J.; Magde, D.; Trogler, W.C. Luminescent oligo (tetraphenyl) silole nanoparticles as chemical sensors for aqueous TNT. *Chem Commun* **2005**, 5465–5467.

34. West, R.; Sohn, H.; Bankwitz, U.; Calabrese, J.; Apeloig, Y.; Mueller, T. Dilithium Derivative of Tetraphenylsilole: An. eta. 1-. eta. 5 Dilithium Structure. *J. Am. Chem. Soc.* **1995**, *117*, 11608–11609.

35. Lee, M.H.; Kim, D.; Dong, Y.; Tang, B.Z. Time-resolved photoluminescence study of an aggregation-induced emissive chromophore. *J Korean Phys Soc* **2004**, *45*, 329–332.

36. Zhao, Z.; Liu, J.; Lam, J.W.Y.; Chan, C.Y.K.; Qiu, H.; Tang, B.Z. Luminescent aggregates of a starburst silole-triphenylamine adduct for sensitive explosive detection. *Dye. Pigment.* **2011**, *91*, 258–263.

37. Sohn, H.; Calhoun, R.M.; Sailor, M.J.; Trogler, W.C. Detection of TNT and picric acid on surfaces and in seawater by using photoluminescent polysiloles. *Angew. Chem.-Int. Ed.* **2001**, *40*, 2104–2105.

38. Seki, K.; Furuyama, T.; Kawasumi, T.; Sakurai, Y.; Ishii, H.; Kajikawa, K.; Ouchi, Y.; Masuda, T. UV photoelectron spectroscopy of substituted polyacetylenes. *J Phys Chem B* **1997**, *101*, 9165–9169.

39. Thomas, S.W.; Joly, G.D.; Swager, T.M. Chemical sensors based on amplifying fluorescent conjugated polymers. *Chem. Rev.* **2007**, *107*, 1339–1386.

40. Shu, W.; Guan, C.; Guo, W.; Wang, C.; Shen, Y. Conjugated poly (aryleneethynylenesiloles) and their application in detecting explosives. *J. Mater. Chem.* **2012**, *22*, 3075–3081.

41. Liu, J.; Zhong, Y.; Lam, J.W.Y.; Lu, P.; Hong, Y.; Yu, Y.; Yue, Y.; Faisal, M.; Sung, H.H.Y.; Williams, I.D. Hyperbranched conjugated polysiloles: synthesis, structure, aggregation-enhanced emission, multicolor fluorescent photopatterning, and superamplified detection of explosives. *Macromolecules* **2010**, *43*, 4921–4936.

42. Sanchez, J.C.; DiPasquale, A.G.; Rheingold, A.L.; Trogler, W.C. Synthesis, luminescence properties, and explosives sensing with 1, 1-tetraphenylsilole- and 1, 1-silafluorene-vinylene polymers. *Chem Mater* **2007**, *19*, 6459–6470.

43. Kim, H.K.; Ryu, M.-K.; Kim, K.-D.; Lee, S.-M.; Cho, S.-W.; Park, J.-W. Tunable electroluminescence from silicon-containing poly (p-phenylenevinylene)-related copolymers with well-defined structures. *Macromolecules* **1998**, *31*, 1114–1123.

44. Shin, B.; Sohn, H. Enhanced explosive sensing based on bis (methyltetraphenyl) silole nanoaggregate. *J Korean Phys Soc* **2018**, *72*, 234–237.

45. Shin, B.; Sohn, H. 1, 3, 5-Trinitrotoluene Sensor Based on Silole Nanoaggregates. *J Nanosci Nanotechno* **2019**, *19*, 991–995.

46. Frisch, M.J.; Trucks, G.W.; Schlegel, H.B.; Scuseria, G.E.; Robb, M.A.; Cheeseman, J.R.; Scalmani, G.; Barone, V.; Mennucci, B.; Petersson, G.A. Gaussian, Inc., Wallingford CT. *Gaussian 09* **2009**.

47. Hong, Y.; Lam, J.W.Y.; Tang, B.Z. Aggregation-induced emission. *Chem Soc Rev* **2011**, *40*, 5361–5388.

48. Jang, S.-H.; Kim, S.-G.; Jung, D.-H.; Kwon, H.-J.; Song, J.-W.; Cho, S.-D.; Ko, Y.-C.; Sohn, H.-L. Aggregation-induced emission enhancement of polysilole nanoaggregates. *B Kor Chem Soc* **2006**, *27*, 1965–1966.

49. Sun, H.; Tang, X.-X.; Miao, B.-X.; Yang, Y.; Ni, Z. A new AIE and TICT-active tetraphenylethene-based thiazole compound: Synthesis, structure, photophysical properties and application for water detection in organic solvents. *Sens. Actuator B-Chem.* **2018**, *267*, 448–456.

50. Qayyum, M.; Bushra, T.; Khan, Z.A.; Gul, H.; Majeed, S.; Yu, C.; Farooq, U.;

Shaikh, A.J.; Shahzad, S.A. Synthesis and tetraphenylethylene-based aggregation-induced emission probe for rapid detection of nitroaromatic compounds in aqueous media. *ACS omega* **2021**, *6*, 25447–25460.

51. Jiang, K.; Luo, S.-H.; Pang, C.-M.; Wang, B.-W.; Wu, H.-Q.; Wang, Z.-Y. A functionalized fluorochrome based on quinoline-benzimidazole conjugate: From facile design to highly sensitive and selective sensing for picric acid. *Dye. Pigment.* **2019**, *162*, 367–376.

52. Giri, D.; Islam, S.N.; Patra, S.K. Synthesis and characterization of 1, 2, 3-triazole appended polythiophene based reusable fluorescent probe for the efficient detection of trace nitroaromatics. *Polymer (Guildf).* **2018**, *134*, 242–253.

53. Sun, X.; Wang, Y.; Lei, Y. Fluorescence based explosive detection: from mechanisms to sensory materials. *Chem. Soc. Rev.* **2015**, *44*, 8019–8061.

54. Zhang, G.; Hu, F.; Zhang, D. Manipulation of the aggregation and deaggregation of tetraphenylethylene and silole fluorophores by amphiphiles: emission modulation and sensing applications. *Langmuir* **2015**, *31*, 4593–4604.

55. Zhang, L.; Jiang, T.; Wu, L.; Wan, J.; Chen, C.; Pei, Y.; Lu, H.; Deng, Y.; Bian, G.; Qiu, H. 2, 3, 4, 5-Tetraphenylsilole-Based Conjugated Polymers: Synthesis, Optical Properties, and as Sensors for Explosive Compounds. *Chem. Asian J.* **2012**, *7*, 1583–1593.

56. Frisch, M.J.; Trucks, G.W.; Schlegel, H.B.; Scuseria, G.E.; Robb, M.A.; Cheeseman, J.R.; Scalmani, G.; Barone, V.; Mennucci, B.; Petersson, G.A.

Gaussian 09 (Revision A. 02)[Computer software]. *Gaussian Inc., Wallingford CT* **2009**.

57. Lakowicz, J.R. *Principles of fluorescence spectroscopy*; Springer, 2006;

58. Kalderis, D.; Juhasz, A.L.; Boopathy, R.; Comfort, S. Soils contaminated with explosives: environmental fate and evaluation of state-of-the-art remediation processes (IUPAC technical report). *Pure Appl. Chem.* **2011**, *83*, 1407–1484.

59. Letzel, S.; Göen, T.; Bader, M.; Angerer, J.; Kraus, T. Exposure to nitroaromatic explosives and health effects during disposal of military waste. *Occup. Environ. Med.* **2003**, *60*, 483–488.

60. Sabbioni, G.; Liu, Y.-Y.; Yan, H.; Sepai, O. Hemoglobin adducts, urinary metabolites and health effects in 2, 4, 6-trinitrotoluene exposed workers. *Carcinogenesis* **2005**, *26*, 1272–1279.

61. Yew, Y.T.; Ambrosi, A.; Pumera, M. Nitroaromatic explosives detection using electrochemically exfoliated graphene. *Sci. Rep.* **2016**, *6*, 1–11.

62. Tang, N.; Mu, L.; Qu, H.; Wang, Y.; Duan, X.; Reed, M.A. Smartphone-enabled colorimetric trinitrotoluene detection using amine-trapped polydimethylsiloxane membranes. *ACS Appl. Mater. Interfaces* **2017**, *9*, 14445–14452.

63. Aparna, R.S.; Devi, J.S.A.; Sachidanandan, P.; George, S. Polyethylene imine capped copper nanoclusters-fluorescent and colorimetric onsite sensor for the trace level detection of TNT. *Sensors Actuators B Chem.* **2018**, *254*, 811–819.

64. Kartha, K.K.; Babu, S.S.; Srinivasan, S.; Ajayaghosh, A. Attogram sensing of trinitrotoluene with a self-assembled molecular gelator. *J. Am. Chem. Soc.* **2012**, *134*, 4834–4841.

65. Dongre, S.D.; Das, T.; Babu, S.S. Dual mode selective detection and differentiation of TNT from other nitroaromatic compounds. *J. Mater. Chem. A* **2020**, *8*, 10767–10771.

66. Mullen, C.; Irwin, A.; Pond, B. V; Huestis, D.L.; Coggiola, M.J.; Oser, H. Detection of explosives and explosives-related compounds by single photon laser ionization time-of-flight mass spectrometry. *Anal. Chem.* **2006**, *78*, 3807–3814.

67. Senthamizhan, A.; Celebioglu, A.; Bayir, S.; Gorur, M.; Doganci, E.; Yilmaz, F.; Uyar, T. Highly fluorescent pyrene-functional polystyrene copolymer nanofibers for enhanced sensing performance of TNT. *ACS Appl. Mater. Interfaces* **2015**, *7*, 21038–21046.

68. Lan, A.; Li, K.; Wu, H.; Olson, D.H.; Emge, T.J.; Ki, W.; Hong, M.; Li, J. A luminescent microporous metal–organic framework for the fast and reversible detection of high explosives. *Angew. Chemie* **2009**, *121*, 2370–2374.

69. Hu, X.; Wei, T.; Wang, J.; Liu, Z.-E.; Li, X.; Zhang, B.; Li, Z.; Li, L.; Yuan, Q. Near-infrared-light mediated ratiometric luminescent sensor for multimode visualized assays of explosives. *Anal. Chem.* **2014**, *86*, 10484–10491.

70. Berliner, A.; Lee, M.-G.; Zhang, Y.; Park, S.H.; Martino, R.; Rhodes, P.A.; Yi, G.-R.; Lim, S.H. A patterned colorimetric sensor array for rapid detection of

TNT at ppt level. *RSC Adv.* **2014**, *4*, 10672–10675.

71. Han, T.; Hong, Y.; Xie, N.; Chen, S.; Zhao, N.; Zhao, E.; Lam, J.W.Y.; Sung, H.H.Y.; Dong, Y.; Tong, B. Defect-sensitive crystals based on diaminomaleonitrile-functionalized Schiff base with aggregation-enhanced emission. *J. Mater. Chem. C* **2013**, *1*, 7314–7320.

72. Dong, Y.; Lam, J.W.Y.; Qin, A.; Sun, J.; Liu, J.; Li, Z.; Sun, J.; Sung, H.H.Y.; Williams, I.D.; Kwok, H.S. Aggregation-induced and crystallization-enhanced emissions of 1, 2-diphenyl-3, 4-bis (diphenylmethylene)-1-cyclobutene. *Chem. Commun.* **2007**, 3255–3257.

73. Fischer, G.M.; Daltrozzo, E.; Zumbusch, A. Selective NIR chromophores: bis (pyrrolopyrrole) cyanines. *Angew Chem Int Ed.* **2011**, *50*, 1406–1409.

74. Grabowski, Z.R.; Rotkiewicz, K.; Rettig, W. Structural changes accompanying intramolecular electron transfer: focus on twisted intramolecular charge-transfer states and structures. *Chem. Rev.* **2003**, *103*, 3899–4032.

75. Jenekhe, S.A.; Osaheni, J.A. Excimers and exciplexes of conjugated polymers. *Science (80-.).* **1994**, *265*, 765–768.

76. Jia, W.; Wang, H.; Yang, L.; Lu, H.; Kong, L.; Tian, Y.; Tao, X.; Yang, J. Synthesis of two novel indolo [3, 2-b] carbazole derivatives with aggregation-enhanced emission property. *J. Mater. Chem. C* **2013**, *1*, 7092–7101.

77. Mei, J.; Wang, J.; Sun, J.Z.; Zhao, H.; Yuan, W.; Deng, C.; Chen, S.; Sung, H.H.Y.; Lu, P.; Qin, A. Siloles symmetrically substituted on their 2, 5-positions with electron-accepting and donating moieties: facile synthesis, aggregation-

enhanced emission, solvatochromism, and device application. *Chem. Sci.* **2012**, *3*, 549–558.

78. Yu, G.; Yin, S.; Liu, Y.; Chen, J.; Xu, X.; Sun, X.; Ma, D.; Zhan, X.; Peng, Q.; Shuai, Z. Structures, electronic states, photoluminescence, and carrier transport properties of 1, 1-disubstituted 2, 3, 4, 5-tetraphenylsiloles. *J. Am. Chem. Soc.* **2005**, *127*, 6335–6346.

79. Li, J.; Rajca, A.; Rajca, S. Synthesis and conductivity of binaphthyl-based conjugated polymers. *Synth. Met.* **2003**, *137*, 1507–1508.

80. Du, P.; Schneider, J.; Brennessel, W.W.; Eisenberg, R. Synthesis and structural characterization of a new vapochromic Pt (II) complex based on the 1-terpyridyl-2, 3, 4, 5, 6-pentaphenylbenzene (TPPPB) ligand. *Inorg. Chem.* **2008**, *47*, 69–77.

81. Shen, X.Y.; Wang, Y.J.; Zhao, E.; Yuan, W.Z.; Liu, Y.; Lu, P.; Qin, A.; Ma, Y.; Sun, J.Z.; Tang, B.Z. Effects of substitution with donor–acceptor groups on the properties of tetraphenylethene trimer: aggregation-induced emission, solvatochromism, and mechanochromism. *J. Phys. Chem. C* **2013**, *117*, 7334–7347.

82. Wang, F.; Bazan, G.C. Aggregation-mediated optical properties of pH-responsive anionic conjugated polyelectrolytes. *J. Am. Chem. Soc.* **2006**, *128*, 15786–15792.

83. Fu, H.-B.; Yao, J.-N. Size effects on the optical properties of organic nanoparticles. *J. Am. Chem. Soc.* **2001**, *123*, 1434–1439.

84. Sathiyaraj, M.; Pavithra, K.; Thiagarajan, V. Azine based AIEgens with multi-stimuli response towards picric acid. *New J. Chem.* **2020**, *44*, 8402–8411.

85. Chen, B.; Jiang, Y.; Chen, L.; Nie, H.; He, B.; Lu, P.; Sung, H.H.Y.; Williams, I.D.; Kwok, H.S.; Qin, A. 2, 5-Difluorenyl-Substituted Siloles for the Fabrication of High-Performance Yellow Organic Light-Emitting Diodes. *Chem. Eur. J.* **2014**, *20*, 1931–1939.

86. Zhao, D.; Swager, T.M. Sensory responses in solution vs solid state: a fluorescence quenching study of poly (iptycenebutadiynylene) s. *Macromolecules* **2005**, *38*, 9377–9384.

87. Kasat, R.B.; Wang, N.-H.L.; Franses, E.I. Effects of backbone and side chain on the molecular environments of chiral cavities in polysaccharide-based biopolymers. *Biomacromolecules* **2007**, *8*, 1676–1685.

88. Sekiguchi, A.; Zigler, S.S.; West, R.; Michl, J. A synthon for the silicon-silicon triple bond. *J Am Chem Soc* **1986**, *108*, 4241–4242.

89. Tamao, K.; Yamaguchi, S.; Shiro, M. Oligosiloles: first synthesis based on a novel endo-endo mode intramolecular reductive cyclization of diethynylsilanes. *J. Am. Chem. Soc.* **1994**, *116*, 11715–11722.

90. Nojima, M.; Kamigawara, T.; Ohta, Y.; Yokozawa, T. Catalyst-Transfer Suzuki–Miyaura Condensation Polymerization of Stilbene Monomer: Different Polymerization Behavior Depending on Halide and Aryl Group of ArPd (tBu3P) X Initiator. *J. Polym. Sci. Pol. Chem.* **2019**, *57*, 297–304.

91. Zhao, Z.; Chen, S.; Lam, J.W.Y.; Jim, C.K.W.; Chan, C.Y.K.; Wang, Z.; Lu, P.;

Deng, C.; Kwok, H.S.; Ma, Y. Steric hindrance, electronic communication, and energy transfer in the photo-and electroluminescence processes of aggregation-induced emission luminogens. *J. Phys. Chem. C* **2010**, *114*, 7963–7972.

92. Freeman, D.M.E.; Musser, A.J.; Frost, J.M.; Stern, H.L.; Forster, A.K.; Fallon, K.J.; Rapidis, A.G.; Cacialli, F.; McCulloch, I.; Clarke, T.M.; et al. Synthesis and Exciton Dynamics of Donor-Orthogonal Acceptor Conjugated Polymers: Reducing the Singlet-Triplet Energy Gap. *J. Am. Chem. Soc.* **2017**, *139*, 11073–11080, doi:10.1021/jacs.7b03327.

Appendix A

Acknowledgement

First and foremost, I would like to express my sincere gratitude to my advisor **Prof. Sohn Honglae** for his guidance and motivation. I can't thank him enough for providing me the great opportunity to pursue my Ph.D. under his supervision. He has been a marvelous mentor to me. I'm grateful for his continuous support, patience and sharing of his immense research knowledge and ideas with me. I always enjoyed the lab meetings and the discussion time with him and have learned a lot from him. His teaching and expertise have made my Ph.D. experience productive and interesting. As my advisor, his understanding and care for me made my tough times in the Ph.D. manageable. His advice on both research as well as on my career have been priceless. Throughout my Ph.D., he gave me the moral support and the freedom to pursue the research I wanted to do. Without his guidance and constant feedback, this Ph.D. would not have been possible.

My sincere thanks to the thesis committee members for evaluating my thesis. Their insightful comments and questions have made my defense enjoyable and memorable.

I owe my gratitude to Chosun University International office team for their academic help in various stages of my Ph.D. They took us on field trips to various parts of Korea which helped me to understand and embrace the culture of Korea and warm gesture of Korean people. I thank the former coordinator **Yushin Jeong** and current coordinator for all their help and kindness and constant feedback throughout my Ph.D. study.

Words cannot express my thankfulness to my parents **Md Abul Hasem and Mst. Ambia Khatun**. Both are my role model in my life, and they sacrificed everything for me. They raised me independently and allowed to decide my career and pursue towards it. Then I am thankful to my wife **Jannatul Ferdous,** she supported me a lot to reach my goal . I also thank my sisters **Tahira** and **Sumaiya**, my sister-in-law **Mr Obaidul Haque** who is more than a brother to me and **Mr Tusar** for all their encouragement and support. I am also thakful to my mother-in-law for his unconditional support. And thanks to my friends to helped me a lot to reach my dream.

My deep appreciation goes to my co-guide and senior **Dr. Ahmed Shamsuddin, Dr. Saiful Islam, Dr. Imrul Khalid** and my senior **Mr. Kyeong Kuk Koh** who have been supportive in many ways. There are innumerable situations we discussed our research and worked together all night to keep up with deadline. I am also grateful to my lab mates for her help and wonderful fun lab time. The time we spent together will always be remembered and cherished.

Besides my lab members, I extend my sincere gratitude to my all friends including **Chosun University** (**Dr. Adnan, Dr. Themmy, Dr. Isabel, Dr. Dui, Dr. Selim, Asadujjaman, Dr. Masud Rana, Dr. Munsur, Golam Taki, Dr. Masud, Dr. Manik** and **Dr. Maruf**) for their help and moral support.

Finally, I would like to thank all of my friends from France and Pakistan for their constant encouragement. My special thanks to my uncles **Mr. Akmol Hussain, Mr. Abul Kalam,** my friend **Abdullah Rasel** and my brother **Waheduzzaman** for their constant support, this journey was not possible without their kind attention. Following this, my special gratitude to my ex-professor **Dr. Abdul Bari** for his countless help

and guiding throughout my Bachelor journey. Also, my special thanks to **Mr. Badsha Alomgir, Hafizul Islam, Hasan Tarek, Golam Hafiz, Khairul Islam, Rubel, and Sojib.**

I thank everyone who helped directly and indirectly to complete my doctoral study successfully.

I dedicate this thesis to my parents and my wife specially to my father who left us just before my finishing line. My mother struggled a lot as women to raise me and always pushed me to the my golden journey. Their unconditional love, constant support and grace has always kept me going. I found my wife always besides me as a friend, supoorter and motivisional.